DEVELOPMENT OF MICRO AND NANOPARTICLE SUBSTRATES FOR SERS DETECTION OF PESTICIDES AND DELIVERY OF CHEMOTHERAPEUTIC DRUGS

and

PILOT SCALE PROCESS DEVELOPMENT AND PRODUCTION OF CANCER TESTIS ANTIGENS

A Dissertation

Presented to the Faculty of the Graduate School

of Cornell University

In Partial Fulfillment of the Requirements for the Degree of

Doctor of Philosophy

by

Cameron Lee Bardliving

May 2013

ABSTRACT

DEVELOPMENT OF MICRO AND NANOPARTICLE SUBSTRATES FOR SERS DETECTION OF PESTICIDES AND DELIVERY OF CHEMOTHERAPEUTIC DRUGS

and

PILOT SCALE PROCESS DEVELOPMENT AND cGMP PRODUCTION OF CANCER TESTIS ANTIGEN MELAN-A

Cameron Lee Bardliving, Ph.D.

Cornell University 2013

Detection or delivery of a diverse range of biomolecules in field portable devices is an important area of research in the fields of environmental pollution, homeland security, and medicine. The demand for hand-held and low cost detection in these fields has led to the development of novel analytical systems such as Surface Enhanced Raman Spectroscopy (SERS) and Molecularly Imprinted Polymers (MIP). SERS is rapidly emerging as a tool for biological assays, chemical sensing, and electrochemistry. Whereas, Molecularly Imprinted Polymers have been developed as systems for solid phase extraction, chemical separation, and controlled release. In this dissertation, several systems were developed using nanotechnology and polymer synthesis to develop chemical sensors and a drug delivery system. A substrate for pesticide detection was developed by conjugating oligonucleotides specific for the pesticide malathion to the surface of a SERS substrate that detected the organophosphorus pesticide malathion down to the micromolar level. A SERS substrate was also developed by grafting a molecularly imprinted polymer of methacrylic acid and ethylene glycol dimethacrylate to surface of a gold coated silica microparticle that was able to capture and detect the pesticide thiabendazole. Molecularly

imprinted polymers were investigated as a drug delivery system for the chemotherapeutic doxorubicin which showed strong imprinting and temperature sensitive controlled release of drug. Lastly, a cGMP pilot scale process was developed to produce gram levels of the cancer vaccine Melan-A for phase I clinical trials.

BIOGRAPHICAL SKETCH

Cameron Lee Bardliving was born on July 10th 1984 in Milford, CT to Clifford Lee Bardliving Jr. and Tanya Lynn Bardliving. He grew up in Norwalk, CT where he attended the Columbus Magnet Elementary School until the age of eleven when he and his family move to Abington, PA. He matriculated through the Abington school district until 10th grade when he moved to Wyndmoor, PA where he graduated from Springfield Township High School in 2002.

Cameron Bardliving attended the University of Maryland, Baltimore County where he received his B.S. in Chemical Engineering in 2007. At UMBC, he was awarded the Meyerhoff Scholarship which is a program dedicated to helping increase diversity among the leadership in the STEM fields by preparing selected undergraduates for doctoral study in science and engineering. In 2007 he entered the PhD program in Biomedical Engineering at Cornell University. As a member of the laboratory of Carl A. Batt, he has worked on projects ranging from pilot scale process development and production of vaccines for phase 1 clinical trials, development of nanoparticle conjugates for pesticide detection using Surface Enhanced Raman Spectroscopy, and imprinted polymers for drug delivery.

ACKNOWLEDGMENTS

I would like to gratefully acknowledge the guidance and support of my advisor Carl A. Batt. His mentorship has been invaluable to me as a graduate student and as person. I still remember my first visit to Cornell and how welcoming Carl was to me. Ever since that time his door has always been open to me. More than anything else he has taught me that science is not an individual endeavor and if you do not look behind to teach others your efforts are wasted. I would like to thank my minor advisors Prof. Matt Delisa and Prof. Esther Angert for serving as great mentors and role models. I would also like to thank Dr. Aaron Stickland and Dr. Francisco Barahona for all their guidance and just being good friends.

I want to give a special acknowledgement to the entire Ludwig Team that I had a chance to work with during my tenure as a graduate student. Adam, Mike, Laura, Kyle, Jack, Leo, Deuce, Brian, Denise; you all made the experience in the facility great and I am grateful for all of the knowledge I was able to gather from working with you. Adam you deserve a special shout out for the countless hours we spent working the Melan-A campaign.

I would like to acknowledge my family who started me on this journey so many years ago. I especially thank my grandma who used to give me all those dinosaurs for my birthday and Christmas and made me study facts on each one. I want to also thank my father and mother for teaching me determination and setting high expectations for me. I want to give a special thank you to Stephanie who puts up with me every day in lab but whose love and support make this journey all the more enjoyable.

TABLE OF CONTENTS

Chapter 1: Introduction

CANCER IMMUNOTHERAPY

The pharmacodynamic effect of immunotherapeutics is defined by various modulations of patient anticancer immune responses to selectively eliminate cancerous tissue. Immunotherapeutics are generally divided into two catergories; passive or active[1-3]. Passive immunization involves the introduction of exogenous immune system components into the body to cause a cytotoxic effect. Active immunization rather stimulates the body's own immune system to combat an infection or chronic disease. For over two centuries, active immunization has been at the forefront of immunotherapeutics beginning with the work of Edward Jenner in developing the first smallpox vaccine from cowpox lesions[3]. Since that time, preventative and therapeutic vaccines for poliomyelitis, typhoid, cholera, diphtheria, and hepatitis B among others have been developed and in some cases used to eradicate the disease[3]. The idea for the development of active immunotherapeutics to combat cancer was first proposed in the 1890s by Paul Ehrlich and William Coley and the first reported successful implementation was by Ronald Levy and colleagues for B-cell lymphomas in 1982 [4].

Cancer immunotherapeutics are presently a main component for cancer treatment regimens. Modern cancer immunotherapeutics include prophylactic vaccines, monoclonal antibodies, systemically administered cytokines for activation of cell signaling cascades, and local delivery of immunotoxins/adjuvants to illicit immune response (Table 1.1). All of these strategies take advantage of the immune system's ability to recognize not only foreign antigens but also abnormal expression of proteins by tumors. Cancer immunotherapies generally need to overcome

several biological hurdles during development including identification of appropriate targets, adequate activation of the immune system, suppression of cytotoxic pathways, and proper interaction with immune system components[2]. Additionally patient heterogeneity[5] and lack of information on the proper dosing schedule for many cancer immunotherapeutics when compared to the measurable pharmacokinetic and pharmacodynamic effects of classic chemotherapy drugs[2, 5] is a deterrent for implementation of immunotherapies. Cancer immunotherapeutics, in particular cancer vaccines, also often lack measurable biomarkers to determine the maximal tolerated and maximal effective dose of the therapy and may have insufficient volumetric response in the tumor in comparison to the effects of cytotoxic drugs[2, 6]. Therefore the current method for clinical assessment of tumor therapies is not necessarily transferable to cancer vaccine assessment. Future work will involve coordination between government, industry, and academia to institute broader definitions for clinical trials design and analysis to incorporate the therapeutic benefits of cancer vaccines [7]. The chapter will focus on two of immunotherapies; monoclonal antibodies and recombinant vaccines.

Table 1.1 Approved Cancer Immunotherapies[1, 7]. Adapted from Dougan *et al*., and Huang *et al*.

Therapy	**Indication**	**Host**
Antibody		
Rituximab	Non-Hodgkin's lymphoma, Chronic lymphocytic leukemia	Chinese Hamster Ovary (CHO)
Ibritumomab tiuxetan	Non-Hodgkin's lymphoma	CHO
Tositumomab	Non-Hodgkin's lymphoma	Mammalian
Alemtuzumab	Chronic lymphocytic leukemia	CHO
Gemtuzumab	Acute myelogenous leukemia	NS0 (murine myeloma)
Trastuzumab	Breast cancer	CHO
Cetuximab	Colorectal cancer	SP2/0 (murine myeloma)
Natalizumab	Multiple sclerosis (MS)	CHO
Tremelimumab	Metastatic melanoma	
Panitumumab	Colorectal cancer	CHO
Bevacizumab	Colorectal cancer, Lung cancer	CHO
Cytokine		
IFN-α	Melanoma, Renal cell carcinoma	*E. coli*, CHO
IL-2	Melanoma, Renal cell carcinoma	*E. coli*
TNF- α	Soft tissue sarcoma, Melanoma	
Peptide Vaccines		
Hepatitis B Virus (HBV)	Hepatocellular carcinoma	*S. cerevisiae*
Human papillomavirus (HPV)	Cervical cancer	*S. cerevisiae*
Recombinant Therapeutic Vaccines		
MAGE-A3	Non-small cell lung cancer (NSCLC) and Melanoma	*E. coli*
NY-ESO-1	Various malignancies	*E. coli*
Melan-A	Melanoma	*E. coli*
SSX2	Synovial sarcoma	*E. coli*

Monoclonal Antibodies

One of the most successful forms of cancer immune therapy is monoclonal antibodies (mAb) treatment[8]. Antibodies, also known as immunoglobulins, consist of two copies of two polypeptide chains which recognize target antigen epitopes and play an essential role in protection from microorganisms. The development of the hybridoma technique for monoclonal antibody production in 1975 by Kohler and Milstein [9], made it possible to engineer antibodies for treatment of chronic disease. In a little over a decade, a murine based mAb therapy, muromonab targeting CD3 in patients with renal transplants, was approved by the FDA[10]. Yet murine derived antibodies were found to have several drawbacks which prohibited their clinical effectiveness. One issue is that animal derived products cause an immune response in the patient which limits its dosage schedule. Additionally, murine mAb generally have short half-lives *in vivo*, and do not elicit antibody-dependent cellular cytotoxicity (ADCC) due to insufficient binding to human compliment[1, 3, 7]. To overcome these limitations new monoclonal antibody therapeutics were introduced that were chimeric, humanized, or full human antibodies. Chimeric antibodies are fusion protein constructs most often consisting of a substituted Fc region. Basliximab (simulect) a chimeric antibody toward CD25 (IL-2Rα) to block binding with IL-2 was approved in 1998 [3]. Research continued into reducing the mouse component of the antibody down to 5-10% which resulted in reduced immunogenicity, improved serum half -life, and cytotoxic effect[11]. Other chimeric or fused antibodies were later commercialized including infliximab (remicade) and etenercept (Enbrel) against the cytokine TNFα[3]. Humanized antibodies, where non-human antibody sequences are modified to have sequence identity with antibodies derived from humans, were developed to take advantage of recombinant expression of

of these constructs in mammalian cell culture systems[12]. The first humanized monoclonal antibody (daclizumab, Zenapax) was approved by the FDA in 1997 targeting CD25 expressing lymphocytes to reduce transplant allograft rejection[2, 3]. These second generation antibodies also targeted cytokine receptors or were conjugated with radiolabels and toxins to improve cytotoxicity. Examples are rituximab which was conjugated with ^{90}Y targeting CD20 for B-cell non-Hodgkin's lymphoma[13]

Monoclonal antibodies therapeutic effect can be characterized by three mechanisms of action: antibody-dependent cellular cytotoxicity (ADCC), compliment dependent cytotoxicity (CDC), and cell signaling interference[1, 8]. In ADCC, mAbs can bind to antigen presented on the tumor cell surface which serves as a target for the natural killer (NK) cells FcγRIII receptor. Cytolytic proteins are then released from the NK cells and the tumor cell is lysed. The cellular debris is taken up by antigen-presenting cells, which present the tumor antigens to B cells and leads to the release of tumor antibodies. Cytotoxic T lymphocytes (CTLs) recognize these antigens and attack the tumor and provide the patient with immunological memory[8]. Compliment dependent cytotoxicity is a part of the innate immune system where by a membrane attack complex is formed as the end product of antibody targeting a specific antigen on the tumor surface[8]. As many of the tumor associated antigens (TAA) are growth factors (i.e. endothelial growth factor receptor) another mechanism of monoclonal antibody action is direct attenuation of a receptor or receptor dimerization leading to decreased proliferation[8]. The reduced growth rate of the tumor also allows for more effective use of chemotherapy agents as the tumor cells are more sensitive at more normal proliferation rates. The mAb trastuzumab (Herceptin) against HER2/neu and

endothelial growth factor receptor has been shown to improve survival in patients when used in combination with paclital or other chemotherapeutics[14-16]

Monoclonal antibody immunotherapy is also generally not as toxic as conventional chemotherapy agents and can activate titer levels rapidly[1]. Over 25 different antibodies are currently in clinical use[17]. With improvements in industrial scale production systems[18], serum half-life, and efficacy monoclonal antibodies will continue to expand the immunotherapeutic market that is growing at a rate of 14% per year as of 2007[19].

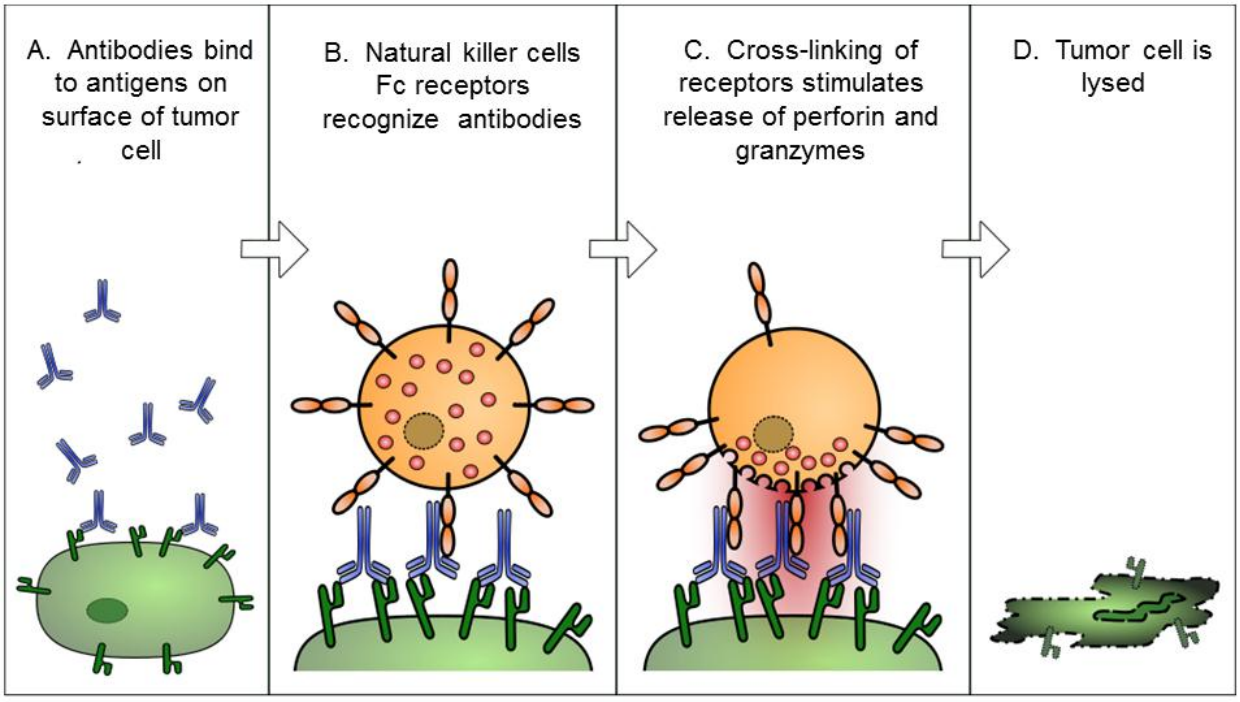

Figure 1.1 Antibody-dependent cell-mediated cytotoxicity. a) Monoclonal antibodies (MAbs) bind to target antigens on surface of tumor cell. b) Natural killer cells expressing the transmembrane isoform of CD16 engage antibodies on surface of tumor cell. c) Cross linking of FCγIIIa receptors stimulates release of cytokines and cytolytic granules. d) Interferons and granzymes enter cell triggering apoptosis.

Recombinant Immunotherapeutics/Vaccines

Vaccines are biological preparations of killed, attenuated, subunit, or polysacchide conjugate of a pathogen used to improve immunity to a disease. While prophylactic or therapeutic vaccines to microbial or viral infectious diseases have been in development for over two centuries, vaccines for chronic illness such has cancer have not seen the same level of success. However, as numerous cancers are caused by microbial infections, traditional vaccination strategies can be used to treat these cancers. Highly conserved epitopes that are expressed by microbes can be used to develop effective vaccination strategies. The first available recombinant prophylactic vaccine for cancer therapy approved by the FDA (1986) was the vaccine for hepatitis B virus (HBV)[20]. Hepatitis B infects the liver leading to hepatitis. This chronic inflammation can eventually cause hepatocellular carcinoma in a subset of patients[21]. The vaccine contained a surface antigen that was administered in combination with an adjuvant to protect against all strains of HBV.

The next breakthrough occurred with the development of the recombinant human papillomavirus (HPV) under the trade name Gardasil. HPV infections can lead to cervical cancer which results in 250,000 deaths per year worldwide and HPV 16 and 18 are associated with 70% of the cervical tumors[22]. Girls vaccinated with HPV 16 and 18 have a 98% prevention rate against cervical intraepithelial neoplasia and cervical cancer[22, 23]. The HPV vaccine is composed of four capsid proteins that can spontaneously assemble into virus-like particles (VLP) which are indistinguishable from native virus[24].

Therapeutic cancer vaccines derived from whole cells, tumor associated antigens (TAA) and viral vectors, have been investigated for cancer treatment. TAA vaccines are of particular interest

because they are gene products that are overexpressed by tumor cells but have basal or no expression in normal cells[25]. Among the well documented TAAs Her-2, p53, and cancer testis (CT) antigens, CT antigens show the most promise as a therapeutic as their expression outside of tumors is often limited to germ cells and trophoblasts which are not recognized by cytotoxic T lymphocytes [25, 26]. John Beard first noted the similarities in biological expression between trophoblasts and cancer (trophoblastic theory of cancer) which eventually lead to the discovery of CT antigens[26]. The first CT antigen, MZ2-E, was discovered through autologous typing and DNA cloning from a melanoma patient with CTLs that recognized the tumor[27, 28]. The gene encoding MZ2-E was named MAGE1 and soon after the CT antigens B melanoma antigen (BAGE) and G antigen 1 (GAGE1) were discovered. The later development of the SEREX technique (serological analysis of cDNA expression libraries), which combined serological analysis with antigen cloning technology[29, 30], led to the discover of the SSX gene family[31] and the potent NY-ESO-1 antigen[32]. Presently, there are 44 known CT antigen gene families which can be divided based on chromosomal mapping either on the X chromosome or non-X chromosome[26]. Table 1.2 lists some of the major CT antigens as well as their expression patterns in normal and cancerous tissue. The function of many of the CT antigens is not understood but expression has been linked to promoter demethylation[33].

Table 1.2 Select cancer testis antigens gene expression in normal and cancerous tissues [34]

Antigen	Normal Expression Pattern	Cancerous Expression Pattern
MAGE	Testis and pancreas	Melanoma, lung, brain, esophageal and stomach, bladder, breast, skeletal muscle
NYESO-1	Testis, placenta, pancreas, liver	Esophageal, melanoma, prostate, transitional cell bladder, breast, lung, medullary thyroid, squamous head and neck carcinoma, cervical carcinoma
BAGE	Testis	Melanoma, bladder, lung
GAGE	Testis	Melanoma, sarcomas, Non-small cell lung cancer, head and neck tumors, bladder
XAGE1	Testis, placenta, pancreas, spleen, thymus, lung, skeletal muscle	Bone, muscle, melanoma, Ewing's sarcoma, breast, lung, prostate
SSX	Testis	Skin, bladder, breast, head and neck, colon, lung

The recombinant MAGE-A3 and NY-ESO-1 have been produced in *E. coli* and have been evaluated in clinical trials as vaccines [35-40]. The recombinant proteins are often preferred over peptide segments as the multiple epitopes on the recombinant protein can stimulate strong activity of $CD4^+$ and $CD8^+$ T cell populations. NY-ESO-1 has been found to be one of most immunogenic CT antigens with expression across a variety of cancers including bladder, lung, ovarian, hepatocellular, and melanoma[34]. In a clinical trial, patients that were given NY-ESO-1

in combination with the adjuvant ISCOMatrix observed higher antibody titers, reduced negative pharmacodynamics and CD4+ and CD8+ T cells specific for a range of NY-ESO-1 epitopes [41].

The differentiation antigen presented in this work, Melan-A, is also a member of the MAGE gene family [42]. Melan-A has been screened as a peptide prophylactic vaccine in a murine model and has been shown to elicit CTL response and tumor growth suppression of up to 60%[43]. The preference of use of recombinant proteins over peptides in clinical trials, has led to the work described here for pilot scale production of cGMP grade Melan-A for clinical trials.

SURFACE ENHANCED RAMAN SPECTROSCOPY

Background and Mechanisms

Raman spectroscopy is a branch of vibrational spectroscopy in which the transitions between vibrational states are studied when a molecule in-elastically scatters light[44]. The Raman effect occurs from the very small fraction of incident photons (e.g., ~1 in every 10^7 photons) that couple to distinct vibrational modes of the molecule, resulting in in-elastically scattered radiation with a change in frequency. The energy difference between the inelastic scattered radiation and the incident light corresponds to the energy involved in changing the molecule's vibrational state. Plotting the intensity of this energy change verses the related frequency shift produces the Raman spectrum. The Raman effect was first reported by CV Raman in 1928 using pure liquids or gases[45]. The utility of Raman as an analytical technique was limited until the 1970s when it was observed that adsorption of molecules to a roughened metal surface greatly enhanced the Raman signal intensity[46-48]. This set of discoveries and later work by Liao and Howard[49, 50], confirmed that noble metal surfaces with nanoscale features can enhance the Raman scattering

signal of molecules adsorbed on the surfaces. This phenomenon became known as Surface Enhanced Raman Scattering (SERS).

After the initial reports on SERS, a debate as to the mechanism of the enhancement raged for several decades[51, 52]. Currently it is believed that there are two synergistic mechanisms that are contributing to the enhancement factors of 10^6 or greater. One mechanism is electromagnetic which results from the excitation of the localized surface plasmon resonance (LSPR)[53]. LSPR is the flow of free electrons that can occur on noble metal nanoscale features, metal tips, or roughened metal surfaces[54]. The electromagnetic mechanism can be characterized by the examples of a metal nanoparticle in an external electric field. Since the particles diameter is smaller than the wavelength of light, the resulting electric field can be thought of as uniform across the entire particle. The magnitude of the electron cloud around the particle is defined by the equation:

$$\mathrm{E}_{out} = \left(\frac{\varepsilon_{in} - \varepsilon_{out}}{\varepsilon_{in} + 2\varepsilon_{out}}\right)\mathrm{E}_{laser}$$

This equation becomes resonant as the denominator approaches zero ($\varepsilon_{in} = -2\varepsilon_{out}$). The resonance excitation of the surface plasmon is believed to increase the local field experienced by the molecule[51, 52]. The particle can then not only enhance the incident light but also the resulting Raman scattering field[51]. The electromagnetic mechanism is thought to contribute as much as 10^4 to the enhancement factor of SERS although higher enhancement factors of 10^{10} are theoretically possible[52, 55].

The second contribution to SERS enhancement comes from the chemical enhancement where there is excitation of molecule electronic states that are in coordination with the noble metal surface. This mechanism was largely speculative but evidence for chemical enhancement could be seen in the drastically different SERS enhancements of two different molecules under the same conditions. A model proposed by Lombardi *et al*. suggests that the transfer of charge from the highest occupied molecular orbital (HOMO) to the lowest unoccupied molecular orbital (LUMO) of absorbed molecule to the metal or vice versa can occurs at half the energy of the difference in the two energy states[56]. This mechanism is thought to contribute less to the enhancement factor of SERS (10^2-10^3)[52, 57] and is highly dependent on the molecule of interest[57, 58].

To measure the signals of molecules with SERS, the distance of the molecule to the surface of substrate is critical. Generally SERS enhancement decays with respect to distance at a rate of r^{-10} [52]. Therefore SERS effect is limited to a range of molecules that can make close contact with the noble metal surface typically less than a few angstroms[52, 59]. Nevertheless, this "limitation" can often be used to one's advantage in SERS-based analyses by tailoring the nanoparticle surface to have affinity for a given analyte; thus, given the insensitivity of standard Raman, analytes that are localized near the noble metal surface are the only detectable species in a given sample. SERS also has little interference from water which gives it great potential for use in chemical and biological sensing systems[52].

Surface Enhanced Raman Substrates

One of the most widely studied areas in SERS applications is the design and fabrication of reproducible substrates. Most SERS substrates rely on the principle that electromagnetic field "hot spots" can be created between the nanosized gaps of clustered of nanoparticles on surfaces[60] or in solution[61]. Toward this end, metal particle aggregation has been one of the most widely employed substrate fabrication techniues[62, 63] and is considered essential for producing a SERS effect[64, 65]; This technique is simple and cost effective as it usually involves the simple reduction of a solution of gold or silver salts[66, 67]. Particles of various shapes and sizes can be produced in this manner such as tetrahedral silver nanoparticles[68], star shaped gold nanoparticles[69], to flower shaped doped silver nanoparticles[70] with varying degrees of shape anisotropy for SERS effect.

Gold nanorods have been widely used as reliable and tunable SERS substrate. By altering the aspect ratio of rods one can adjust of the longitudinal plasmon over a range of wavelengths to absorb at the excitation of the Raman source. Guo *et al.* showed that overlap of the surface plasmon resonance with the excitation of the laser increases the SERS enhancement effect using cetyltrimethylammonium bromide (CTAB) coated gold nanorods[71]. The plasmon matching to the excitation source wavelength has been shown to result in at least a 10-100 fold increase in enhancement compared to unmatched nanorods[72] Liao *et al.* developed gold nanorod arrays using anodic aluminum oxide (AAO) template assisted nanofabrication which showed that ordered gold nanorod arrays had SERS hot spots localized along the longitudinal end of the rods whereas NaOH etched and aggregated rods localized hot spots at the junctions between the polar ends of the rods[73].

Recent efforts have focused on the production of more ordered SERS substrates for more batch to batch reproducibility. The ideal SERS substrate would have several characteristics including but not limited to homogenous signal across the entire substrate, large enhancement factor, and cost efficient straight forward preparation[74]. In order to obtain large arrays of metallic nanoparticles, different surface functionalization approaches have been taken to either bind metal nanoparticles to a surface using linker molecules or self-assembly. Self-assembled monolayers (SAMs) have been used to great effect to assemble gold and silver nanoparticles for analyte detection on surfaces modified with thiol, amine, or oxide groups[75-77]. Fan *et al.* self-assembled silver nanoparticles onto glass slides functionalized with 3-mercaptopropyltrimethoxysilane (MPTMS) and achieved a substrate with relatively uniform distribution of SERS signal across the entire surface[75]. A novel concept of coating a material to be studied with a shell of gold nanoparticles in a silica shell was introduced by Li *et al.* and named Shell-isolated nanoparticle-enhanced Raman spectroscopy (SHINERS) [78]. Some other template assisted fabrication methodologies include atomic layer deposition[79] and film over nanosphere (FON) substrates created from deposition of thin films of Au or Ag nanoparticles on polystyrene or silica spheres[80, 81]. There are also some novel materials such as quantum dots[82], graphene[83], and TiO_2[84] which are coming into use as SERS substrates. However, these substrates rely primarily on the chemical enhancement mechanism which limits their capabilities when compared to conventional SERS materials[55]. Lithography techniques such and nanoimprint lithography and electron-beam lithography have also become powerful tools for patterning SERS substrates with uniform geometry. However, these techniques are often more expensive than other methods of fabricating SERS substrates.

Applications

Surface Enhanced Raman is a powerful tool for the detection of small molecules and biomolecules. These SERS based sensors either use an intrinsic method where the spectra of the target analyte is sensed directly or an extrinsic method where a commercially available reporter molecule is sensed in the presence of or after interaction with the analyte. Some examples of applications using intrinsic sensing are CTAB coated Au-nanorods functionalized with thiolated beta-cyclodextrin that have been shown to detect the fungicide carbendazim at micromolar concentrations [85] and CTAB-coated nanorods have been developed as system for detection of the pesticide 2,4-dichlorophenoxyacetic acid [86]. SERS has been utilized for clinical applications, as the Van Duyne group has made progress toward an intrinsic *in vivo* glucose sensor that can accurately measure glucose in the presence of other biomolecules[87-90] for real time measurement of blood glucose levels through the skin. Intrinsic SERS has been used to address bio-warfare applications as well[91]. The Van Duyne group has also reported work on a SERS sensor for detection of calcium dipicolinate using silver FON for rapid identification of anthrax spores[92, 93] where silver substrates were coated with a thin layer (< 1 nm) of alumina by ALD for binding of the analyte to the surface[93]. Intrinsic SERS biosensors of DNA and aptamers have also been in development over the last decade. Barhoumi *et al*. reported a method for producing reliable SERS spectra of DNA on Au-coated silica shells bound to glass slides by measuring the adenine vibrational band at 729 cm^{-1} [94]. Neumann *et al.* also showed detection of conformational changes in aptamers when bound to their specific targets[95]. SERS has been investigated in microbiology applications pertaining to identification of bacterial strains[96-98] as well as in the study of cancers[88, 99-102] and other chronic illnesses[103, 104].

MOLECULARLY IMPRINTED POLYMERS

Molecularly Imprinted Polymers (MIPs) are synthetic polymers with specific recognition sites to rebind a target analyte within the material scaffold[105]. These materials are comprised of functional monomers that are polymerized around a template molecule with cross linking molecules which leads to template specific cavities within the polymer matrix. MIPs have been prepared with binding characteristics similar to that of enzymes and immunoglobulins[106-109]. The template, monomers, cross linker, initiator, and method/extent of polymerization are all factors that need to be adjusted to achieve the desired effect of the molecularly imprinted polymer[110]. For example, MIPs prepared for analytical chemistry applications require highly specific binding cavities with low levels of unmediated diffusion out of the polymer matrix. However a drug delivery application might not need as strong of a binding pocket and require faster diffusion out of the polymer matrix[111].

There are three approaches to creating imprinted polymers: covalent, semi-covalent and non-covalent[110]. The covalent approach involves a reversible covalent attachment of the template to the functional monomers where the bonds are cleaved and then reformed once the template interacts with the monomer units inside the specific cavity[112]. Covalent imprinting can only be used for small compounds containing alcohols, carboxylic acids, amines, and ketones[113]. Reaction of boronic acid with 1,2 and 1,3-diol functional groups on the templates has been explored in the imprinting of amino acids[114, 115], sugars[116, 117], carboxylic acids[118-120]. The semi-covalent approach mirrors the covalent method except that rebinding is through non-covalent interactions. The advantages of semi-covalent approach are specific and more uniform distribution of binding sites as well as diffusion limited rebinding kinetics[113].

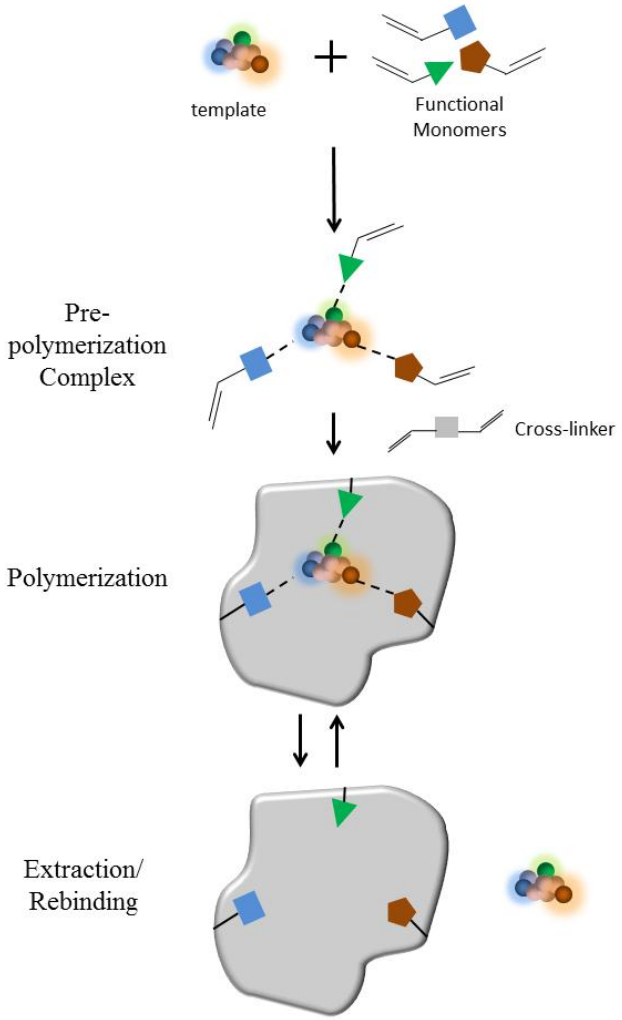

Figure 1.2 Schematic representation of the molecular imprinting process. The imprinting process begins with formation of prepolymerization complex of functional monomers around template molecule. The functional monomers coordinating around template form a specific cavity for the template in the polymer matrix. Polymer synthesis by free radical polymerization proceeds after addition of cross linking monomer and initiator molecule. The template is finally extracted from the matrix and can be specifically reabsorbed.

The non-covalent imprinting method was developed by *Mosbach et al* [121] where the complex between template and monomers during the polymerization steps is based on a combination of hydrogen bonding and hydrophobic interactions[111, 113]. The simplicity of the imprinting protocols

and availability of a variety of monomer substrates have made non-covalent imprinting the preferred imprinting method in the field[113].

Non-covalent interactions usually use an excess of functional monomers to shift the thermodynamics of the system to favor assembly of template/monomer complex[122]. A rule of thumb for template/monomer ratio is begin with a ratio of 1:4, although larger amounts of monomer are also used[123]. The most common functional monomer used for non-covalent imprinting is methacrylic acid and has been adapted for use with a variety of templates[124-126]. Other common monomer units are 4-vinylpyridine, 2-hydroxyethyl methacrylate (HEMA), and acrylamide.

Selection of the cross linker which forms the bulk of the polymer matrix and serves to stabilize the binding site is critically important in MIP preparations. It determines the morphology and mechanical stability of the polymer scaffold[123]. High cross linking ratios (~80%) are preferred because it leads to a material with minimal deformation and ample stability. One of the more common cross linking agents, ethylene glycol dimethacrylate (EGDMA) works well at high cross linked ratios and has been used in a variety of drug delivery applications[127-129]. Previous work has shown MIPs composed of EGDMA form stable macromolecular networks resistant to extreme fluctuations in pH and temperature *in vitro*[130-133]. Several studies have comparing the performance of EGDMA to another common cross linking agent, divinylbenzene (DVB), showed that polymer synthesized with EGDMA had an improved separation factor[134-136]. This feature is thought to arise from the fact that EGDMA is not only short and flexible but also has rigid centers at the methacrylate functional groups[113].

MIP polymer synthesis is usually carried out using free radical polymerization due to simplicity of the reaction and the commercial availability to a broad range of monomer, cross linkers, and initiators[113]. Azo-initiators are the standard inititators used in methacylate based MIPs. Most MIP preparations use the thermal decomposition of azobisisobutyronitrile (AIBN) to initiate free radical polymerization. 2,2'-azo-bis-(2,4-dimethylvaleronitrile) (ABDV) which has a lower decomposition temperature is used for low temperature polymerizations[137]. Other initiators used in preparation of MIPs are known as iniferter molecules (usually dithiocarbamate derivatives) that can act as initiator (*ini*), chain transfer agent (*fer*), and terminator (*ter*)[138]. The advantage of using an initiator with more than one mode of decomposition is that one can change the polymerization conditions if the template is photochemically or thermochemically unstable [123].

The solvent used for polymerization plays an important role in the formation of pores in the macromolecular network. The type of solvent (also called porogen) used will determine the morphology, porosity, swellablity, and rigidity of the final matrix[139]. The solvent also plays an important role in stabilization of the prepolymerization complex between template and monomers for non-covalent MIPs. Water in a mixture with a polar solvent such as methanol has been shown to promote hydrophobic interactions[140] while increasing the organic content of a porogen mixture favors ionic interactions between template and monomers[141, 142].

Taking all of these factors into consideration, it is possible to create a molecularly imprinted polymer with specific recognition to a template for many applications. Molecular imprinted polymers for liquid chromatography[143-146], solid-phase extraction[147-154], sensing[155], and drug-delivery[105, 111] have all been developed using non-covalent imprinting approach.

CONCLUDING THOUGHTS

This dissertation research addresses or examines several needs in the fields of cancer immunotherapy, SERS sensing, and drug delivery. The second chapter of this dissertation examines strain development, process development and implementation of pilot scale cGMP production of the cancer testis antigen, Melan-A, for possible phase I clinical trials. The third chapter deals with development of a novel SERS sensor using DNA aptamers specific for the pesticide malathion, for rapid capture and detection of the contaminant. The fourth chapter focuses on a molecularly imprinted polymer for drug delivery of doxorubicin using a controlled release mechanism. The fifth chapter of this dissertation deals with development of a sensor which combines the specificity of a MIP with the analytical power of SERS to detect the fungicide thiabendazole. In this system the imprinted polymer is grown from the surface a gold coated silica particle modified with the iniferter molecule sodium diethyldithiocarbamate. The sixth chapter details a curriculum plan develop through the NSF GK-12 program designed to teach 8^{th} grade students principles of marine biology, microbiology and nanotechnology. Student were lead through a series of activities focused on mapping of sea turtle locations using GSP data, calculating the distance a sneeze travels, PCR identification of bacteria in samples taken from aquatic animals, and fabrication of Surface Enhanced Raman substrates using gold nanoparticles.

Chapter 2: Process Development and Production of cGMP Grade Melan-A for Cancer Vaccine Clinical Trials

ABSTRACT

Melan-A is a cancer testis antigen commonly found in melanoma, and has been shown to stimulate the body's immune response against cancerous cells. We have developed and executed a process utilizing current good manufacturing practices (cGMP) to produce the 6x-His tagged protein in C41DE3 Escherichia coli for use in Phase I clinical trials. Approximately 11 gm of purified Melan-A were produced from a 20 L fed-batch fermentation. Purification was achieved through a three column process utilizing immobilized metal affinity, anion exchange, and cation exchange chromatography with a buffer system optimized for low-solubility, high LPS binding capacity proteins. The host cell proteins, residual DNA, and endotoxin concentration were well below limits for a prescribed dose with a final purity level of 91%.

INTRODUCTION

Melan-A, also known as MART-1, has been used as a diagnostic marker [156] for melanoma as well as an immunotherapeutic agent [43]. This tumor associated antigen (TAA) contains 118 amino acids, with a 21 amino acids predicted transmembrane domain and a 92 solvent exposed domain[157]. Melan-A was originally cloned by Coulie et al.[158] and was independently cloned by the Kawakami et al. [159] who termed it MART-1 (Melanoma Antigen Recognized by T-cells) [42]. The protein is expressed only in melanocytes, the retina, and most melanoma cancers. While it is expressed in virtually all metastatic melanomas, some primary, cutaneous melanomas have stained Melan-A negative [160].

Melan-A is a member of the MAGE gene family [42], which includes many TAAs that are recognized by cytotoxic T lymphocytes (CTL). Once recognized, CTLs lyse the cancerous cell[161]. NY-ESO-1[162] and SSX-2 [163] are two related TAAs which provoke similar reactions from CTLs and have had some success as cancer vaccines[164, 165]. Interestingly, it has been demonstrated that Human Leukocyte Antigen (HLA) phenotype strongly influences the efficacy of Melan-A vaccination due to the ability of the HLA molecule to present the antigen [166]. Other TAAs appear to be antigenic when displayed by multiple HLA phenotypes [167, 168].

Melan-A peptides have been delivered through viral vectors and directly as peptide solutions for use as cancer vaccine antigens. Virally, Melan-A has been expressed using lentiviral [168], adenoviral [169], and poxviral vector [170, 171] systems. The studies' results strongly supported the use of Melan-A as an immunotherapy. This is especially well supported by the phase I/II clinical trials using inactivated vaccinia virus. Individuals have also been vaccinated with Melan-A

peptides intravenously as part of clinical trials. In order to elicit a stronger CTL response, adjutants [172] and combination therapies have been used. There has been significant evidence that masking the CTLA-4 protein on helper T-cells can significantly increase the immune response to vaccine antigens [173-175]. As with any selective agent, resistance to CTLs has been observed [176] and is further evidence that combination therapies are required for these vaccine treatments.

We have developed a process to produce His-tagged current Good Manufacturing Process (cGMP) grade Melan-A at the pilot-scale for clinical trials. The process utilizes a 20 L fed-batch fermentation and a three column purification scheme to remove contaminating host proteins and endotoxin. Together with the protein's initial success in limited trials [177-180], we have filled the gap between laboratory and industry scale to provide cGMP grade Melan-A for use in vaccine clinical trials.

MATERIALS AND METHODS

Materials

All materials used were obtained at the highest purity level possible. All equipment was cleaned and tested in accordance with cGMP protocols detailed in the harmonized International Conference on Harmonisation (ICH) quality guidelines[181]. Production staff followed strict cGMP training and operating procedures during production of the biopharmaceutical material. Water for injection grade water was used for all solutions (Hyclone Inc. Logan, UT). All column chromatography purification steps were performed using an Akta Purifier FPLC system (GE Healthcare, Piscataway, NJ) equipped with either a BPG 200/500 or 100/500 column (GE Healthcare, Piscataway, NJ) controlled by Unicorn software version 4.12 (GE Healthcare,

Piscataway, NJ). Our production technicians packed all chromatography columns. The columns were then checked for symmetry and plate count as directed by the manufacturer. Protein and endotoxin concentrations were measured using Bradford and Limulus Amebocyte Lysate assays respectively, as previously described [182].

Buffer Composition

Lysis buffer: 50 mM Tris Base, 100 mM NaCl, 1 mM $MgSO_4$, 1 mM β-mercaptoethanol, $2.5x10^{-3}$ % (v/v) "Turbo" DNase (Ambion, Inc., Austin, TX) at pH 8.0. **Solubilization buffer**: 2% m/v deoxycholate (sodium salt), 1% v/v Triton-114, 8M urea, 50 mM phosphate, 200 mM NaCl, 100 mM KCl, 10 mM imidazole, 2.5 mM ß-mercaptoethanol at pH 7.5. **Urea buffer**: 4M urea, 50 mM phosphate, 2.5 mM ß-mercaptoethanol at pH 7.5. **Imidazole buffer**: Formulated as urea buffer with 500 mM imidazole. **Carbonate buffer:** 4M urea, 10 mM Carbonate, 1 mM 2-Mercaptoethanol at pH 10.5 **Carbonate elution buffer:** Formulated as carbonate buffer with 1M sodium chloride at pH 10.5 **Final Bulk Buffer:** 4M urea, 50 mM phosphate, 145 mM NaCl, 50 mM glycine at pH 6.5**.** All buffers cleared endotoxin testing before use.

Description of Facility

The manufacturing facility is approximately 1,100 sq. ft. and consists of five (5) process suites: Bioreactor, Cell Disruption, Downstream Purification, Buffer Prep & Wash, and Storage. In addition there is a common hallway and a gowning room. Interlocking pass-throughs are positioned between the Downstream Purification Room and Cell Disruption as well as between the Downstream Purification Room and Buffer Prep & Wash Room. Adjacent to the

manufacturing suite is the mechanical room housing an oil-free air compressor for process and instrument air, HVAC system with dedicated air conditioners, on-demand dry steam humidifier, dedicated purified water-USP water system and a dedicated recirculating refrigerated chiller. The facility has a dedicated boiler for plant (dirty) steam. The GMP manufacturing facility suites are classified as ISO level 8 with the exception of the downstream purification room which has an ISO classification level 7.

Data analysis

The standard curve, spike recovery, and sample dilutions for all quantitative assays were analyzed for linearity, accuracy, and intra-assay precision. For linearity, the mean corrected value versus expected concentration was plotted and a best fit line using linear regression analysis was generated. For endotoxin assay, $\log_{10}$ of the mean onset time versus the $\log_{10}$ of the expected endotoxin concentration was plotted. The accepted correlation coefficient and the residual sum of squares were ≥ 0.98 and ≥ 0.97 respectively. Accuracy was determined by equation 1. The accepted accuracy of the lowest standard was ±20% of its expected concentration and all other standards had an accepted accuracy of ±10%. The precision was calculated using the coefficient of variation. The accepted CV for the standard was ≤20% for the lowest concentration and ≤10% for all other samples. Spike recovery was calculated by equation 2. The accepted spike recovery was within 70%-130% of the expected value.

1. $accuracy(\%) = \left(\frac{Calculated\ Mean\ Concentration - Expected\ Concentration}{Expected\ Concentration}\right) \times 100$
2. $Spike\ Recovery\ (\%) = \left(\frac{Spiked\ Sample - Sample}{Spike}\right) \times 100$

Assay Validation

Preparation and execution of assay validation was the responsibility of the Facility Manager and assigned personnel. Approval of the qualification protocol and completed qualification report was the responsibility of Quality Assurance. All designated test instruments and standards used in assay validation and in the exercise of the assay were calibrated as NIST traceable where applicable. References used for assay validation include FDA(Food and Drug Administration)-Code of Federal Regulations (21 CFR Part 211): Subpart I-Laboratory Controls, TGA (Therapeutic Goods Administration) –Australian Code of Good Manufacturing Practice for Medicinal Products; Chapter 6 – Quality Control, ICH (International Conference on Harmonization) Q2A – Validation of Analytical Procedures, and ICH (International Conference on Harmonization) Q2A – Validation of Analytical Procedures: Methodology.

Picogreen dsDNA Quantification assay

PicoGreen dsDNA quantitation assay was developed from Molecular Probes PicoGreen® dsDNA Quantitation Kit (Molecular Probes). 8 µg/mL of working solution of dsDNA was diluted in 1X TE working solution (10 mM Tris-HCl, 1 mM EDTA, pH 7.5). Eight dsDNA standards were prepared from 2000 mg/mL- 0 ng/mL. 90 µL of each dsDNA standard and experimental sample was loaded into the corresponding microplate well, in triplicate. Two dilutions of selected experimental samples were spiked with 9 µL of 8000 ng/mL dsDNA standard. 90 µL of 1X PicoGreen® dsDNA quantitation reagent was transfer into each well containing blank, standard, or sample. The fluorescence intensity of the samples at 515 nm (ex.485 nm) was measured on a Tecan Genios Microplate Reader (Tecan, San Jose, CA).

Endotoxin Quantification assay

Endotoxin quantification assay was adapted from Endosafe® Endochrome-K™ reagent protocol. First, Endochrome-K™ was rehydrated in 3.2-3.4 mL of LAL reagent water. Endosafe® Control Standard Endotoxin (CSE) was reconstituted in manufacturer specified volume using LAL reagent water to a final concentration of 50 EU/mL. Standards were prepared in depyrogenated glass test tubes and vortexed for 30 seconds. If necessary, samples were diluted with LAL reagent water until concentrations were within the range of the standard curve. Dilutions were based on the calculated Maximum Valid Dilution (MVD) where *MVD = (Endotoxin Limit x Product Potency)/λ*. 10 µL of 5 EU/mL CSE spike for each selected experimental sample was loaded into the corresponding microplate well, in triplicate, prior to adding the sample. 0.1 mL of endotoxin standard and experimental samples is added to the corresponding wells, in triplicate, as defined by the S.O.P. 100 µL of LAL is added to each well and the absorbance is measured at 405 nm using a Tecan Genios Microplate reader (Tecan; San Jose, CA). Endotoxin limit for the bulk drug substance is calculated as K/M; where K is the maximum human pyrogenic dose of endotoxin per kg of body weight (5 EU/kg) and M is the maximum recommended human dose per kg of body weight per hour. The dosage levels for Melan-A were taken from recommended dosage levels in clinical trials involving Melan-A [179, 180].

NanoLC-MS/MS analysis

Peptide mapping and purity levels were determined by mass spectrometry. All assays and data analysis were completed by the Proteomics and Mass Spectrometry Core Facility at Cornell University. A sample from each final filtered bulk was analyzed by direct in-solution digest with

trypsin and separated by a nano-HPLC interfaced with a LTQ Orbitrap Velos Hybrid FT mass spectrometer (Thermo Scientific). The CID fragmentation method was used for both samples. The raw data files were screened using the Mascot search engine against the NBCI database. Purity levels were estimated by the Exponentially Modified Protein Abundance Index (emPAI) method [183]

Plasmid & Strain Development

The Melan-A gene is 357 base pairs encoding a protein of 118 amino acids with a deduced mass of 13.2 kDa. Sequence coding for a polyhistidine-tag was added to the 3' end of the codon optimized Melan-A gene. The modified Melan-A gene was synthesized by Integrated DNA Technologies (IDT) (Coralville, IA). Its sequence was determined by Sanger (3730XL) DNA sequencing and the resulting 124 amino acid sequence with a deduced mass of 13.9 kDa was deposited in Genbank under accession number NM_005511.1.

The expression construct was obtained by digesting the pET9a24a and IDT Melan-A plasmid with *NdeI* and *NotI*, and isolating the fragments of 4.5 kb and 0.4 kb respectively. The DNA digest was then separated by gel electrophoresis using a low melting point, 1% agarose gel and purified using a Wizard PCR Preps kit (Promega).The two DNA fragments were then ligated together and transformed into TOP10F'cloning strain, (Invitrogen). The transformed cells were plated on LB plates containing 100 mg/L kanamycin. One colony was selected, grown in LB broth with 100 mg/mL kanamycin and the DNA plasmid isolated using a Wizard Plus SV Miniprep kit (Promega). The resultant plasmid is pET9a24a-Syn-Melan-A. Plasmids were then characterized by digestions with *NdeI* and *BamHI* indicating the presence of Melan-A insert, and

by digestion with *ClaI* and *PstI* showing the correct orientation of plasmid. The expected 4.5 kb and 0.4 kb bands for *NdeI/BamHI* digest, and 3.3 kb and 1.5 kb bands for *ClaI/PstI* digest were observed. The Melan-A gene in the expression plasmid was sequenced with four fold redundancy, two forward and two backward sequencing reactions. The amplification primers used were T7-F: 5'-taatacgactcactataggg-3' and T7-R: 5'-caaaaaacccctcaagacccgttta-3. Host strain characterization was carried out following protocols provided by Lucigen (Middleton, WI). C41(DE3) and BL21(DE3) expression strains were transformed with the pAVD10 expression vector and were plated onto APS LB plates containing 100 µg/ml ampicillin with and without 1 mM isopropyl β-D-1-thiogalactopyranoside (IPTG). The plates were then incubated overnight at 37 °C and the resulting colonies observed. No colonies should be observed on plates containing IPTG induced C41 strain.

The transformation was carried out by incubating 50 µl of purchased competent C41(DE3) cells on ice. 100-200 ng of the expression vector, pET9a24a-Syn-Melan-A was added to C41(DE3) competent cells. The cells were put in a 0.1 cm gap cuvette and eletroporated at 25µF, 200 Ohms and 1500 Volts for 3 to 4 msec. Within 10 second after the pulse, 975 µL of SOC media was added to cuvette. The cells were gently mixed and placed in a sterile tube to incubate at 250 rpm/37 °C for an hour. 50µL of the transformed cells were spread on APS-LB Agar containing 100 µg/ml of kanamycin. The plates were then incubated at 37 °C overnight and kanamycin-resistant colonies were selected. Four transformants were selected and placed into 5 mL of the fermenter medium in sterile 50 mL conical bottles. The cells were grown overnight at 25 °C with shaking at 200 rpm. Aliquots of the cultures were transferred aseptically into fresh 5 mL of medium in conical tubes, so that the final OD_{600} was about 0.1-0.2. The cultures were allowed to

grow at 37 °C with shaking at 250 rpm to an OD_{600} of 0.5-1.0. The cultures were then induced with IPTG at a final concentration of 0.4 mM and allowed to grow for 4 more hours. The culture with the highest yield of Melan-A was selected for 250 ml scale expression screening experiments.

For scale up expression screening, an aliquot of an overnight culture was transferred to 50 mL of bioreactor medium in a 250 mL baffled flask (Nalge Nunc), so that the OD_{600} was about 0.1 to 0.2. The culture was allowed to grow at 37 °C with shaking at 250 rpm to an OD_{600} of 0.5-1.0. After removing 15 mL of the culture as the uninduced sample, IPTG was added to the remainder to a final concentration of 0.4 mM and allowed to grow for 4 hours. Equivalent amounts of cell pellet were then aliquotted, lysed and resolved on commassie stained SDS-PAGE and Anti-Melan-A western blot.

The Melan-A expression strain was grown for 16S ribosomal DNA analysis. A single colony was grown overnight at 37 ºC with shaking in 5 mL of APS LB containing 100 µg/ml of kanamycin. Genomic DNA was obtained using a DNeasy Tissue Kit (Qiagen; Valencia, CA). The ~1.5 Kb 16S rRNA gene sequence was amplified using the following forward and reverse primers: 5'-AGA GTT TGA TCC TGG CTC AG-3' and 5'-AAG GAG GTG ATC CAA CCG CA-3', respectively. The PCR protocol began with a 10 minute denaturing step at 94 ºC. A PCR cycle consisting of a 30 second denaturing step at 94 ºC, a 30 second annealing step at 51 ºC, and a 2 minute elongation step at 72 ºC was repeating 29 times. The PCR reaction finished with a final extension step at 72 ºC for 10 minutes and was maintain at 4 ºC until it was removed from thermocycler. The PCR product was cloned using a TOPO® TA cloning® kit (Life Technologies, Cal). Two colonies were picked from each plate and these cultures were grown

overnight at 37 ºC. The plasmid DNA was then purified via minipreps (Promega; Fitchburg WI) and the insert confirmed by digestion with EcoRI. The resulting DNA was then sequenced at both ends using the M13 reverse and T7 high temp primers (M13R:5'-AACAGCTATGACCATG-3', T7H:5'-GTAATACGACTCACTATAGGGC-3'). The sequences were compared to the published BL21 16S rRNA sequence, accession # AJ605115. Although there were several point mutations, no significant deviations from the control sequences were detected.

Single colonies of the expression strain were selected and placed into 5 ml of the bioreactor medium in sterile 50 ml conical tube. The cells were grown overnight at 25 °C with shaking at 250 rpm. Aliquots of the cultures were then taken and transferred aseptically into fresh 5 ml of medium in conical tubes, so that the final OD_{600} was about 0.1. The cultures were allowed to grow at 37 °C with shaking at 250 rpm to an OD_{600} of 1.0-1.5. 1 ml of cell culture was aliquoted into cell bank cryovials and sterile 80% glycerol was added to a final concentration of 10 % (v/v). Cells were then placed into a -80 °C freezer immediately for storage.

A vial containing the transformed C41 strain was obtained from the bioprocess research laboratory and the contents were plated on solid growth medium containing 100 µg/ml kanamycin. Plates were then incubated at 37ºC until the colonies were 1-2 mm in diameter. A single colony from a plate was selected and transferred to a 50 mL conical tube containing 5 mL of liquid growth medium containing 100 µg/ml kanamycin and 34 µg/ml chloramphenicol. The inoculum was incubated with shaking (250 rpm) at 25°C overnight. One mL of the overnight culture was transferred into a 125 mL flask containing 25 mL of the liquid growth medium, 100 µg/mL of kanamycin and 34 µg/mL chloramphenicol. The inoculum was incubated with shaking

at 37ºC for 2-3 hours or until and OD600 of 0.5 to 1.0 was reached. The inoculum was used to prepare the Master Cell Bank (MCB). The inoculum was aseptically mixed with sterile glycerol (9 parts culture: 1 part 80% glycerol) and dispensed as 1 mL aliquots into tubes compatible with storage in an ultra-low freezer. The master cell bank vials were frozen for 48 hours before proceeding with establishment of the working cell bank.

A single vial from the MCB was thawed and the contents used to inoculate a 50 mL conical tube containing 5 mL of liquid growth medium (see table in section 2.4.4.1) containing 100 µg/mL kanamycin. The inoculum was incubated with shaking (250 rpm) at 25°C overnight. The 5 mL overnight culture was added to 50 mL of liquid medium, 100 µg/mL of kanamycin in a 250 mL flask. The inoculum was incubated with shaking at 37ºC for 4-6 hours or until an OD600 of 0.5 to 1.0 was reached. Cells were aseptically mixed with sterile glycerol (9 parts culture to 1 part 80% glycerol) and dispensed as 1 mL aliquots into tubes compatible with storage in an ultra-low freezer. Master and working cell banks were produced from the research cell bank and characterized by Gram Stain Analysis, Microscopic Purity Identification, Plasmid Stability, *Escherichia coli* Identity Test, 16S rDNA Analysis (UV, agarose gel, and sequencing), Plasmid DNA Analysis (UV, agarose gel, and sequencing), Protein Quantitation by Bradford, SDS-PAGE, and Western Blot analysis before cGMP production.

Fermentation

A 1 ml vial from the working cell bank was used to inoculate 50 ml of production culture medium, as described in a previous report [182], in a sterile 250 ml flask. The culture was shaken at 250 rpm overnight at 37˚C. The entire culture volume was then aseptically inoculated into 350

ml of production medium in a sterile 2 L shake flask. Cells were shaken at 37˚C for two hours, after which they were aseptically inoculated into a 25L BioFlo 4500 Bioreactor (New Brunswick Scientific, New Brunswick, NJ) containing 7L of production media. AFS-Biocommand Bioproessing software version 2.6 (New Brunswick Scientific, New Brunswick, NJ) controlled the fermentation and logged all reaction conditions. During fermentation, dissolved oxygen (DO) was maintained at 40% of saturation and was controlled by a DO cascade of agitation (maximum of 1000 rpm) followed by supplementation with pure oxygen as needed. The temperature, pH, and gas flow were set to 37°C, 6.8, and 20 standard liters per minute respectively. A solution of 5M NaOH controlled the reactor pH during the batch phase. Upon exhaustion of the glucose in the batch phase, the base feed was turned off and 12.5 L of glucose feed containing 1M IPTG was initiated, as previously formulated [182]. A pH-stat feedback mechanism regulated the feed rate by feeding in a controlled volume of feed (acid) in response to an increase in pH inside the bioreactor as a result of accumulation of ammonium ions.

Harvest & Lysis

The fermentate was harvested into a sterile 20 L Hyclone® bioprocess bag , and then fed into a Carr Powerfuge Pilot (Pneumatic Scale Corp., Cuyahoga Falls, OH) operating at 14500 rpm, from which the cell pellet was periodically collected, once the powerfuge bowl was full (approx. 1L of solids). The powerfuge was cleaned, reassembled and an additional volume of fermentate was fed into the powerfuge until the bowl was full of solids. This process was repeated until the entire fermentate was processed. The centrate discharge was analyzed during operation to determine when bowl was full by checking for accumulation of solids in the supernatant. Approximately one half of the concentrated biomass was frozen at -20°C to be processed later,

while the second half was resuspended in 15 L of lysis buffer. Portions of the cell suspension were sequentially disrupted in a 4 L Waring laboratory blender and transferred to a clean, sterile bioprocess bag. The disrupted cells were subjected to three passes through a Microfluidics Microfluidizer M100EH (Microfluidics International Corp., Newton, MA) at 23 Kpsi.

Solubilization and Filtration

The lysate was solubilized for 18 hours while mixing in 35 L of solubilization buffer. The solution was then passed through a 10" 1.2 μm low protein binding filter (LPBF) (Millipore Corp., Billerica, MA) and subsequently a 10" 0.5 μm LPBF (Millipore Corp., Billerica, MA).

Immobilized Metal Affinity Chromatography (IMAC) & Buffer Exchange

All chromatography was carried out using an Akta Purifier FPLC (GE Healthcare, Piscataway, NJ) controlled by Unicorn software (GE Healthcare, Piscataway, NJ). The 42L of filtered lysate was loaded at 90,800 cm/hr onto a 5 L column containing nickel-bound Chelating Sepharose Fast Flow resin (GE Healthcare, Piscataway, NJ), previously equilibrated with two column volumes (CV) of solubilization buffer. Each chromatography fraction was collected into sterile bioprocess bags. The purification program used the scheme: 11 CV load, 7 CV solubilization buffer wash, 5 CV urea buffer wash, 5 CV 15% imidazole buffer diluted into urea buffer, and 3 CV elution with 100% imidazole buffer. The elution fraction was concentrated to 1 L using a Millipore ProFlux M12 TFF system with two 4 KDa Centramate cassettes (Pall). The retentate was then exchanged five-fold volumetrically with carbonate buffer and collected into a sterile bioprocess bag. The M12 system was run at 25% pump speed producing an inlet pressure of 30 PSI and outlet pressure of 20 PSI for both the concentration step and diafiltration step.

Anion & Cation Exchange Chromatography (AXC & CXC)

A 1 L column containing Q Sepharose XL resin (GE Healthcare, Piscataway, NJ) was equilibrated for 3 CV at 50 mL/min with carbonate buffer. The retentate was then loaded with carbonate buffer at a 70:30 ratio at 45,400 cm/hr for 3.8 CV. The protein was then washed with 2.5 CV of carbonate buffer and subsequently eluted with 5 CV of carbonate elution buffer. Each fraction was collected in a separate, sterile bioprocess bag. The cation exchange column was conducted as a flow through column using 45,400 cm/hr as a constant flow rate. The column was equilibrated with 2 CV carbonate elution buffer then was loaded with the anion exchange elute for approximately 5 CV. The column was then washed out with 1.5 CV of carbonate elution buffer. The load flow-through and the wash out fractions were collected into a single, sterile bioprocess bag.

Final Buffer Exchange and Terminal filtration

The fraction collected from the cation exchange column was concentrated to 1 L as described above in an M-12 TFF system and then buffer exchanged with 6 L of final bulk buffer. The system was flushed with 500 ml of final bulk buffer to collect any residual protein for a final retentate volume of ~1.5 L. The protein solution was then passed through a sterile 0.22 µm disc filter (Millipore) under sterile conditions into a bioprocess bag for storage.

RESULTS AND DISCUSSION

Plasmid and Cell Bank Construction

A synthetic version of Melan-A was developed to aid in its production in the host system and purification using affinity based column chromatography. The DNA sequence was codon

optimized for *E. coli* to avoid stringent responses from amino acid starvation due to codon bias [184]. The synthetic Melan-A sequence was further modified with a 6x-polyhistidine tag on the C terminus for purification. This version of Melan-A (Syn-Melan-A) has 375 base pairs encoding 124 amino acids with a mass weight of 14.1 kDa. The expression plasmid was constructed from the Syn-Melan-A insert and the pET9a24a plasmid (Figure 2.1A). The C41 strain of *E. coli* derived from BL21 was used as the host expression strain for its ability to produce high levels of membrane-derived recombinant proteins [185]. It has the genotype F- *ompT hsdSB* (rB- mB-) *gal dcm lon* and one uncharacterized mutation which inhibits cell death resulting from expression of toxic recombinant proteins. To characterize the host expression strain, an expression based selection system using a plasmid verification vector was used to select for C41(DE3). The pAVD10 vector contains *uncF* gene which encodes for the beta-subunit of *E. coli* ATPase under control of the T7 promoter. This vector is lethal to BL21 and induced C41(DE3). No C41(DE3) colonies were obtained in the presence of 1 mM IPTG. The BL21(DE3) strain did not grow under either condition. The host strain was then transformed and selected for kanamycin resistance.

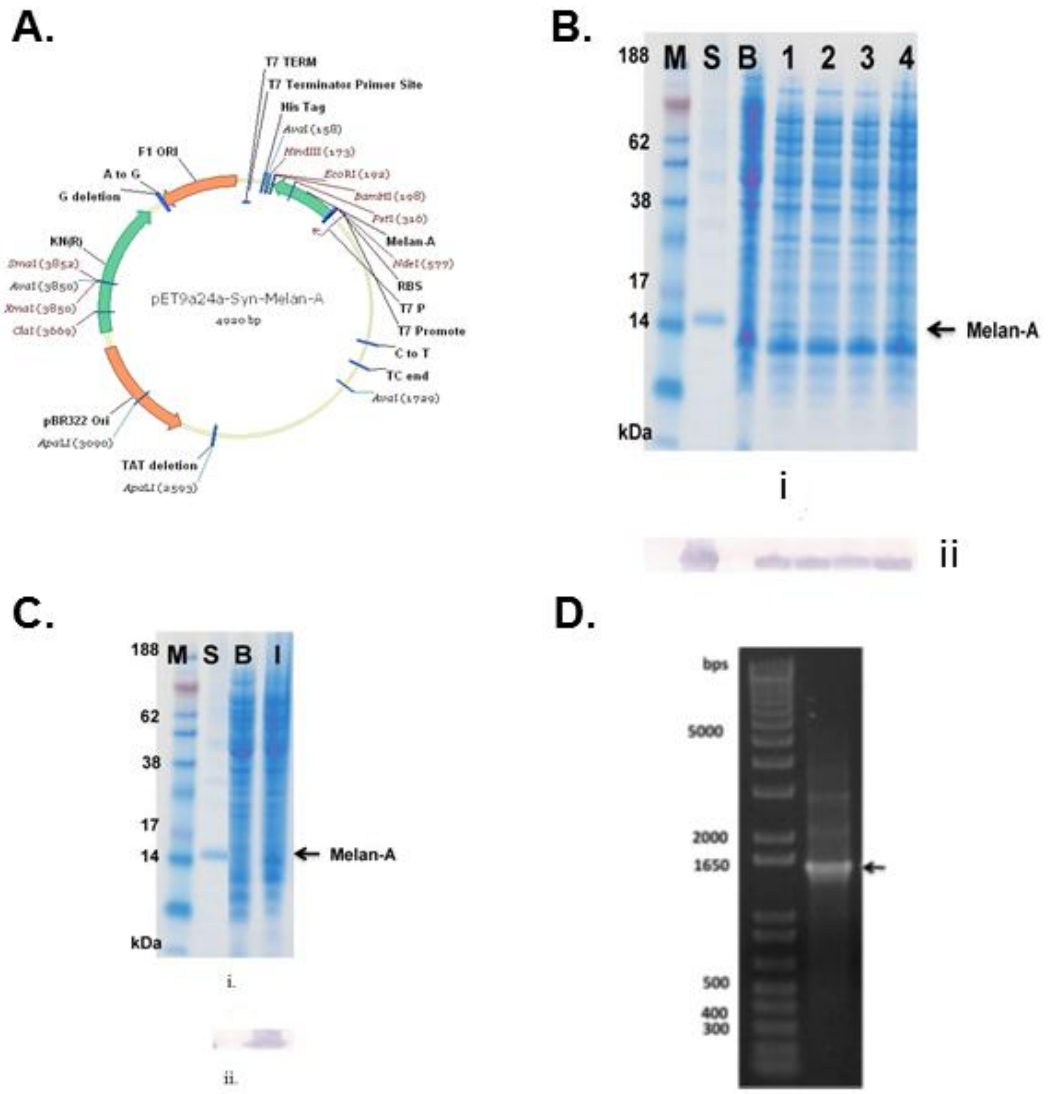

Figure 2.1 a) pET9a24a plasmid map containing Syn-Melan-A. b) (i) Commassie stained SDS-PAGE and (ii) Anti-Melan-A western blots of four tested Melan-A expression strains. M, molecular weight marker; S, Melan-A standard; B, before Melan-A induction cell lysate; 1 to 4 indicate the after induction cell lysate of four different transformants. c) (i) Coommasie stained SDS-PAGE and (ii) Anti-Melan-A western blots of strain numbered 4 expression Melan-A. M, molecular weight marker; S, Melan-A standard; B, before Melan-A induction cell lysate; I, after induction cell lysate. d) PCR amplification of 16S DNA of Melan-A expression strain number 4.

Expression screening was carried out by selecting four kanamycin resistant colonies and growing the colonies in 5 ml of bioreactor media at 37 ºC. Melan-A expression was induced with the addition of IPTG for four hours after which the cell pellet was lysed and equivalent amounts of lysate from each colony were analyzed by commassie stained SDS-PAGE (Figure 2.1Bi) and Anti-Melan-A western blot (Figure 2.1Bii). Colony number four (N4) showed the highest level of expression and was selected for 50 ml level expression screening.

Larger scale expression screening was carried at the 50 ml scale. The culture was grown at 37 ºC/250 rpm until an O.D. of 0.5-1.0. 15 ml of the culture were removed as the T0 sample and 1 M IPTG was added to the remaining media to final concentration of 4 mM. The culture was induced for four hours and the cell pellet harvested. Figure 2.1Ci & ii shows a commassie stained SDS-PAGE and anti-Melan-A western blot for the 50 ml expression screen with the Melan-A monomer band at 14 kDa appearing in the induced sample. Next, transformant N4 was grown for 16S rDNA sequencing for species identification. The gene for 16S rRNA was amplified by PCR using methods adapted from Martinez-Murcia et al [186]. The ~ 1.5 Kb PCR product was analyzed by gel electrophoresis (Figure 2.1D) and subsequently subcloned into a Topo TA vector. Two transformed colonies were isolated from each plate and the plasmid DNA was used in an analytical digestion with EcoRI to confirm correct insertion of the insert. The plasmid was then sequenced using the M13 reverse and T7 high temperature primers. The entire 16s region was sequenced twice in the forward and reverse directions for a total of 4 fold coverage. The sequences were then compared to a published BL21 16 sequence (accession # AJ605115). Although there were several point mutations, no significant deviations from the control sequences were detected. Isolated colonies from this strain were grown designated as the

research cell bank. Master and working cell banks were established from the research cell bank. After the master and working cell banks were established, vials were tested according to validated SOPs. Two random vials were selected from each bank for characterization testing. In addition, one research vial was selected from the bioprocess research laboratory as a control, labeled Melan-A in pET9a24a in C41 (DE3). The vials were cultured and examined microscopically to verify that the cells were rod shaped with no apparent contamination. The Melan-A cell banks as well as the research vial met all acceptance criteria.

Fermentation

The fed-batch fermentation was conducted under pH control using a feedback control loop. The DO, pH, glucose feed volume, base feed volume, and oxygen flow rate were all recorded during vessel preparation and post-inoculation. The vessel was inoculated at hour 21 of the fermentation. The batch phase is marked by acidification of the medium by the cells triggering addition of a P.I.D. controlled volume of sodium hydroxide into the vessel to maintain pH at 6.8. After approximately 30 ml of base was added to the vessel, the glucose feed loop was initiated and base was not added until the pH of the media rose above the set point. As shown in Figure 2.2, the dissolved oxygen concentration (DO) begins to plummet at hour one into the fermentation indicating initiation of glucose consumption by the cells. The DO concentration then spiked 4 hours after induction indicating an exhaustion of the initial carbon source in the bioreactor medium. As the bioreactor medium pH increases due to an accumulation of ammonium ions after the depletion of the primary carbon source [187, 188], we used this process variable to control the glucose feed rate into the vessel. The glucose feed, containing IPTG, was

introduced into the vessel using empirically determined proportional control algorithm that resulted in a constant growth rate during the induction process. Oxygen was supplemented to maintain the dissolved oxygen level at 40% during the feed stage. The cells were deemed ready to harvest when the DO levels continued to rise above the set point despite additional feed. The fermentation completed reproducibly after 23 hours with the consumption of 12 L of glucose feed. The final wet cell weight prior to lysis was 245.81 g/L. Table 2.1 details the optical densities and wet cell weights for each of the steps in the fermentation process. A single fermentation produced enough biomass for two pilot scale GMP production batches.

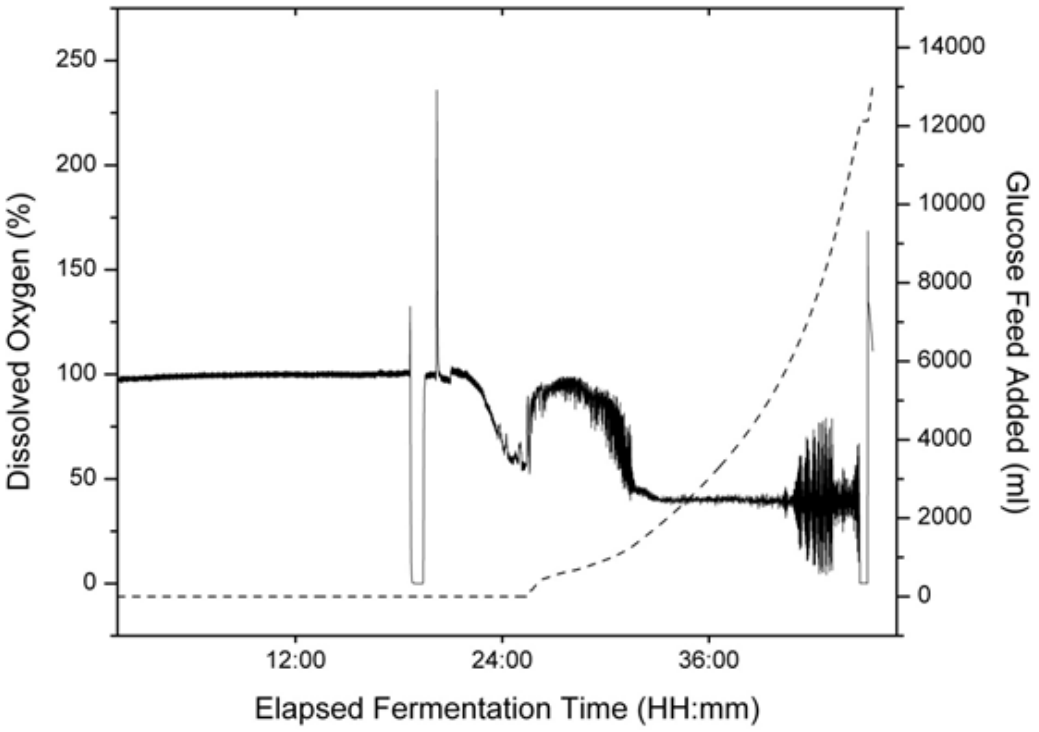

Figure 2.2 Fermentation profile for Melan-A. Dissolved oxygen concentration (solid line) follows the profile seen for pH stat control. Glucose feed (dash line) increases exponentially at the conclusion of the batch phase of the fermentation.

Table 2.1 **Profile of fermentation process including optical density and wet cell weight.**

Sample Description	OD_{600} Reading	OD_{600} Neat Sample	Wet Cell Weight (g/L)
Pre-Inoculum	0.962	9.62	NA
Inoculum	0.328	3.28	NA
Before Feed	0.335	3.35	21.426
Before Harvest	0.839	167.8	237.47
Harvest	0.845	169.0	245.81

Purification

Half of the cell pellet from the harvest was lysed in a microfluidizer to release inclusion bodies containing Melan-A. The cell lysate was mixed with lysis buffer to a final ratio of 4.0 kg buffer/kg solids. The lysate was solubilized in phosphate buffer containing 8M urea, 1% Triton-114 and 2% w/v deoxycholate for 16 hours. The solution was then filtered through a 1.2 µm and 0.5 µm low-protein binding capsule filter and 42 L loaded onto a 5L nickel column. Immobilized metal affinity chromatography (IMAC) was used as the initial purification column for Melan-A. The chromatogram in Figure 2.3A shows the results for the IMAC purification. Following a protocol developed previously by our group [162], the solubilized lysate was loaded onto the column (Figure 2.3AI) and subsequently washed with a solution of 8M urea, 2% w/v deoxycholate, and 1.0% v/v Triton X-114 (figure 2.3AII) which lowered endotoxin concentration from 197 EU/µg in the IMAC load to 0.4 EU/µg in the subsequent urea wash (Table 2.2). As described in our previous reports, we determined that the therapeutic antigens SSX-2, Melan-A,

and NY-ESO-1 bind the lipopolysacchrides produced by *E. coli* to high concentrations [162, 189]. For example, the CT-antigen NY-ESO-1 had endotoxin levels at 1,362.95 EU/µg prior to loading onto the IMAC column. Additionally NY-ESO-1 had latent endotoxin which gradually diffused out during storage if a deoxycholate wash step was not included in the IMAC purification [162]. Despite Melan-A solubilized inclusion bodies having a 10,000 fold lower endotoxin concentration as compared to NY-ESO-1 (197.0 EU/µg in IMAC load); even at these concentrations, the detergent wash step on the IMAC is essential to reduce endotoxin before the downstream columns as the regulatory limit for endotoxin is 1.7 EU/µg for 115 µg dose of drug substance. Table 2.2 details the endotoxin levels measured at several points in the purification process. For the two GMP batches, the majority of the endotoxin eluted either with the host proteins in the load flow through or in the deoxycholate wash step. The excess detergent on the column was washed away with an 8M urea buffer. It is important to remove as much of the residual detergents as possible before downstream processing as these contaminants are difficult to separate from the bulk material even by rigorous buffer exchange. The detergents used in our process contribute to an elevated 280 nm absorbance (Figure 2.3AII) that plummeted after 1.5 column volumes of urea wash. A small amount of endotoxin is removed in this step as well (Table 2.2). Using our purification scheme, the endotoxin levels were reduced to $6.7*10^{-4}$ EU/µg in the IMAC High Imidazole elution. The quality of the IMAC purification was analyzed by Coomassie gel and Anti-Histidine western blot. As shown in figure 2.3B, a large portion of the host proteins elute in the load flow through (lane 4) but no his-tagged product was lost in the flow through as shown in figure 2.3C (lane 4). The deoxycholate wash removes a small fraction of target protein (not shown) and an undetectable level of protein exits in the urea wash step

(figure 2.3B, lane 6). Approximately, 13 grams of total protein were collected in the high imidazole elution with very low levels of endotoxin which is an improvement in both yield and endotoxin purity when compared to our previously reported IMAC purification of NY-ESO-1. The eluted product was concentrated to 1 L and buffer exchanged using tangential flow filtration (TFF) into 10 mM carbonate buffer for anion exchange chromatography.

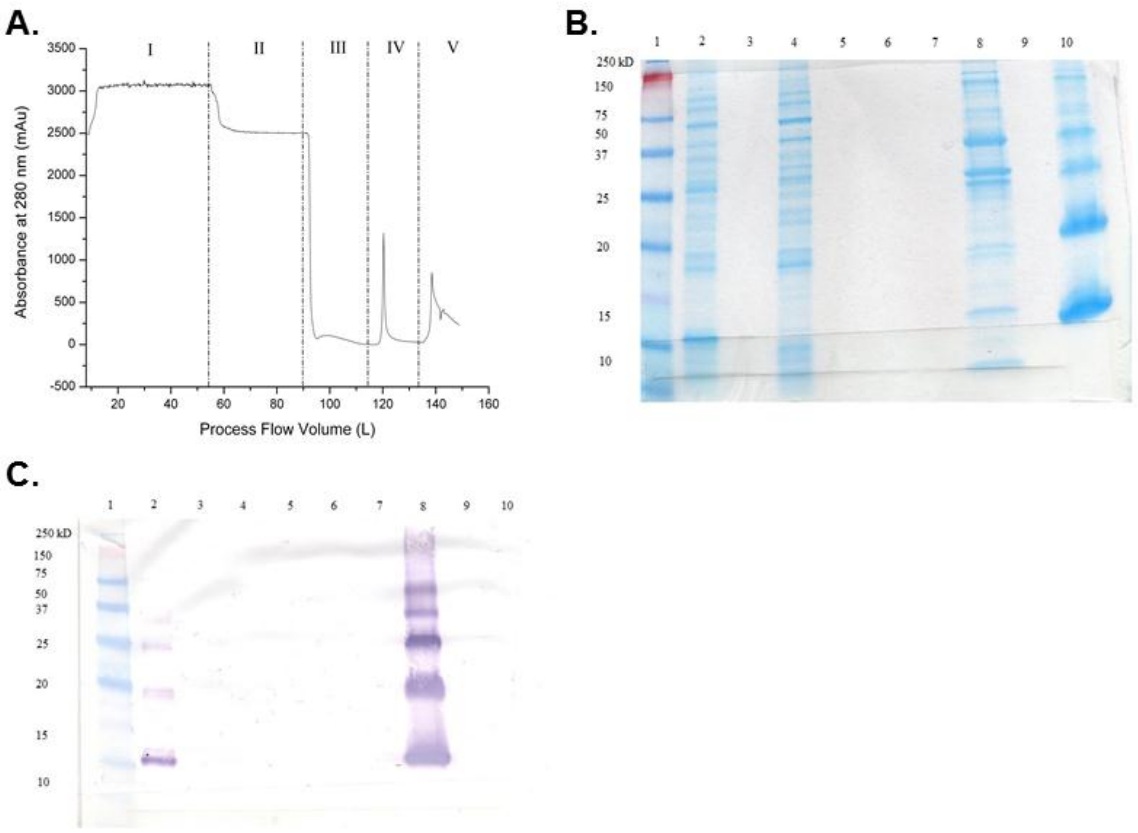

Figure 2.3 a) Immobilized metal affinity chromatography (IMAC) column chromatogram for Melan-A. Sections I-V correspond to load, deoxycholate wash, urea wash, low imidazole, and high imidazole respectively. b) Coomassie stained SDS-PAGE gel for IMAC column purification steps. Lanes 1-10 correspond to protein ladder (1), Load (2), blank (3), Load flow-through (LFT) (4), blank (5), Urea flowthrough (UFT) (6), blank (7), IMAC low imidazole (8), blank (9), and IMAC high imidazole (10). c) Anti-Histidine Western Blot for IMAC column purification. Lane 1-10 correspond to protein ladder (1), Load (2), blank (3), LFT (4), blank (5), UFT (6), blank (7), IMAC high imidazole (8), blank (9), IMAC low imidazole (10). Samples were analyzed under reducing conditions. Primary antibody was diluted 1/20,000. The Melan-A monomer band appears at 14 kDa.

In our previous report on the production of NY-ESO-1, an anion exchange column was used as a flow though column followed by final polishing with a hydrophobic interaction column (HIC). During process development for Melan-A, we found the HIC column to be impractical for purification of Melan-A due to inefficient elution off of the column even with the addition of non-polar excipients. Additionally, detergent or alcohol removal after the HIC column is extremely difficult and results in a significant loss of product. Therefore, the downstream polishing column process was improved by converting the AXC into an elution column and replacing the HIC with a flow through cation exchange column. Figure 4A shows the chromatogram of the AXC purification. The retentate from the post-IMAC buffer exchange was loaded onto the column in a 70:30 dilution ratio (V/V) with carbonate buffer. This dilution step allowed for increased loading capacity of the column compared to undiluted load by preventing resin fouling at the top of the column. The product is eluted over six column volumes with carbonate buffer containing 1M NaCl (Figure 2.4A-IV). Figure 4C shows a Coomassie stained SDS-PAGE gel of samples from the AXC polishing step. There was a slight loss of protein in the load flow through (Table 2.2) and no detectable loss of total protein in the wash step (figure 2.4C). Most of the Melan-A monomer is collected in the AXC elution.

For cation exchange, the column was equilibrated with two column volumes of the AXC elution buffer to ensure no binding to the column by the product. In this instance, the net negative charge of the protein and competition from other charged species would cause the product to flow through the cation resin. The product flow through was collected over 6.0 column volumes, which includes 1.0 column volumes of washout with AXC elution buffer (Figure 2.4B). The

CXC flow through was concentrated and buffer exchanged into the final formulation bulk buffer. Figure 2.4D shows the Coomassie gel of samples from CXC column flow through and final bulk retentate. The permeate fraction had no detectable levels of protein by SDS-PAGE and only a negligible amount of protein (0.03 mg/ml) was detected by Bradford. The product was subjected to dead-end sterile filtration through a 0.22 µm disk filter for final storage. Dead-end filtration resulted in a 15% loss in protein concentration (Table 2.2). Other types of filters were explored during process development, in particular low protein binding capsule filters that would reduce the percent loss of product in the final filtration. However, the filter used for final filtration was the only filter that could pass our validated bubble point test protocol needed for regulatory compliance.

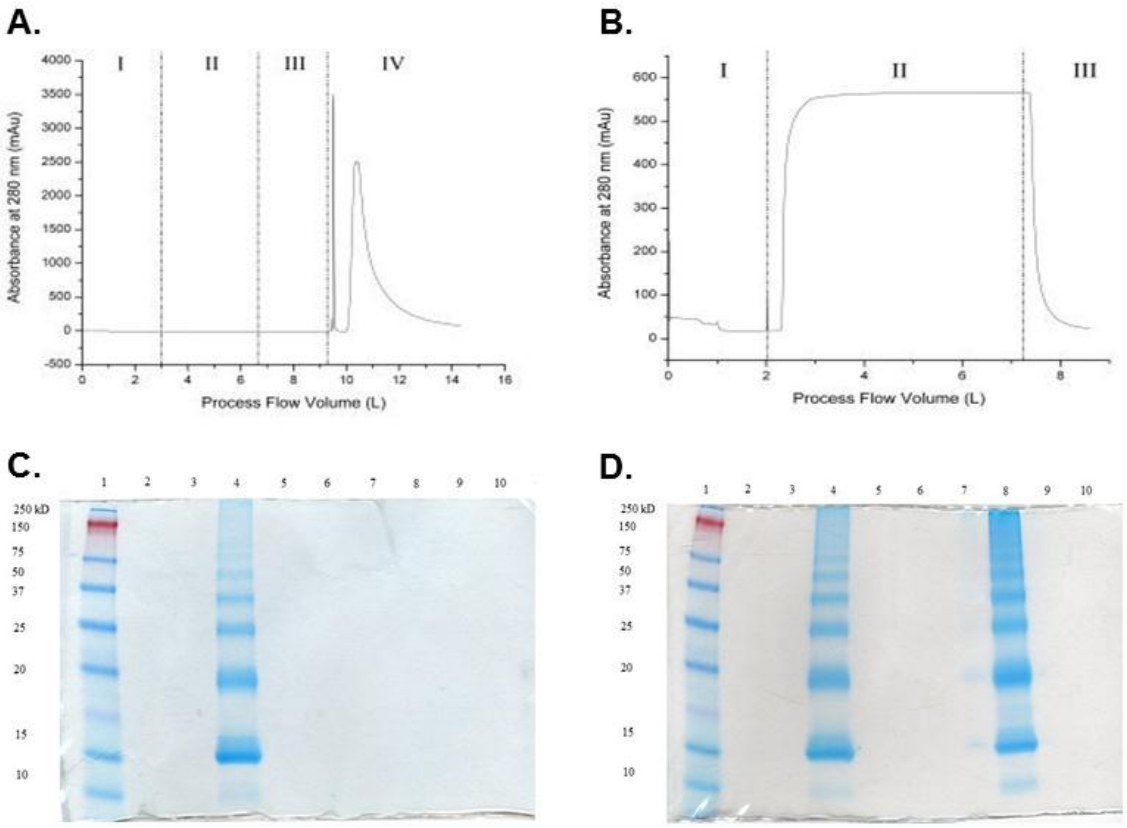

Figure 2.4 a) Chromatogram for anion exchange chromatography. Section I-III are column equilibration, load flow through and wash respectively. Section IV shows the elution peaks for Melan-A with 1M NaCl. b) Chromatogram for cation exchange chromatography. The antigen flows through the column in section II and the wash is completed in section III c) Coomassie stained SDS-PAGE gel for anion exchange column. Lanes 1-8 are as follows: protein ladder (1), blank (2), blank (3), AXC elute (4), blank (5), AXC load flow through (6), blank (7), AXC wash (8). d) Coomassie stained SDS-PAGE gel for cation exchange chromatography and final buffer exchange. Lane assignments (1-8) are as follows: protein ladder (1), blank (2), blank (3), CXC flow through (4), blank (5), final concentration permeate (6), blank (7), final bulk retentate (8). Samples were analyzed under reducing conditions. The Melan-A monomer appears at 14 kDa.

Table 2.2 Endotoxin, protein concentration, and % monomer measured during several points in the production process. Endotoxin limit is 1.7 EU/µg for a dose of 115 µg.

Sample Description	Average Protein Concentration (mg/ml)	Average Endotoxin Concentration (EU/µg Melan-A)	% 14 kDa band
IMAC Load	9.2	197	32%
IMAC Load Flow Through	4.9	405	13%
Deoxycholate Wash	1.9	7.89	--
Urea Wash	$2.5*10^{-2}$	$4.0*10^{-1}$	--
IMAC High	0.9	$6.7*10^{-4}$	63%
AXC Load Flow Through	0.1	$1.4*10^{-2}$	--
AXC Elute	1.7	$9.0*10^{-3}$	53%
CXC Flow Through	0.98	$1.3*10^{-2}$	44%
Final Bulk Buffer Retentate	4.6	$1.1*10^{-2}$	41%
Filtered Final Bulk Melan-A	3.9	$6.4*10^{-3}$	38%

Product Quality Testing

In accordance with ICH guideline Q6B [190] for process related impurities derived from cell substrates in biotechnological products, we tested the final product for host cell proteins and residual DNA. Various processing points in the two GMP batches were analyzed by anti-*E. coli* western blot for the presence of *E. coli* surface antigens. As shown in figure 2.5A & B the only samples that contain *E. coli* antigens are the crude lysate and crude filtrate (IMAC load). The levels of host proteins were below the detectable limit of the assay in all of the samples after the IMAC load, including in the final product, confirming loss of host proteins in the IMAC deoxycholate and urea wash steps (Table 3). Residual DNA was analyzed in several process samples using Pico Green dsDNA reagent. The specification limit for residual DNA in the bulk API is < 1ng/dose and for both GMP batches the final filtered Melan-A product contained < 0.002 ng/dose (330 µg) of dsDNA (Table 3).

A final summary Coomassie gel and Western blot for both GMP batches are shown in figure 2.6. The bands were quantified by SDS-PAGE image densitometry using ImageJ software. The intensity of the 14 kDa monomer band peaks in the IMAC high (Table 2); suggesting that this step provides a majority of the purification of the monomer. The downstream purification steps show retention of monomer and higher molecular weight oligomers. The Melan-A monomer is 38.0 % of the total protein in the final the final filtered bulk API as estimated by gel densitometry. To further characterize the final product, a sample of final filtered bulk product from each GMP batch was analyzed by mass spectrometry for peptide mapping and purity. The N-terminal peptide MPREDAHFIYGYPK and C-terminal peptide LSAEQSPPPYSPHHHHHH of Melan-A were manually identified and verified in both batches (Table 3). An average purity

level of 91% was calculated for Melan-A with the remaining percentage of protein divided amongst trace level of *E. coli* proteins (Table 3). Among the host strain contaminants are protein chain elongation factor -Tu, glutamine synthetase, and chaperone Hsp70. Chaperone Hsp70 (DnaK) has been shown to be strongly associated with bacterial inclusion bodies (IB) and EF-Tu is commonly associated with DnaK in inclusion bodies [191-193]. A total yield of 11.1 g of product was produced from the campaign. Endotoxin levels in the final filtered product were less than 0.01 EU/µg which was two orders of magnitude below the 1.7 EU/µg for a 115 µg dose (Table 3).

Table 3 Analysis of GMP batches of Melan-A Protein Drug Substance

Assay	Specification/Limit	CULICR11302010-Melan-A	CULICR11302010-2-Melan-A
Total Yield	Report	6.3 g	4.8 g
SDS-PAGE	Percent ~14 kDa monomer	36.38%	40.49%
Western Blot	Major band at ~14 kDa	14 kDa	14 kDa
Anti-*E. coli* Western Blot	Report	None Detected	None Detected
Purity by MS	Report	92.27% total Melan-A	90.48% total Melan-A
N-Terminal Sequencing	Consistent with theoretical sequence	Complies	Complies
C-Terminal Sequencing	Consistent with theoretical sequence	Complies	Complies
MW by Mass Spec.	13.980 kDa	13.434 kDa	13.434 kDa
Residual DNA	< 1 ng/dose	< 0.002 ng/dose	< 0.002 ng/dose
Endotoxin	≤ 1.7 EU/µg	< 0.01 EU/ µg	< 0.01 EU/ µg
Appearance	Report	Clear, colorless, free of visible particulates	Clear, colorless, free of visible particulates

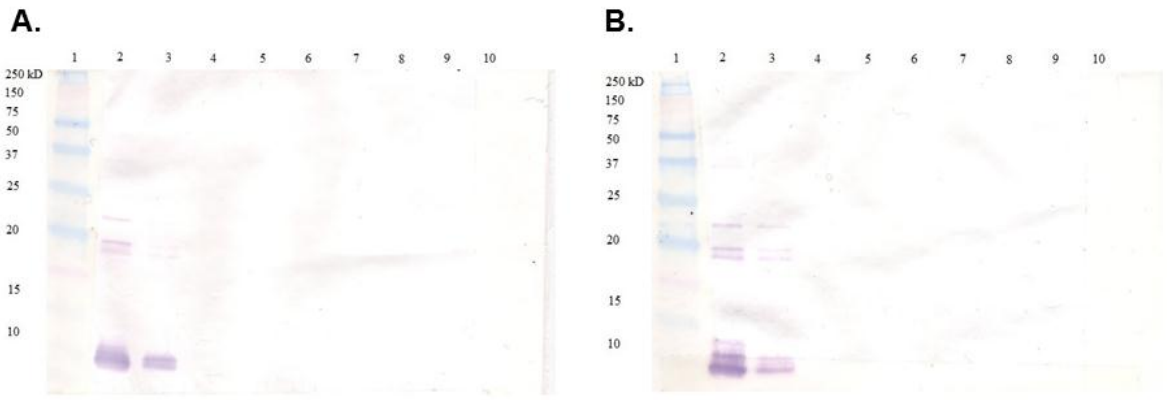

Figure 2.5 a) Anti-*E.coli* Western Blot of several process samples from first GMP run. Lane assignments (1-10) are as follows: protein ladder (1), crude lysate (2), Filtrate (3), IMAC low imidazole (4), IMAC high imidazole (5), Post IMAC TFF retentate (6), AXC elute (7), CXC flow through (8), CXC bulk purified Melan-A (9), Final Filtered Melan-A (10). b) Anti-*E.coli* Western Blot of several process samples from second GMP run. Lane assignments (1-10) are as follows: protein ladder (1), crude lysate (2), Filtrate (3), IMAC low imidazole (4), IMAC high imidazole (5), Post IMAC TFF retentate (6), AXC elute (7), CXC flow through (8), CXC bulk purified Melan-A (9), Final Filtered Melan-A (10). Samples were analyzed under reducing conditions and primary antibody was prepared at a 1/5000 dilution.

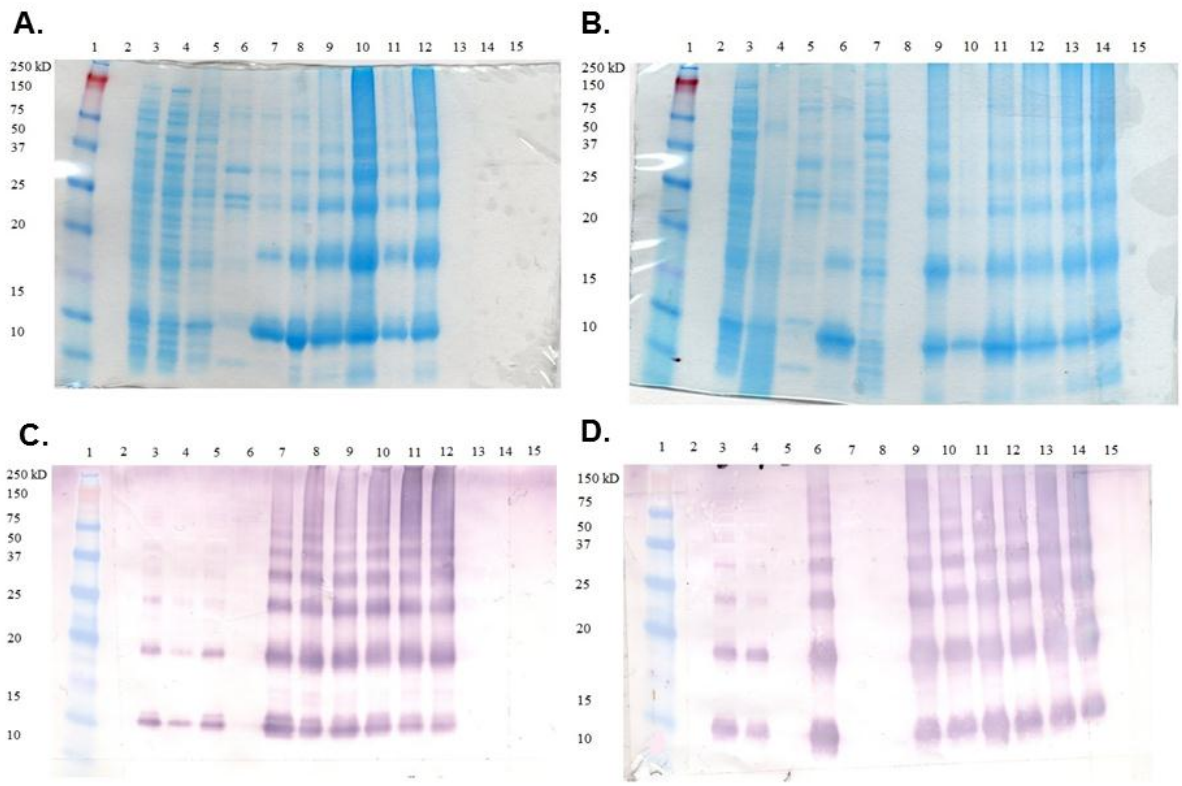

Figure **2.6** a) Coomassie stained SDS-PAGE gel summarizing the first GMP production run of Melan-A. Lane assignments (1-12) are as follows: protein ladder (1), blank (2) crude lysate (3), Tris Permeate (4), IMAC Load (5) IMAC low imidazole (6), IMAC high imidazole (7), post IMAC TFF retentate (8), AXC elute (9), CXC flow through (10), final bulk retentate (11), final filtered Melan-A (12). b) Anti-Histidine western blot of Melan-A summary gel for first GMP run. Lane assignments (1-12) are as follows: protein ladder (1), blank (2) crude lysate (3), Tris Permeate (4), IMAC Load (5) IMAC low imidazole (6), IMAC high imidazole (7), post IMAC TFF retentate (8), AXC elute (9), CXC flow through (10), final bulk retentate (11), final filtered Melan-A (12). c&d) Coomassie stained SDS-PAGE summary gel and Anti-Histidine western blot of second GMP production run. Lane assigments are protein ladder (1), blank (2), crude lysate (3), IMAC load (4), IMAC low (5), IMAC high (6), IMAC LFT (7), blank (8), post IMAC TFF retentate (9), AXC load FT (10), AXC elute (11), CXC flow through (12), final bulk retentate (13), final filtered Melan-A (14). Samples were analyzed under reducing conditions. Primary antibody was used at a 1/20,000 dilution. Melan-A monomer appears at 14 kDa.

ICH quality guidelines on the production of biotechnological products calls for testing to ensure stability of the active components in the final container [184]. The product can be sensitive to a variety of environmental conditions including but not limited to temperature, shear, and light. Therefore, a 500 µl aliquot of final filtered Melan-A was aliquoted into a glass vial or plastic cryovial for primary and secondary stability testing. Primary stability testing calls for samples to be analyzed 1 day, 1 week, 1 month, 2 months, and 3 months at 4 ºC, -20 ºC, and -80 ºC. Secondary testing required samples be analyzed 1 day, 1 week, and 1 month into storage at the following conditions: 4 ºC inverted/right side up, Room temperature inverted/ right side up, 37 ºC right side up, UV exposed for -80 ºC/4 ºC, Extended vortexing (20 min) for -80 ºC/4 ºC, and freeze-thaw at -80ºC to RT. After one day no discernible effects of temperature were recorded. At one week in storage, primary stability showed normal consistency while secondary stability showed some discoloration in the samples stored at 37 ºC. The vortexed samples showed some protein precipitation but no degradation. Figure 2.7a&b shows a coomassie stained SDS-PAGE and Anti-His western blot of the secondary stability test samples after 1 month. The samples exhibited fair stability after one month with the exception of the samples stored at 37 ºC which was expected under the accelerated degradation condition. A fair amount of degradation can be seen in the SDS-PAGE gel correlating to a reduce intensity of the Melan-A monomer band in the western blot of the 37 ºC sample. Under refrigerated and frozen storage our product is clear, colorless, and absent of visible particulate and can be reliably stored in glass or plastic vials.

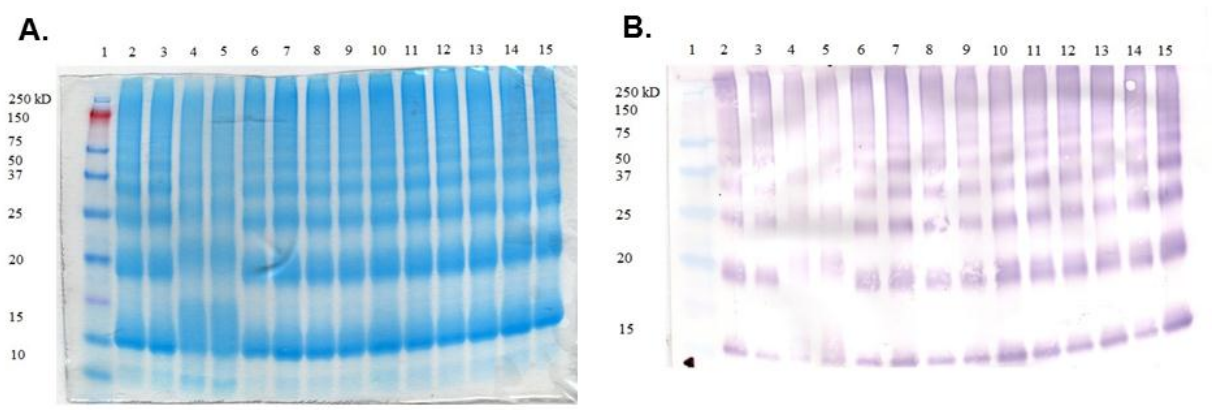

Figure 2.7 a) Coomassie stained SDS-PAGE gel of secondary stability test samples. Lane assignments are protein ladder (1), RT-glass (2), RT-cryovial (3), 37 ºC-glass (4) 37 ºC cryovial, (5), 4 ºC-glass-UV (6), 4 ºC-cryovial-UV (7), -80 ºC-glass-UV (8), -80 ºC-cryovial-UV (9), 4 ºC-glass-vortex (10), 4 ºC-cryovial-vortex (11), -80 ºC-glass-vortex (12), -80 ºC-cryovial-vortex (13), -80 ºC-glass-freeze/thaw (14), -80 ºC-cryovial-freeze/thaw (15). b) Anti-Histidine western blot of secondary stability test samples. Lane assignments are as follows: protein ladder (1), RT-glass (2), RT-cryovial (3), 37 ºC-glass (4) 37 ºC cryovial, (5), 4 ºC-glass-UV (6), 4 ºC-cryovial-UV (7), -80 ºC-glass-UV (8), -80 ºC-cryovial-UV (9), 4 ºC-glass-vortex (10), 4 ºC-cryovial-vortex (11), -80 ºC-glass-vortex (12), -80 ºC-cryovial-vortex (13), -80 ºC-glass-freeze/thaw (14), -80 ºC-cryovial-freeze/thaw (15). Samples were analyzed under reducing conditions. Primary antibody was used at a 1/20,000 dilution.

CONCLUSION

GMP pilot scale production of Melan-A showed similar challenges to those seen in our previous report on NY-ESO-1 [162]. Melan-A is highly insoluble in aqueous solution and requires the presence of high concentrations of urea to stay in solution. Melan-A also has a strong affinity for endotoxin and like NY-ESO-1 requires a detergent wash step during IMAC purification to significantly reduce endotoxin levels before downstream purification [189]. The modifications to purification process from our previous report on NY-ESO-1, specifically a chromatographic anion exchange step and flow through cation column, resulted in higher yields per fermentation for Melan-A. Yields can be further improved with careful section of filtering units in

downstream processing. Endotoxin and Residual DNA levels in the final bulk product were well below the specified limit for a recommended 330 µg dose. Our final yield was 11.1 grams of protein from one twenty liter fermentation with a purity level of 91% as determined by mass spectrometry. This material meets the standards for use in phase 1 clinical trials.

ACKNOWLEDGEMENTS

The authors would like to acknowledge the financial and logistical support by the Ludwig Institute for Cancer Research.

Chapter 3: Aptasensor Based on Polymer-Gold Nanoparticles Composite Microspheres for the Detection of Malathion Using Surface-Enhanced Raman Spectroscopy

Adapted with permission from "Aptasensor Based on Polymer-Gold Nanoparticles Composite Microspheres for the Detection of Malathion Using Surface-Enhanced Raman Spectroscopy" Industrial Biotechnology (2013)

ABSTRACT

In this paper, we present a new format of apta-sensing composite particles for Surface-Enhanced Raman Spectroscopy (SERS) detection of malathion. The developed apta-sensing microspheres comprise extraction capability by aptamer-target analyte interaction and Raman signal enhancer for SERS detection of the pesticide.

Micron-sized polymer particles were synthesized by polymerization by precipitation using methacrylic acid (MAA) and ethylene glycol dimethacrylate (EGDMA) as co-monomers in acetonitrile. Conjugation with colloidal gold nanoparticles (AuNPs) via modification with 2-aminoethanethiol led to polymer-AuNP composites with controlled aggregation of AuNPs onto the polymer surface. The thiolated aptamer targeting malathion was attached to the metal surface by thiol-gold interaction, resulting in polymer-AuNP-aptamer composite microspheres. The new material was characterized by imaging using Scanning Electron Microscopy (SEM) and Dynamic Light Scattering (DLS) measurements. The polymer-AuNP-aptamer particles were incubated with a phosphate buffer solution containing malathion at a suitable concentration level for 30 min, washed with water and then dried on a microscope glass slide, prior to spectra acquisition. The proposed apta-sensing SERS substrate successfully allows the direct detection of the target molecule at 3.3 μg mL-1. Because of only basic equipment is required for analyte separation, the apta-sensing microspheres are well suited for potential industrial applications that require on-site analyte detection.

INTRODUCTION

In the 1970s it was first reported that the Raman signal intensity of molecules could be dramatically increased by chemi-adsorption onto a roughened noble metal surface. [46, 48] Since then, interest of researchers has grown in Surface-Enhanced Raman Spectroscopy (SERS) and SERS-based technologies. In recent years, the detection of small molecules, peptides, proteins or DNA, has been addressed using SERS, resulting in an increasing number of publications. Some features of SERS make it a particularly versatile and effective technique for sensing in bioanalytical [59, 194] and homeland security [91] applications, such as its high sensitivity, molecular fingerprinting ability, multiplex capability, minimal background signal from water, and the speed and cost effectiveness compared to standard procedures. Moreover, the electromagnetic enhancement mechanism of SERS can create localized surface plasmons (LSP) from the matching of the resonance frequency of the valance electrons of a noble metal with the frequency of the incident light that can further enhance the Raman signal of the target [52].

Malathion is the most common organophosphate insecticide applied in the United States, [195] used primarily in agriculture and domestic use for eradication and control of pests. The structure of malathion is shown in figure 1. Presently, there is no definitive information showing effects of chronic toxicity of malathion [195] and due to its low toxicity to humans [196] it is considered safe to use. However, because of its widespread use, it is necessary to develop detection methods to monitor the presence of malathion in different environmental compartments (eg. surface waters, soil, etc.). Analytical methodologies for malathion, together with other organophosphorous pesticides have recently been developed through gas chromatography-mass spectrometry (GC-

MS), [197-199] gas chromatography-nitrogen phosphorus detector (GS-NPD) [200-202] or high performance liquid chromatography-diode array detector (HPLC-DAD), [203, 204] among others. These methods successfully analyzed the target analyte with satisfactory limits of detection. However, these types of procedures often involve time and labor intensive sample preparation, and separation prior to the final detection, [205] taking up to 80% of total time spent on analysis. [205, 206]

SERS-based sensors can be classified into two categories: intrinsic and extrinsic sensors. With intrinsic (or direct) sensing, the molecular fingerprint of the target analyte is acquired directly. This method has been applied to wide variety of small biological molecules [59] and microfluidic devices for detection of dyes. [207] Extrinsic sensors employ SERS-active nanotags consisting of distinguishable SERS-active reporters or molecules with unique spectral fingerprints, for indirect measurements of the analyte of interest. Some extrinsic systems have been developed for small molecule detection including Au NPs functionalized with a 16 amino acid peptide selective to protective antigen (PA) coupled with the Raman reporter molecule 5,5′-dithiobis(succinimidyl-2-nitrobenzoate) to detect PA for anthrax screening [208] or displacement of rhodamine 6G by glutathione on nanoparticles for reverse detection in aqueous solution. [209]

In order to provide molecular affinity to SERS sensors toward the aim of improving reliability, the use of cyclodextrin inclusion complexes (CICs) or molecularly imprinted polymers (MIPs) for direct detection of analytes has been reported. [210, 211] An alternative strategy to chemical modifications for molecular recognition is to use DNA aptamers which can bind to selected targets with high affinity. Aptamers present unique advantages over chemical modifications:

from well-established screening protocols to versatility in modifications for labeling and surface chemistry. Use of aptamers in SERS sensors has been reported for extrinsic detection of cocaine by analyzing the conformational changes to the aptamers upon binding the target analyte. [95, 212] For this purpose it is necessary to obtain a reliable and highly reproducible DNA signal, which can be a limitation on the development of this class of methods. In this study we exploit the specificity of DNA aptamer recognition capability with the simplicity of intrinsic analyte detection by demonstrating a method of direct detection of malathion using DNA apta-SERS substrates.

EXPERIMENTAL

Materials

Ethylene glycol dimethacrylate (EGDMA), methacrylic acid (MAA), 2-aminoethanethiol, N-(3-Dimethylaminopropyl)-N′-ethylcarbodiimide hydrochloride (EDC), azobisisobutyronitrile (AIBN), tetrachloroauric (III) acid, sodium citrate, 2-(N-morpholino) ethanesulfonic acid (MES) were obtained from Sigma-Aldrich (MO, US); (3-aminopropyl)triethoxisilane (APTES) and analytical grade malathion were purchased from Fluka (Buchs, Switzerland). EGDMA and MAA were freed of inhibitors prior to use using a disposable, pre-packed column (22.5 x 2.0 cm), obtained from Aldrich. AIBN was recrystallized from methanol prior to use. All the organic solvents were at least HPLC grade and purchased from Sigma-Aldrich. All other chemicals were used as received. Ag-coated SERS Diagnosis Membranes were kindly supplied by iFyber (SER-DM^{TM}, iFyber LLC, Ithaca, NY, US).

Preparation of SERS substrates

Synthesis of gold nanoparticles

Colloidal gold nanoparticles (AuNP) were prepared by reduction of chlorauric acid with sodium citrate, according to a methodology adapted from Frens. [66] In brief, 50 mL of a $HAuCl_4$ (1mM) aqueous solution were heated to boil and a fixed amount of sodium citrate solution (1%) was then added. The reaction mixture was cooled after 20 min of boil. The concentration of AuNPs in the resulting solution was determined by absorbance measurements (λ=520nm) using a Nanodrop ND-1000 spectrophotometer (Thermo Scientific; Rockford, IL) and molar extinction coeffiecients for AuNPs derived from Yguerabide et al. [213]

Preparation of glass-gold nanoparticle substrates

Glass bottom microwell dishes with an uncoated coverslip (P35G-14-C, MatTek Corporation, Ashland, MA, US) were cleaned with nitric acid, thoroughly rinsed with deionized water and dried under nitrogen flow. Then, 100 µL of aqueous 5 mM APTES were deposited on the glass surface. After 15 minutes, the substrates were again rinsed with deionized water and dried under nitrogen. Subsequently, 100 µL of colloidal gold solution were located on the modified glass and allowed to dry. The glass-gold substrates were finally rinsed with DI water and dried prior to use.

Synthesis of polymer microspheres

Cross-linked polymer microspheres were prepared by precipitation polymerization. Purified MAA (0.46 mmoles, 39.4 µL), EGDMA (2.32 mmoles, 453.2 µL) and initiator AIBN (0.2 mmoles, 33 mg) were mixed with 20 mL of acetonitrile and placed in a glass vial fitted with a screw-cap which served as reaction vessel. The mixture was degassed by a gentle N_2 stream for

10 min. The bottle was sealed and introduced into a temperature controllable incubator equipped with a Spindrive orbital shaker platform (Bel-Art, Wayne, NJ, US) powered by a standard magnetic stirrer that allowed slow agitation of the solution during the course of the polymerisation. The temperature was maintained at 60 ºC for 20 h. The polymer microspheres formed were separated from the reaction medium by vacuum filtration on a Magna nylon membrane filter with 0.45 µm of pore size (Osmonics, Minnentoka, MN, US) and then sequentially washed with acetonitrile.

Preparation of Polymer-Gold nanoparticle composite microspheres

Polymer microspheres were functionalized taking advantage of the presence of available carboxyl groups from the MAA. An amount of 0.2 g of polymer microspheres was dissolved in 15 mL of MES buffer at pH 5.5 and mixed with 200 mg of EDC previously dissolved in 5 mL of water. The mixture was stirred during 30 min and 75 mg of 2-aminoethanethiol (cysteamine) in 2 mL of water were added. The suspension was kept under stirring for 3 hours after which the polymer-cys functionalized particles were filtered, washed with water and resuspended in 5 mL of water. An aliquot of 1 mL of this suspension was added to 10 mL of AuNP solution under stirring, leading to the formation of polymer-AuNP composite microspheres.

DNA aptamer development

The aptamer targeting malathion was developed using the modified Systematic Evolution of Ligands by EXponential enrichment (SELEX) method of Bruno et al. [214] Briefly, analytical grade malathion from Fluka was immobilized on a PharmaLink affinity column (Thermo Scientific; Rockford, IL) per instructions detailed by the manufacturer. The column was

incubated with the SELEX DNA library and the bound DNA was eluted and amplified by polymerase chain reaction (PCR). The PCR product was used for six subsequent rounds of SELEX. The aptamer designated as M17 Forward (M17-F) [215] was purchased from Integrated DNA Technologies, Inc. (IDT; Coralville, IA) with the following sequence: 5'-ThioMC6-ATCCGTCACACCTGCTCT-TATACACAATTGTTTTTCTCTTAACTTCTTGACTGC-TGGTGTTGGCTCCCGTAT-3'. Aptamer structure is schematically depicted in Figure 3.1C. The aptamer contained a thiol C-6 modifier on the 5' end for conjugation to gold nanoparticles attached to the surface of the polymer microspheres. The secondary structure and sequence are shown in figure 3.1 C. A stock solution was made by reconstituting the aptamer to 100 µM in nuclease free water. The stock was stored at -20 ºC for further use.

Preparation of polymer-AuNP-aptamer conjugates

Polymer-AuNP particles functionalized with DNA-aptamers on the surface were prepared according to the methodology developed by Taton et al. [216] The equation *mol conjugated aptamer*=$A_n \times C_n \times D_o \times V$ (**eq. I**) was used to calculate the amount of aptamer to attach to the polymer-AuNP particle; where A_n is the surface area of the microsphere, c_n is the concentration of the original AuNP solution (particles L^{-1}), D_o is the aptamer density on the particle (35 pmol cm^{-2}), and V is the volume of the reaction (L). A mole excess (1.5 times) of the amount of aptamer calculated with equation 1 (~10 µL) was then added to 500 µL polymer-AuNP particles suspension and rotated on a rocking table at 1 Hz in the exclusion of light for 16 h. Next, 0.250 vol of 1M NaCl/0.1 M sodium phosphate buffer (buffer I) was added and the particles were rotated for an additional 4 hours. The conjugated particles were centrifuged at 3000 rpm for 4 min to remove excess aptamer and were resuspended in 500 µL of 0.1 M NaCl/10 mM sodium

phosphate buffer (buffer II). The particles were centrifuged and resuspended two more times and finally resuspended in 125 µL of buffer II.

Characterization techniques

Dynamic Light Scattering measurements

The sizes of AuNP, the polymer microspheres and the polymer-AuNP-aptamer conjugates were analyzed through dynamic light scattering (DLS). Suspensions of the three different types of particles were prepared using water as dispersant and transferred to 400 µL disposable sizing cuvettes, measuring the diffusion of the particles moving under Brownian motion using a Zetasizer Nano-ZS (Malvern Instruments Ltd, Worcestershire, UK).

Scanning Electron Microscope Imaging

Scanning Electron Microscope (SEM) was used to characterize the polymer-AuNP. The images were obtained using a LEO 1550 FESEM (Keck SEM). The dried particles were first coated with an electrically conductive gold-palladium coating approximately 10 nm thick and then placed on a silicon wafer for imaging. The resolution at 5 KeV was 2.5nm.

SERS Measurements

SERS spectra were obtained using a Renishaw InVia Confocal Microscope system (Renishaw Inc; Hoffman Estates, IL) equipped with a 785 nm edge laser and Renishaw CCD Camera (Renishaw Inc; Hoffman Estates, IL) fitted to a Leica microscope. The spectra for polymer-AuNP-aptamer and glass-Au-aptamer substrates were taken with a 50x objective at an exposure time of 10s and a laser power of 1%. The ~1.0 µm laser spot was focused on a single particle on

the surface. All spectra were obtained using a 785 nm excitation. The spectra were analyzed using GRAMS AI spectroscopy suite (Thermo Scientific; Rockford, IL).

Glass-gold substrates

To the glass-gold substrates a 10 µL aliquot of 1 µM thiolated aptamer solution in buffer I was added and incubated at 4ºC overnight. The substrates were rinsed with DI water and dried before SERS measurements. In the same manner, glass-gold substrates were incubated with a 1 mM (330 µg mL^{-1}) solution of malathion in ethanol for 24 h.

SERS Diagnosis Membrane

The membranes were cut into small squares (0.5x0.5 cm size) and incubated with 1mM (330 µg mL^{-1}) solution of malathion in ethanol for 24 hours. The membranes were then rinsed with DI water and placed onto a glass slide for SERS measurements.

Glass-gold-aptamer-malathion experiments

For the glass-gold-aptamer-malathion experiments, 100 µL aliquot of 3 nM thiolated aptamer solution in buffer I was incubated on the glass-gold substrate at 4ºC for 24 hours. After this incubation time, 100 µL aliquot of malathion in buffer II was added. After 15 min, the substrates were thoroughly rinsed with DI water, allowed to dry and SERS spectra were finally obtained.

Polymer-AuNP-aptamer-malathion binding experiments

The polymer-AuNP-aptamer particles were aliquoted (125 µL in buffer II) and incubated with the same volume of a solution of buffer II containing malathion at a suitable concentration level for 30 min. After this time, the particles were centrifuged, separated from the supernatant and washed with an equal volume of DI water three times. Finally, a volume of 100 µL was allowed

to dry on a microscope glass slide, previously cleaned with nitric acid, prior to spectra acquisition.

RESULTS AND DISCUSSION

We propose a new composite material based on polymer-AuNP-aptamer sensing particles capable of acting as capture and signal-enhancer for SERS detection of malathion (Figure 3.1A). A schematic representation of this composite materal is shown in Figure 3.1 A. Fabrication of multimeric SERS substrates is better suited than the methods based on aggregation of gold nanoparticles through changes in the electrostatic charge, which can affect reproducibility. In order to obtain reference SERS spectra of the analyte malathion, we used Ag-coated SERS diagnosis membranes as a positive control substrate. For the same purpose, SERS substrates of AuNPs aggregated on the surface of APTES-coated glass slides were prepared to obtain a reference SERS signal of each component of our multimeric system.

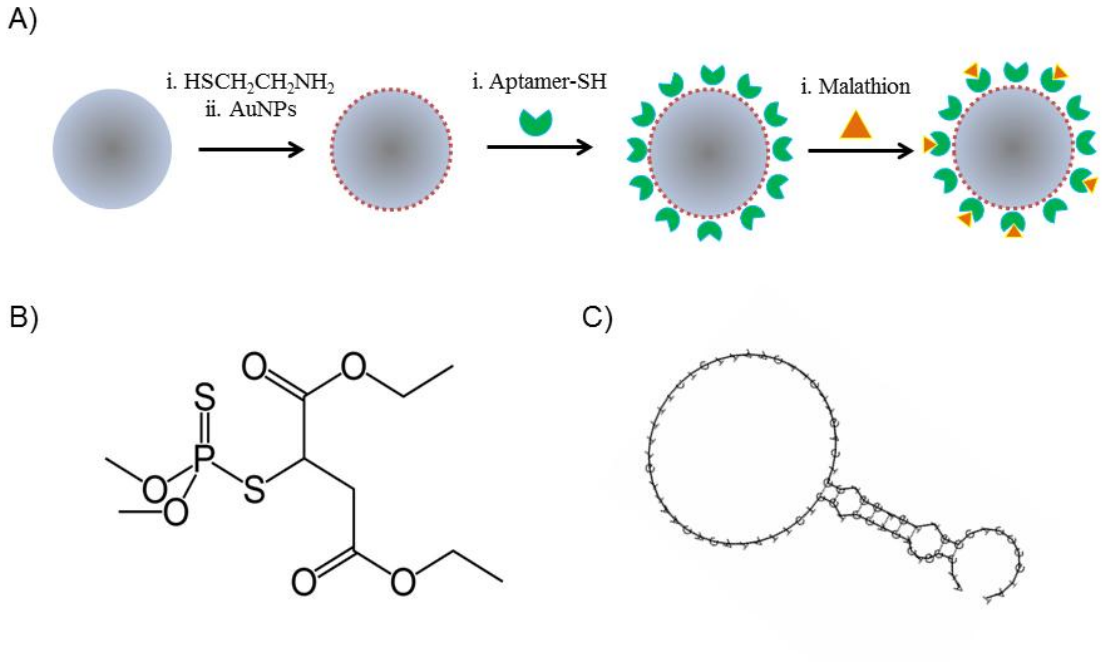

Figure 3.1 A) Illustration demonstrating preparation of polymer-AuNP-aptamer subtrates for SERS detection of malathion. B) Chemical structure of malathion. C) Sequence and predicted secondary structure of DNA aptamer M17-F used to bind malathion.

Preparation and characterization of polymer-AuNP-aptamer substrates

Polymer-AuNP microspheres

When designing our composite SERS substrate, different parameters such as the morphology of the polymer support, as well as the type, size and organization of the AuNP, were taken into account. In this work, we have adapted the methodology proposed by Prasad et al. [217] to form polymer-AuNP composites with controlled aggregation of AuNPs onto the polymer surface. Dyanamic light scattering (DLS) analysis of the synthesized AuNPs indicated a size of ~ 40 nm with a Gaussian distribution shown in figure 3.2C.

Studies have shown that whereas the signal resulting from measurements obtained using colloidal nanoparticles is highly dependent of the number of nanoparticles in the laser beam, the variation in signal using microsphere-AuNP composite substrates is independent of the number of microspheres in the sample. [218] We decided to use as support polymer microspheres with a diameter size comparable with the focal volume of the laser, so that each Raman measurement is restricted to a single microsphere surface. Figure 3.2A shows an image taken with the microscope coupled to the Raman spectrometer with a single bead (center of picture) illuminated by the laser. For practical considerations, particles in the range of μm size are also easier to handle and can be subjected to routine processes such as centrifugation or filtration, preserving its performance. Additionally, it was important to minimize the porosity of the polymer beads in order to restrict the distribution of AuNP onto the surface of the microspheres. The polymer microspheres should show a suitable chemical functionality to allow for subsequent preparation of polymer-AuNP composite particles. Polymer microspheres were prepared by polymerization by precipitation using MAA and EGDMA as co-monomers and acetonitrile as porogen.

Acetonitrile permits formation of particles with a low level of porosity, and MAA provides carboxyl groups on the surface for the conjugation with AuNP via modification with 2-aminoethanethiol. It was important to obtain a narrow size distribution which may affect the quality of the Raman signal. In our case, based on prior knowledge in our laboratory, the polymerization was conducted directly with 2.5% monomer concentration and produced monodispersed polymer particles of an appropriate size (diameter of 1.6 μm), with no obvious signs of aggregation and a narrow size distribution obtained by DLS measurements displayed in figure 3.2D.

Figure 3.2B is a SEM image of the surface of a composite particle prepared as described in the experimental section, based on the methodology proposed by Prasad et al. [217]. AuNPs can be seen distributed throughout the polymer surface either in a monodispersed manner or forming small aggregates. Although beyond the scope of the work, it was found that the addition of smaller amounts of AuNP provided poorer coverings, whereas the addition of a greater amount of gold caused the formation of independent gold clusters. It is of note that there were no signs of irreversible aggregation of polymer-AuNP composite particles over several months. Although the particles sedimented after approximately two hours in suspension, it was possible to resuspend them easily by vortex. This provides an additional advantage of the proposed composite material, compared to the instability of the AuNPs by themselves, which is one of its main limitations. [219]

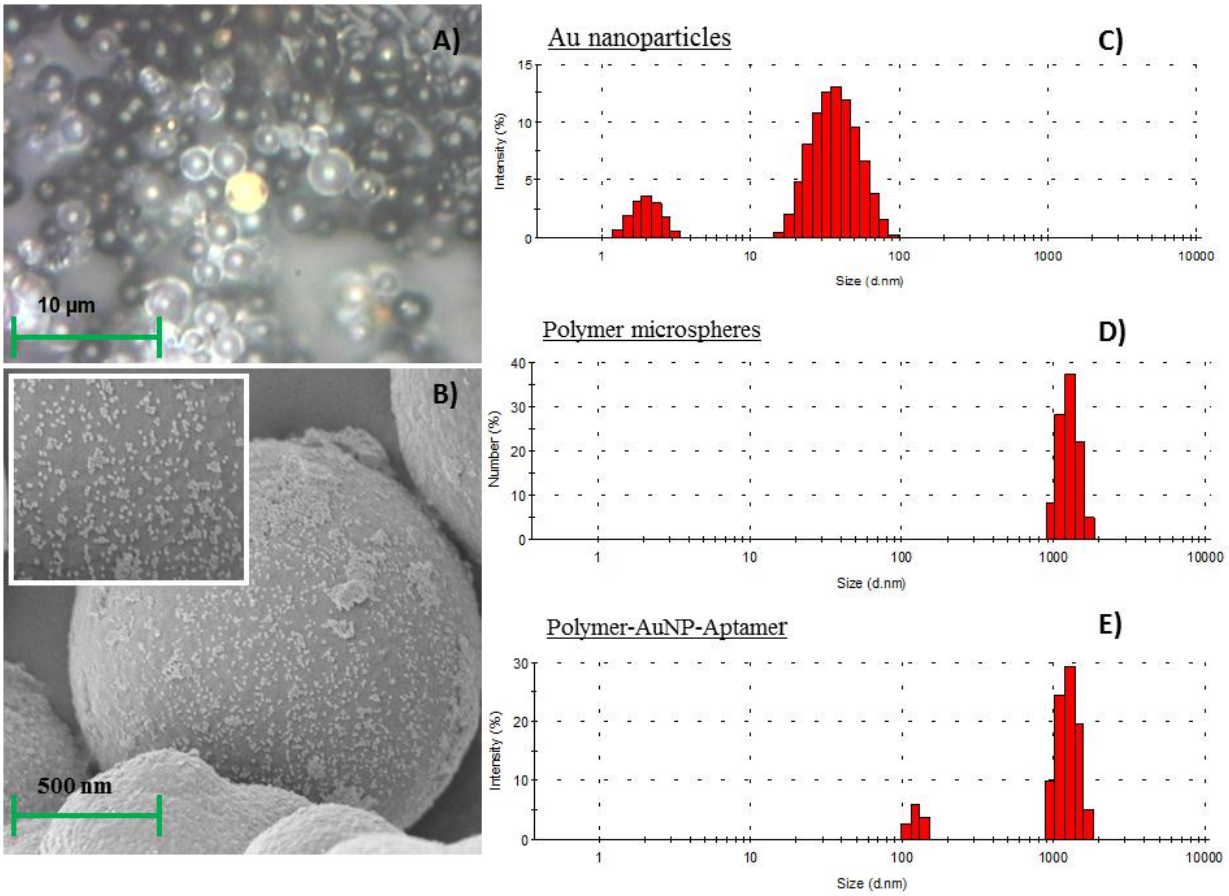

Figure 3.2. A) Light microscope images of polymer-AuNP-aptamer substrates immobilized on glass surface. B) Representative SEM image of polymer-AuNP-aptamer substrates. The inset illustrates clustering of 40 nm gold nanoparticles on surface of polymer substrate. (C-E) Histogram showing the size distribution of Au-NPs, Polymer microspheres, and Polymer-AuNP-Aptamer subtrates respectively as measured by Dynamic Light Scattering.

Polymer-AuNP-aptamer conjugates

The conjugation of the aptamers to the polymer-AuNP particles was carried out following a methodology adapted from Taton et al. [216] The maximum number of units of oligonucleotide per nanoparticle is limited, and it depends on the area of the nanoparticles and the sequence and length of the aptamer. [220] The amount of aptamer used in the conjugation was calculated according to equation I considering the entire polymer microsphere as a gold particle. After functionalization with aptamer, the particles remained in suspension without settling to the bottom of the vial for longer than polymer-AuNP particles, suggesting an effective surface coverage with aptamer. Figure 3.2E shows the size distribution of the polymer-AuNP-aptamer particles obtained by dynamic light scattering. It can be observed that the composite microspheres retained their morphology after the conjugation with AuNPs and aptamers and only a small excess of gold appears in the histogram.

In order to distinguish between the background signal of DNA and the signal characteristic of the target analyte, SERS measurements were conducted using with previously reported substrates. Figure 3.3 shows the SERS spectra obtained using glass-gold substrates prepared as described in the experimental section, after incubation with different amounts of aptamer thiol-C_6-M17-F. Although the obtained signal appears in a region of the spectrum where the signal of citrate has been reported, [218, 221] the increase in the intensity of the signal by increasing the amount of DNA immobilized on the substrate indicates that the observed signal between ~ 800 cm^{-1} and ~ 1800 cm^{-1} corresponds to the DNA. Similarly, bands corresponding to DNA can be observed in the same region of the spectra for our polymer-AuNP-aptamer system, as shown in figure 3.4. This result is consistent with previous studies reporting SERS detection of DNA. [222] According to that

work, it is possible to obtain a highly reproducible signal of DNA, by applying an appropriate thermal treatment. This kind of process is required for indirect measurements, where the molecule bound to the aptamer is detected via a target-induced conformation change. [95, 223, 224] However, direct sensing of malathion can be carried out using our polymer-AuNPs-aptamer system in a suitable solution without any previous thermal treatment by directly measuring characteristic peaks of the target analyte.

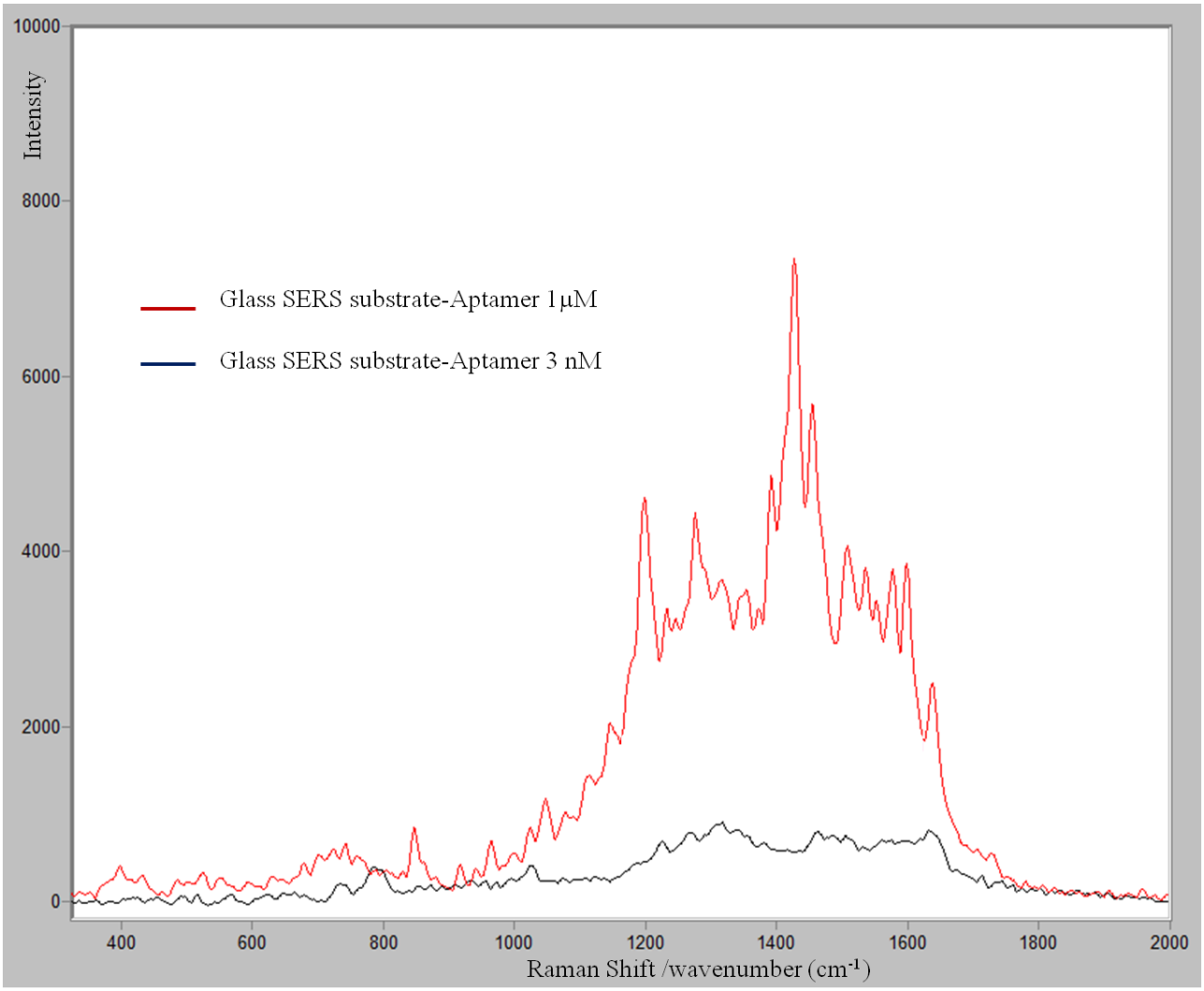

Figure 3.3. SERS spectra taken on glass SERS substrate conjugated with 1 µM or 3 nM concentration of aptamer M17-F modified with a 5' thiol group containing a six carbon spacer.

Sensing experiments for malathion

Although the electromagnetic enhancement mechanism does not require the analyte to be in direct contact with the SERS substrate, for best enhancement the distance between the analyte and the metal surface should be in the range of a 0.01 to 10 nm. [52] In order to perform direct measurements of the analyte, the polymer-AuNPs-aptamer system can operate as an extractant of the pesticide from the solution by specific interaction between the aptamers and the analyte for which they were designed. Conformational changes produced by the rearrangement in the presence of target analyte allow the molecule to be in close proximity to the metal surface. Given that Raman measurements were made with the samples dried on a glass slide, the aptamers exhibited different conformations on the surface of the particles, resulting in variability in the DNA signal. However, operating in a suitable concentration range, characteristic peaks of malathion were clearly observed in every measurement, indicating that the aptamer-analyte interaction was preserved in the vicinity of the surface. Figure 3.5B shows the SERS spectra of polymer-AuNP-aptamer particles incubated as described in the experimental section with a 16.5 μg mL^{-1} (20 μM) solution of pesticide, together with the spectra obtained using SERS Diagnosis Membrane, as reference substrate (Figure 3.5A). . Multiple matches can be observed in the wavenumbers of the peaks assigned to malathion, (eg 500 cm^{-1}, 527 cm^{-1}, 714 cm^{-1}) in a region of the spectra free of DNA signal, enabling the direct detection of the pesticide. These peaks assigned to malathion were not present in the spectra obtained from blank samples (Figure 3.4A). Finally, we selected the peak at ~ 495 cm^{-1} which was better defined and provided a greater sensitivity. As shown in Figure 3.6, such a peak (~ 497 cm^{-1}) is also present in the spectra obtained after incubation of the pesticide with the reference glass-gold substrates functionalized

with thiolated aptamer on the surface. According to previous data, 495 cm^{-1} can be assigned to P-S stretching mode [225] of malathion.

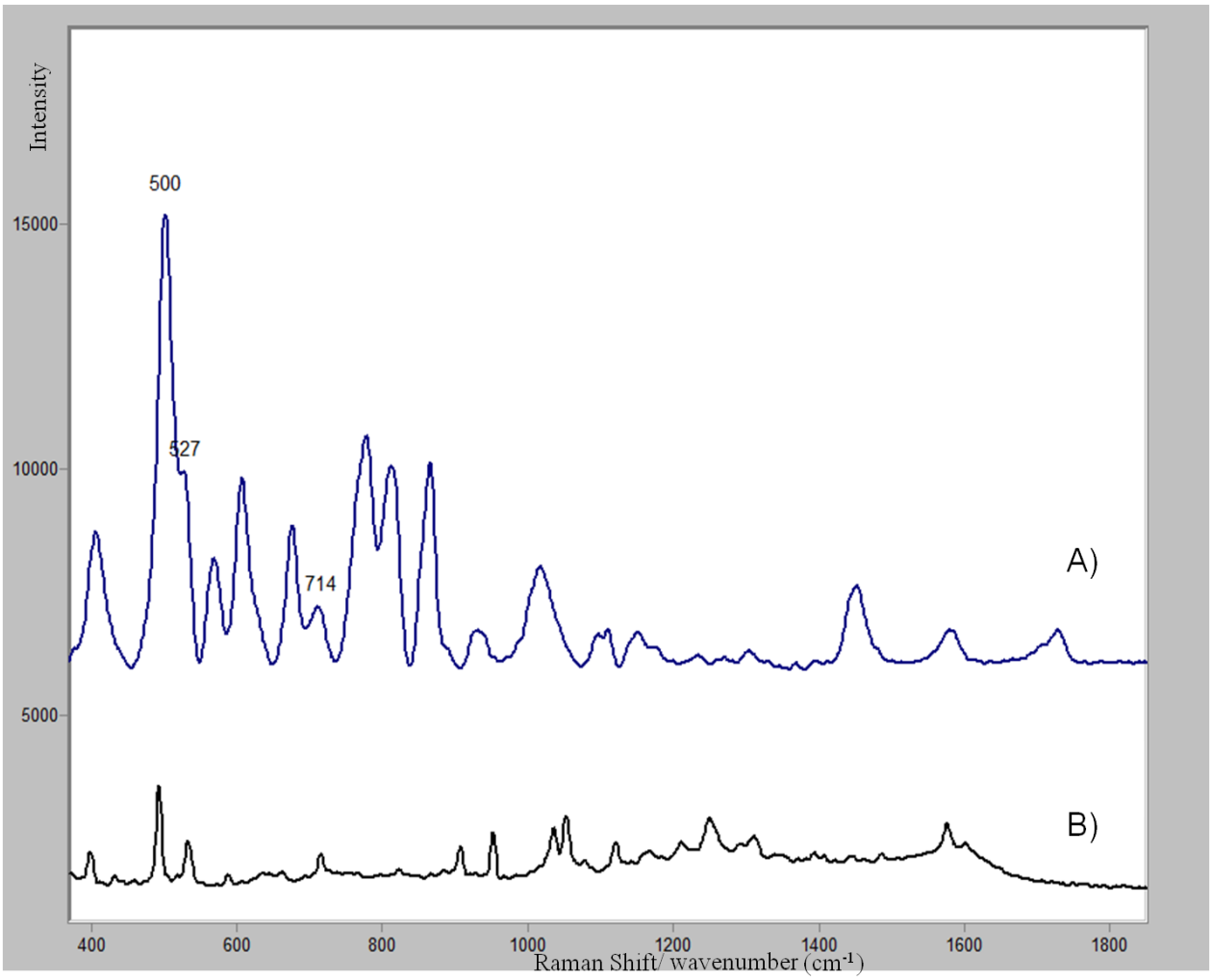

Figure 3.4 Comparison of: A) SERS spectra of 330 µg mL^{-1} malathion in ethanol incubated 24 h on iFyber™ SERS Diagnostic Membrane and B) SERS spectra of 16.5 µg mL^{-1} malathion in buffer solution incubated 30 min with polymer-AuNPs-aptamer substrates. Spectra are offset for clarity.

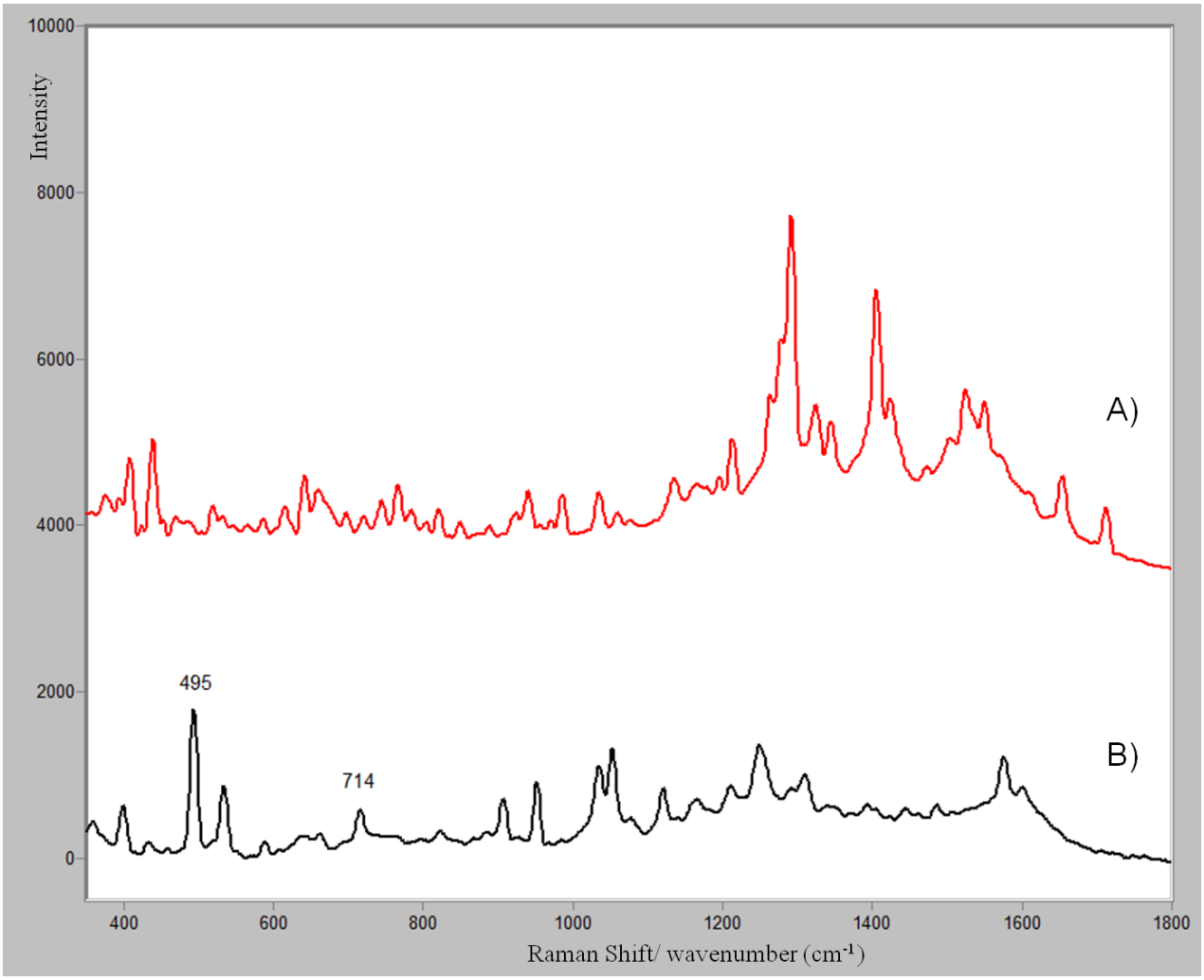

Figure 3.5 SERS spectra of: A) polymer-AuNPs-aptamer substrate incubated with a blank buffer solution; B) polymer-AuNPs-aptamer substrate incubated with a 16.5 µg mL^{-1} malathion in buffer solution. Incubation time was 30 min. Spectra are offset for clarity and characteristic peaks for malathion are highlighted.

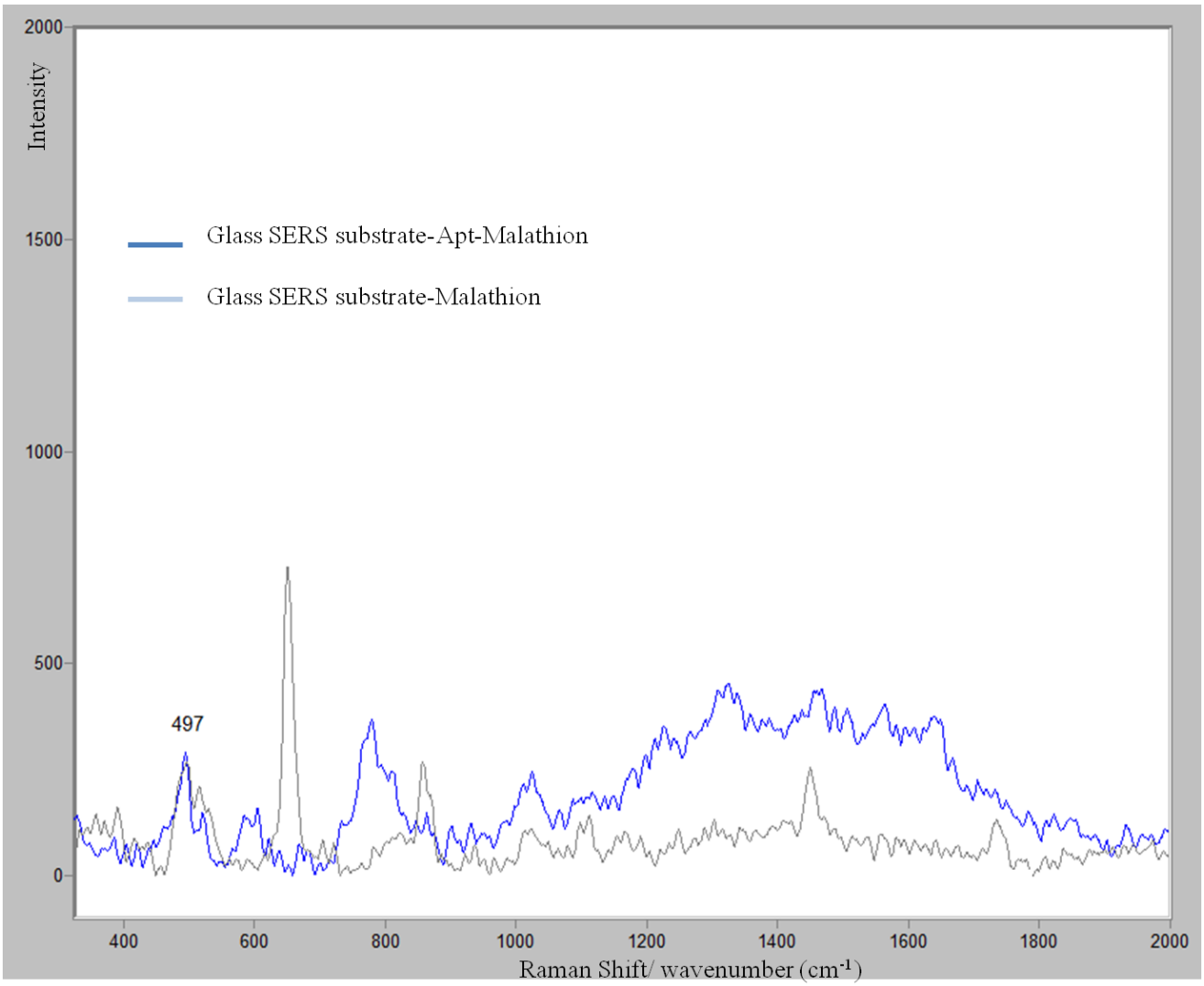

Figure 3.6 SERS spectra of glass SERS substrate incubated with 330 µg mL^{-1} malathion in ethanol for 24 h (grey); and SERS spectra of glass SERS substrate-aptamer (blue) incubated with 6.6 µg mL^{-1} malathion in buffer for 30 min.

It is of note that malathion could not be detected with the polymer-AuNP microspheres lacking modification with the aptamer following washing with DI water. The washing step was able to remove all material nonspecifically adsorbed onto the surface during the 30 min incubation period. This suggests that the modification of the polymer-AuNP beads with the aptamer promotes binding of the pesticide by specific interaction with the aptamer.

Analytical performance and application

The apta-sensing system for malathion was applied to pesticide solutions at different concentration levels. Selectivity for the target molecule in a sample which would also likely contain potential interfering molecules may be an issue. In this sense, experiments with tap water spiked with malathion have been also carried out. The ionic content usually present in tap water is also a challenge for the operation of our system.

Limits of detection

The theoretical limits of detection calculated as three times the average signal of the background noise obtained in the analysis of six blank samples [226] were 0.3 and 0.75 μg mL^{-1} for standard solutions and spiked tap water solutions, respectively. However, in practice such a value is in a concentration range where the variability in the signal is very high. Consequently, an experimental limit of detection of 3.3 μg mL^{-1} was estimated considering the smallest concentration of analyte in the test sample that was reliably distinguished from zero according to the judgment of the researchers (Figure 3.7). This experimental LOD is comparable with the value provided by other studies that address the direct SERS detection of malathion[227].

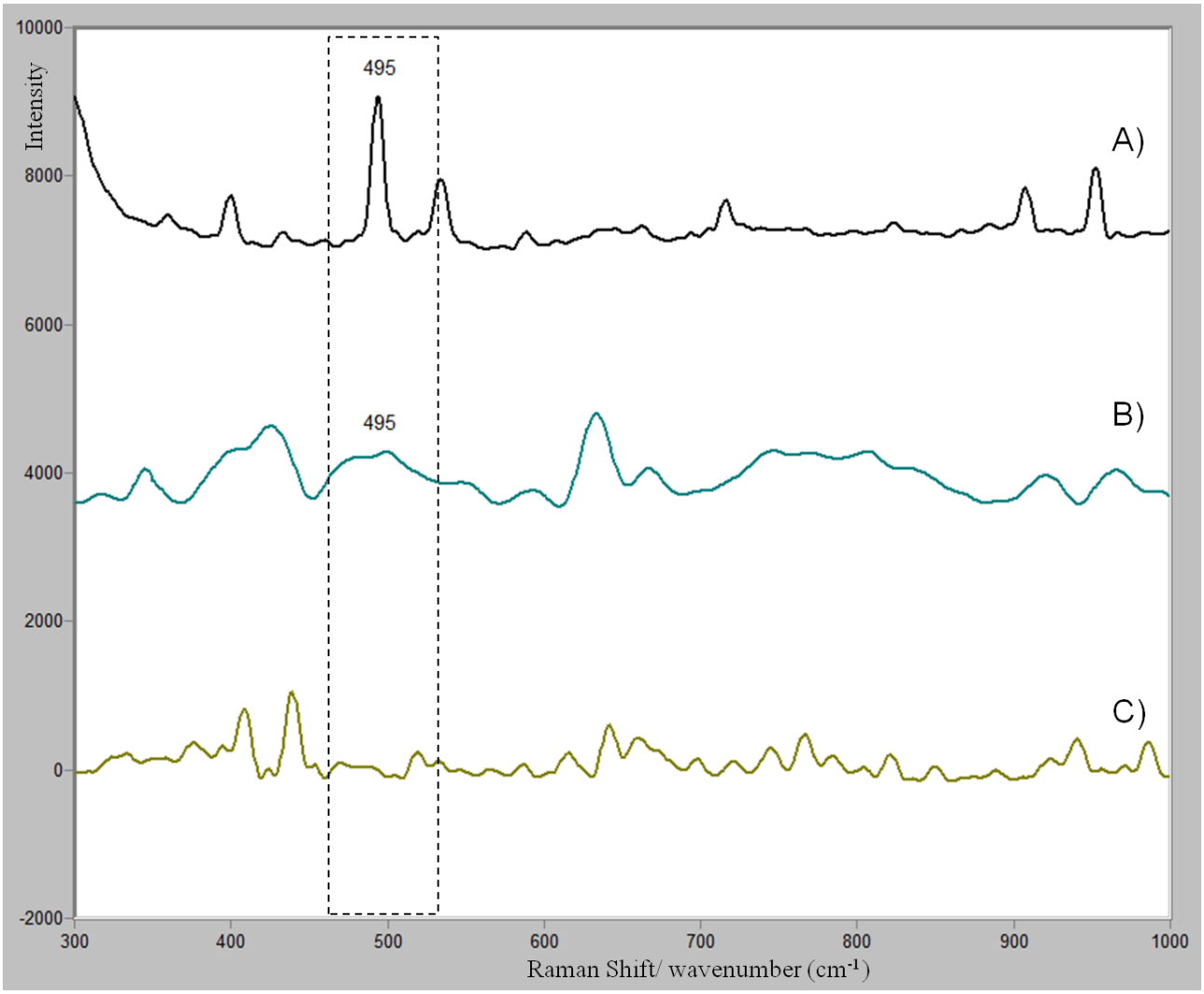

Figure 3.7 Comparison of SERS detection of malathion using 495 cm^{-1} peak with polymer-AuNPs-apt substrates at: A) 16.5 µg mL^{-1} of malathion; B) 3.3 µg mL^{-1} of malathion; C) blank buffer solution. Spectra are offset for clarity.

Linearity

It is important to stress that the poor solubility of malathion in aqueous solution (145 µg mL^{-1}, log P_{ow} 2.75) [228] is the primary limiting fact of the apta-sensor for this specific pesticide. Above a concentration level of 33.3 µg mL^{-1}, it is possible to observe the formation of a film of malathion which prevents focus of the laser on the sample resulting in no Raman signal. Taking these facts into account, the range of application can be reliably restricted to one order of magnitude and thus, the polymer-AuNP-aptamer successfully allows the detection of the target molecule in a concentration range between 3.3 µg mL^{-1} and 33.3 µg mL^{-1}. Linearity was checked with fortified tap water samples and good correlation was observed in the range of concentration studied, with r=0.998.

Precision

The repeatability was studied in terms of the relative standard deviation (RSD) of the values of concentration found obtained at different spiking levels in tap water samples. Table 1 shows the expected and calculated concentrations of malathion with their respective RSDs values. Although the value of RSD for concentration levels close to the estimated limit of detection is 25%, for a higher level of concentration (16.5 µg mL^{-1}) the RSD drops to acceptable levels of 14%.

CONCLUSIONS

In this paper, we present a new format of apta-sensing composite particles for SERS detection of malathion. The developed polymer-AuNP-aptamer microspheres combine extraction capability by aptamer-target analyte interaction and Raman signal enhancer for SERS detection of the

pesticide. Working under described experimental conditions, the polymer-AuNP-aptamer successfully allows the direct detection of malathion at 3.3 μg mL^{-1}, which compares well other SERS substrates reported. [227] The apta-sensing microspheres are a system well suited for industrial and agricultural applications as only basic equipment is required for analyte separation. As hand held and bench-scale Raman spectroscopy systems become more powerful, apta-sensing microspheres can become a reliable method for on-site pesticide detection.

ACKNOWLEDGEMENTS

The authors thank Dr. Kit Umbach and the Cornell Center for Materials Research for assistance and access to the facilities. The authors gratefully acknowledge financial support received from the United States Department of Agriculture (Grant 2009-35603-05066).

Chapter 4: Synthesis and Characterization of doxorubicin molecularly imprinted polymers for sustained release drug delivery system

INTRODUCTION

In the past 50 years the pharmaceutical industry has explored a variety of techniques to incorporate drugs into polymers. A majority of the polymer systems employed by the industry are either cellulose derivatives, micelle forming polymers, or acrylamide derivatives [229]. In most polymeric drug delivery systems (DDS) an inert polymer is loaded with a compound which is released via burst, controlled, or pulsatile delivery. The pharmacokinetic properties of the bioactive agents are often greatly enhanced in polymer DDS through increased plasma half-life and protection from enzymatic degradation that leads to dosage reduction for patients [230, 231]. Combined with the potential for active targeting, polymer DDS field is a rapidly growing field for anti-cancer drug therapeutics, which often have a variety of well documented side-effects[232].

The most common carriers for drug therapeutics are N-(2-hydroxypropyl)-methacrylamide (HPMA) copolymer drug conjugates. Polymer-drug conjugates are advantageous over systemically administered drug through limit of drug uptake to endocytosis, increase in the circulation time of the drug, and accumulation of drug in the leaky vasculature of tumors[231]. Several HPMA polymer conjugates for the anthracyline doxorubicin have been reported in the literature [233-237].

In addition to polymer-drug conjugates, an emerging field in polymer drug delivery systems is molecular imprinting of polymers for drug delivery. Molecularly imprinted polymers (MIPs) are polymer networks with specific recognition sites for a target molecule [238]. Molecularly imprinted

polymers have been used to a wide extent in the field of analytical chemistry in liquid chromatography[239-242], solid-phase extraction[243-246], biomimetic sensors[247-249], and catalysts[250]. MIPs work by providing shape specific cavities for a template with exposed functional groups inside the cavity to form multiple stable interactions with the template[122]. This feature provides specific recognition for a molecule or family of molecules that are complementary in shape and functionality to the template used in the preparation which can be exploited for drug delivery. The interactions can be specific enough as to even allow for the enantioseparation of molecules[251-255]. The template can be removed by disruption of the specific interactions between the monomers and template and specific empty cavities can be reloaded with an established dose of therapeutic drug. As opposed to polymer conjugate systems, MIPs do not require local degradation of the polymer to release drug[256]. MIPs can act as a stable reservoir for drug and decelerate the rate of drug release in a given media[129, 257] and characteristics such as particle size, porosity, and monomer interactions can be used to control the release of drug. If the therapeutic window of the drug is narrow the MIP can keep the concentration of the drug below toxicity level but above the minimum effective dose[258]. The highly cross-linked MIP polymer networks are also resistant to degradation and a variety of stimuli (pH, temperature, irradiation, electric current) can be used to control the release of therapeutic drug into the local environment[105]. In summary, MIPs are cheap, versatile, rationally designed materials with tailor-made properties that make them suitable for drug delivery. In this work we describe the production of nanometer range MIP particles for doxorubicin from methacrylic acid (MAA), 4-vinylpyridine (4-VP), and ethylene glycol dimethacrylate (EGDMA).

EXPERIMENTAL

Materials

Methacrylic acid (MAA), ethylene glycol dimethacrylate (EGDMA), 4-Vinylpyridine (4-VP), and azobisisobutyronitrile (AIBN), were obtained from Sigma-Aldrich (MO, US); Doxorubicin (DOX) was obtained from Santa Cruz Biotechnology Inc. (Santa Cruz, CA). EGDMA, MAA, and 4-VP were freed of inhibitors prior to use using a disposable, pre-packed column (22.5 x 2.0 cm), obtained from Aldrich. AIBN was recrystallized from methanol prior to use. All the organic solvents were at least HPLC grade and purchased from Sigma-Aldrich. All other chemicals were used as received.

Preparation of polymer substrates

Synthesis of polymer microspheres

Cross-linked non-imprinted and imprinted polymer nanospheres were prepared by polymerization by precipitation. Doxorubicin imprinted polymers were synthesized by first dissolving 5 mg of doxorubicin into 1 mL of acetonitrile/toluene solution by sonication. Once dissolved, 4-VP (69.0 µmoles, 7.444 µL) and MAA (69.0 µmoles, 5.85 µL) were added to the mixture and allowed to incubate for 10 minutes. EGDMA (0.69 mmoles, 136 µL) was added after the incubation step and the mixture was brought up to a final volume of 12 mL with acetonitrile/toluene solution (25% toluene v/v). 60.7 µmoles, 10 mg of the initiator AIBN was dissolved into the MIP solution and the mixture was degassed by a gentle N_2 stream for 10 min. A glass vial fitted with a screw-cap served as the reaction vessel. The vial was sealed and placed into a temperature controllable incubator equipped with a Spindrive orbital shaker platform (Bel-

Art, Wayne, NJ, US) powered by a standard magnetic stirrer that allowed slow agitation of the solution during the course of the polymerisation. The temperature was maintained at 60 ºC for 20 h. The polymer nanospheres that were formed were separated from the reaction medium by vacuum filtration on a Magna nylon membrane filter with 0.1 µm of pore size (Osmonics, Minnentoka, MN) and then washed with acetonitrile to remove excess monomer and initiator. Entrapped doxorubicin was extracted from MIPs by 5 extractions in 25 mL of methanol/acetic acid (2.5% v/v) until there was no detectable levels of doxorubicin in the extract. The particles were then washed a final time in acetonitrile and allowed to dry. Non-imprinted polymer was prepared following the same protocol in the absence of template.

Characterization

Dynamic Light Scattering measurements

The size of the polymer nanospheres was analyzed through dynamic light scattering (DLS). Dilute suspensions of the different types of particles were prepared using water as dispersant and transferred to 400 µL disposable sizing cuvettes, measuring the diffusion of the particles moving under Brownian motion using a Zetasizer Nano-ZS (Malvern Instruments Ltd, Worcestershire, UK).

Scanning Electron Microscope Imaging

Scanning Electron Microscope (SEM) was used to characterize the polymer particles. The images were obtained using a LEO 1550 FESEM (Keck SEM). The dried particles were first coated with an electrically conductive gold-palladium coating approximately 10 nm thick and then placed on a silicon wafer for imaging. The resolution at 5 KeV was 2.5nm.

Fourier Transform - Infrared Spectroscopy (FT-IR)

FTIR spectra for the polymer particles were generated using a Bruker Optics - Vertex80v FTIR spectrophotometer equipped with a diamond ATR crystal accessory for analysis of bulk samples. FTIR spectra were acquired between 450-7000cm^{-1}. Particles were washed thoroughly before analysis as stated previously.

Polymer Evaluation

Fluorescence Evaluation of Polymers

Imprinted and non-imprinted polymer particles (10 mg) were incubated in 1.5 mL of 1 µg/mL, 10 µg/mL, 25 µg/mL, 50 µg/mL, and 66 µg/mL solutions of doxorubicin in acetonitrile for 12 hours. After the incubation, the samples were centrifuged at 9,000x g for 6 minutes and the supernatant was collected. The particles were washed with 500 µL of acetonitrile to remove loosely associated template. The template was extracted from the polymer matrix in two steps by re-suspending the particles in 1 mL of methanol/acetic acid (2.5% v/v) and samples were sonicated for 25 minutes at 50 ºC. The particles were centrifuged and the extract collected. Analysis of each extraction was performed using a LS50B luminescence spectrometer (Perkin Elmer; Waltham, MA) with a low volume special optical glass cuvette. The samples were excited at λ = 479 nm and the emission spectrum of the solution were collected and analyzed. The peak height at λ = 549 nm was chosen for quantification based on emission maxima from standard curves and studies by Karukstis et al.[259]

Polymer-Doxorubicin Release Kinetics

Dried polymer (20 mg) samples were incubated in 1, 10, 25, and 50 µg/mL solutions of 1.5 mL of doxorubicin in acetonitrile for 12 hours. The particles were subsequently centrifuged, the supernatant discarded, and the excess of solvent was removed to produce a dry powder.

The drug loaded polymers were then suspended in 2 ml of water and transferred to SnakeSkin® Pleated dialysis tubing (MWCO 10,000, flat width 34 mm, diameter 22 mm, volume/length 3.7 ml cm^{-1}, Thermo Scientific; Rockford, IL). The tubing was sealed and transferred to a capped 100 ml Pyrex® flask containing 14 ml of water. The dissociation of doxorubicin was determined by spectroscopic analysis of the water (ex: $\lambda_{479\ nm}$; em: $\lambda_{558\ nm}$) at specified time intervals. Aliquots were returned to the samples after analysis.

RESULTS AND DISCUSSION

Polymer preparation and characterization

The macromolecular specificity of MIPs stems from the formation of cavities inside the polymers that are complementary to the shape of the template, and functional groups around the template that form multiple stabilizing interactions [105]. When choosing the interaction type, whether covalent or non-covalent imprinting, the type of drug delivery system to be explored and the release mechanism need to be considered [111]. For most drug delivery systems, non-covalent interactions are favored as it allows for drug release to reach the minimum effective concentration without exceeding the therapeutic window of the drug through controlled release mechanism [258].

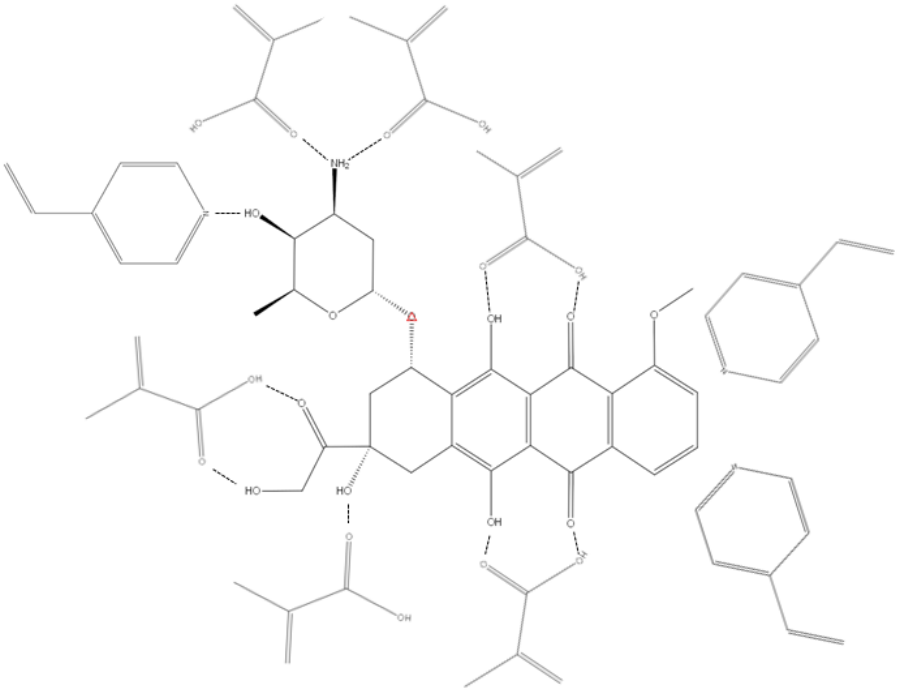

Figure 4.1 Representation of hypothetical prepolymerization complex with doxorubicin, methacrylic acid (MAA) and 4-vinylpyridine (4-VP). Combinations of functional monomer units are used to increase binding capacity of MIPs compared to polymers formed from a single monomer. The basic functional monomer 4-VP can provide hydrogen bonding through the lone pair electrons on the nitrogen atom in the pyridine ring as well as hydrophobic interactions.

The ratio of template to functional monomer units is one major factor in developing precise interactions for non-covalent molecular imprinting[111]. Too much functional monomer promotes non-specific interactions because its favors the formation of randomly distributed functional monomers throughout the polymer network that can non-specifically interact with the analyte. Too little functional monomer leads to weak specific interactions. Additionally, MIPs need to restrict the non-specific interactions in aqueous solutions as MIPs could potentially absorb small proteins and lipids on the polymer surface [105]. Finally, the polymers need to have a high degree of water solubility to be used as drug delivery systems. While much work has been done in the

field of imprinting in aqueous media, the strong interaction of water with the template often curtails the interactions of the monomer units thereby reducing specificity and binding capacity [260]. Through precipitation polymerization in organic solvents; whereas the polymer forms it becomes immiscible with the solvent and precipitates out of solution, it is possible to produce water soluble imprinted particles. In this work, molecularly imprinted polymers were synthesized for doxorubicin by varying types of monomer units, molar ratio of template to monomer units, and the final weight percent of monomer in polymerization reaction to produce MIPs with a strong affinity for doxorubicin. After careful selection of solvent which plays a critical role in template recognition and overall porosity of the particles[261, 262], doxorubicin MIP and non-imprinted polymer particles were prepared first by examining the effect of the types of monomers on water stability and imprinting effect. As doxorubicin contains a large aromatic region, 4-vinylpyridine was chosen as one of the co-monomer units for the template due to its potential to promote π-π stacking and hydrophobic interactions with the template with some electrostatic interactions. The polymers were prepared by polymerization by precipitation using 4-VP with EGDMA was the cross linker in acetonitrile/toluene mixture (3:1, v/v) to a molar ratio of 0.5:8:40 of doxorubicin to 4-vinylpyridine/EGDMA (1.5 wt %). The large ratio of monomer units was chosen to create a enough stable interactions for the doxorubicin which would prevent leakage of the drug since the ratio of template to functional monomer units is one major factor in developing precise interactions for non-covalent molecular imprinting[111]. Investigation into the optimal solvent for polymerization was limited by the low solubility of doxorubicin in several organic solvents. A mixture of acetonitrile/toluene (3:1, v/v) permitted the formation of particles with an intermediate level of porosity with toluene potentially promoting imprinting effects in

the polymer between the dox and 4-VP. In order to examine the morphology of the NIP and MIP under these conditions, a comparison of the SEM images of the polymerization products for the NIP and MIP are illustrated in Figure 4.2A & B. Under these conditions the particles exhibit a high level of aggregation in water and resemble more of a bulk polymer than isolated particles as shown in the images. The particles were loaded with a 50 µg/ml dox solution in acetonitrile, toluene, or water for 12 hours and extracted with MeOH/AcOH mixture. Analysis of the fluorescence of the extract showed no evidence of imprinting effect when imprinted polymers were compared to the control (data not shown). Any isolated particles were also 1-5 µm in diameter which is beyond the desired threshold. Other monomer formulations included using divinylbenzene (DVB) as a cross linker along with MAA and 4-VP to form a more stable cavity for the doxorubicin via a combination of hydrogen bonding and π-π interactions as previously explored in the work of *Ye et al* with MIPs for inhibitors of kallikrein[263, 264]. However, particles made with DVB were as expected highly insoluble in aqueous media and tended to readily form aggregates despite numerous warm sonications.

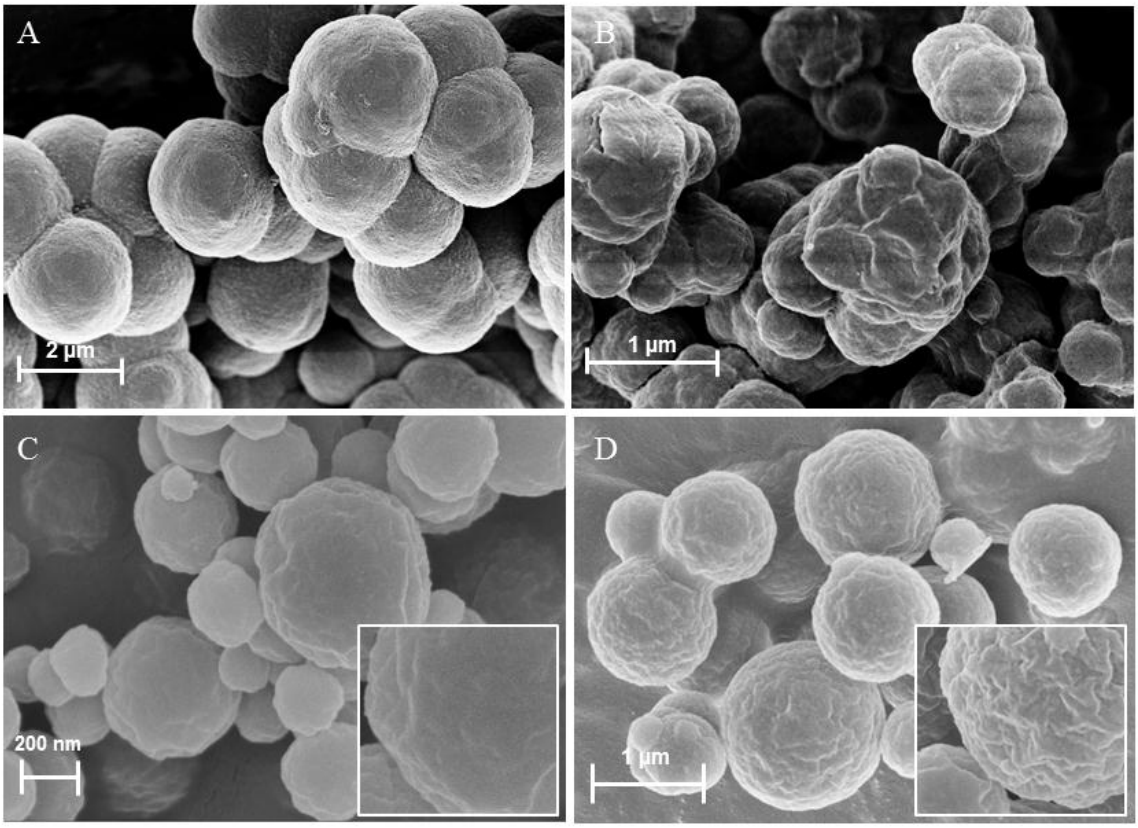

Figure 4.2. Representative SEM images of (a) non-imprinted 1.5 wt% 4-vinylpyridine/ethylene glycol dimethacrylate polymer particles (b) 1.5 wt% imprinted 4-vinylpyridine/ethylene glycol dimethacrylate polymer particles (c) 1.25 wt% non-imprinted methacrylic acid/4-vinylpyridine/ethylene glycol dimethacrylate polymer particles (d) 1.25 wt% imprinted methacrylic acid/4-vinylpyridine/ethylene glycol dimethacrylate polymer particles.

In order to improve the imprinting performance of the particles, MAA was added as a co-monomer unit to a final molar ratio of 0.5:4:4:40 of dox to MAA, 4-VP, and EGDMA. Methacrylic acid can potentially create a more stable pre-polymerization complex with the template since it is smaller and less rigid than 4-VP and does not promote non-specific interactions as does the pyridine group. Use of MAA has been cited in many studies [257, 265, 266] and it is suitable for compounds with optimal stability a lower pH[267], such as doxorubicin. The monomer weight percent was also reduced 1.25% in an attempt to decrease particle size. The particles formed using MAA/4-VP as functional monomers and EGDMA as cross linker are shown in the SEM images in figure 4.2C & D. The images show that the addition of MAA provided particles with a more uniform morphology than those obtained only with 4-VP (figure 4.2A & B) and with less visible differences in polymer morphology between NIP and MIP. The effect of decreasing the monomer concentration is seen in the controlled size of the particles as measured by dynamic light scattering (figure 4.3). The non-imprinted and doxorubicin imprinted particles obtained with the polymerization mixture containing MAA/4-VP/EGDMA had an average diameter of less than 400 nm with small differences between MIP and NIP.

A.

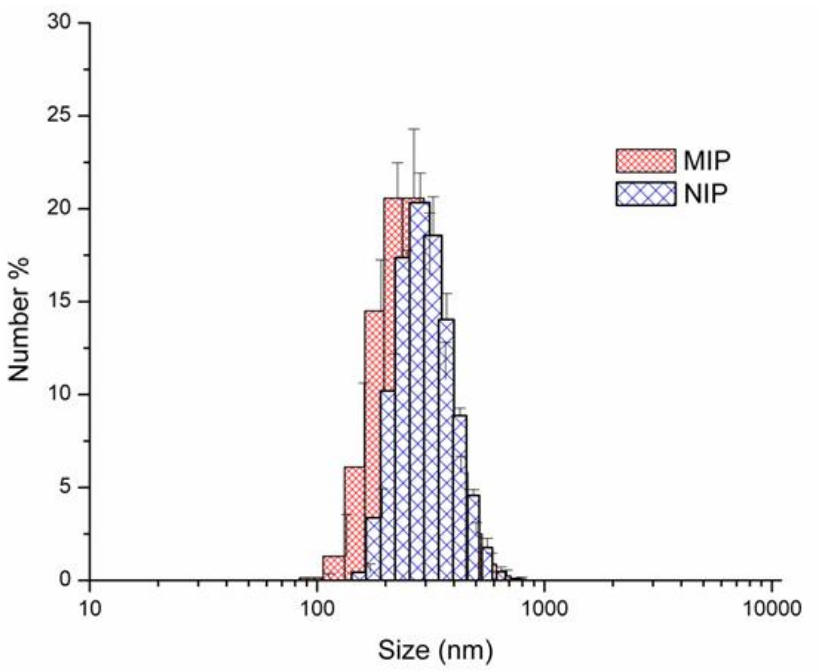

B.

	Pk. Ave. (d. nm)
NIP	362.0
MIP	328.9

Figure 4.3 Dynamic light scattering (DLS) particle characterization of methacrylic acid, 4 vinylpyridine, and ethylene glycol demethacrylate imprinted and non-imprinted polymers (A) Comparison of particles size distribution for MAA/4-VP/EGDMA non-imprinted (NIP) and imprinted (MIP) polymers. (B) Average peak diameter of NIP and MIP.

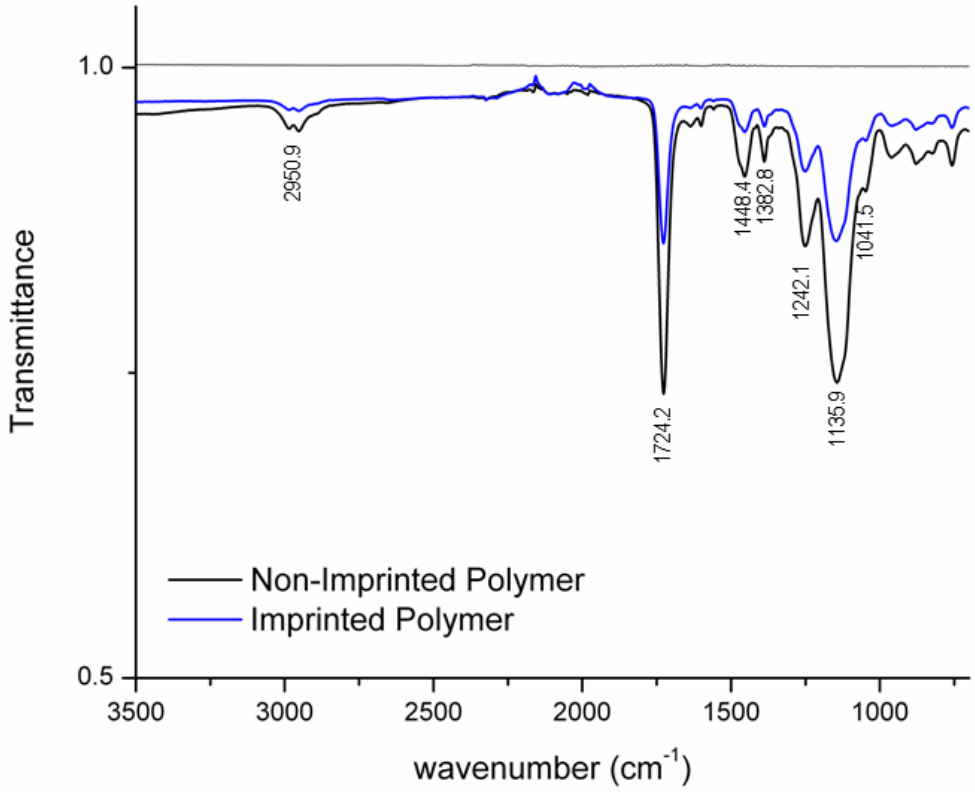

Figure 4.4 FTIR spectra of MAA/4-VP/EGDMA non-imprinted (black) and imprinted polymer (blue). The particles contained 1.25 wt% functional monomer polymerized in a 3:1 (v/v) mixture of acetonitrile and toluene.

The FTIR spectra of unloaded NIP and MIP are shown in figure 4.4. In the FTIR spectra for the NIP and MIP the medium peak at 2950.9 cm^{-1} and the peak at 1382.8 cm^{-1}correspond to C-CH_3 bending from the methyl groups of the MAA and EGDMA. The peak at 1724.2 cm^{-1} is a typical vibration of a conjugated C=O stretching vibration contributed by the MAA with some contribution from the ester bonds found in EGDMA. The peaks at 1040 and 1242 cm^{-1} are assigned to aromatic C-H bending of the pyridine group. The strong peak at 1448.4 is indicative of an aromatic ring stretch also contributed by the 4-VP. [268]

Evaluation of Adsorption Capacity

Evaluation of the adsorption capacity of the MIP to doxorubicin is critical to determining the performance of the MIP and its capability to be used as a drug delivery system. The imprinted polymer should have higher retention of the template when compared to the control polymer across a range of concentrations. Doxorubicin MIP and non-imprinted polymer particles were evaluated by measuring the fluorescence signal of the extracts obtained according to the procedure described in the experimental section. 10 mg of MIP and NIP particles incubated with varying amounts of doxorubicin (0.15 – 10 μg/mg polymer). The particles were centrifuged to remove unbound drug that remains in the supernatant. Particles were then washed with 500 μL of acetonitrile, centrifuged and drug bound specifically was finally extracted in a mixture of methanol/acetic acid and the amount of doxorubicin recovered in the extract was determined by monitoring the fluorescence at 549 nm. The washing step with acetonitrile helps remove any non-specifically bound template or template concentrated in non-specific binding sites. Each set of particles underwent a second extraction step to determine whether any sorbed template

remained in the polymer after the initial extraction. In comparing the adsorption capacity of the particles, there is a marked increase in selectivity for the template over the range of loading concentrations in the doxorubicin imprinted polymer particles (figure 4.5). The differences in the amount extracted between MIP and NIP can be seen in the loading supernatant and wash for the imprinted polymer which was visually clear compared to the control. The washing supernatant of the NIP had a significant level of drug indicating solvation of drug from non-specific or large binding sites. The amount of drug extracted in each stage was also consistent with a strong imprinting effect. After the first extraction, the MIP and NIP particles underwent a second extraction in methanol/acetic acid. Table 4.1 details the extraction levels for five different loading concentrations from two subsequent extraction steps. It can be observed that the amount of doxorubicin extracted in the second stage is greater for the MIP, which clearly indicates stronger specific interactions between the molecule of interest and the polymer taking place in the specific cavities. The precise loading and dose control capability of MIPs

Table 4.1 The amount of drug (µg) extracted in two successive extractions with a mixture of methanol/acetic acid (2.5% AcOH v/v). The extraction mixture was analyzed by fluorescence at 549 nm. The samples were taken in triplicate and mean with standard deviations reported.

	NIP		MIP	
Concentration	Extraction 1	Extraction 2	Extraction 1	Extraction 2
1 µg/mL	0.89 ± 0.027	0.24 ± 0.025	1.01 ± 0.015	0.43 ± 0.018
10 µg/mL	7.77 ± 0.02	0.95 ± 0.012	10.5 ± 0.054	1.79 ± 0.018
25 µg/mL	18.1 ± 0.043	3.09 ± 0.014	26.2 ± 0.057	9.91 ± 0.027
50 µg/mL	29.7 ± 0.125	5.62 ± 0.047	33.9 ± 0.035	13.6 ± 0.063
66 µg/mL	19.9 ± 0.10	2.41 ± 0.036	33.1 ± 0.09	9.08 ± 0.029

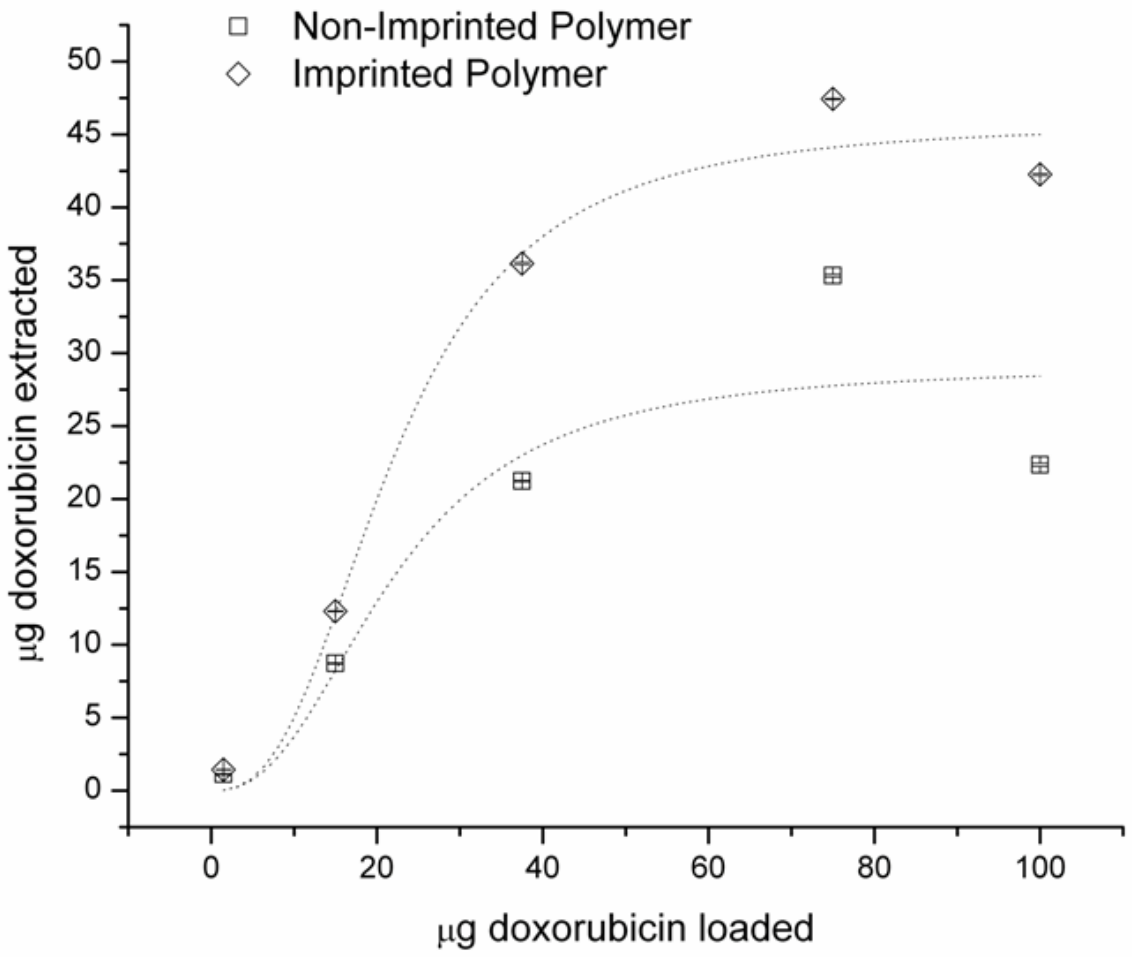

Figure 4.5 Plot of adsorption isotherm of NIP (□) and MIP (◊) loaded with doxorubicin measured by fluorescence at 549 nm. The difference in extracted doxorubicin between MIP and NIP reaches a maximum at a loading of 75 μg doxorubicin.

Evaluation of Imprinting Effect

To further characterize the recognition properties of the material, the extraction data was fit to the Langmuir isotherm model that describes a theoretical saturation value for adsorption of molecules into a surface with a discrete number of binding sites. The adsorption constant (*k*) and binding site density (*N*) were calculated by the Langmuir model expressed as:

$$B = \frac{NkC}{1 + kC}$$

where *B* is the amount of adsorbed template and *C* is the concentration of unbound template in solution respectively. *N* and *k* are the Langmuir constants for binding site density/adsorption capacity and adsorption constant. The Langmuir isotherm is derived based on the assumption (a) adsorption does not exceed beyond monolayer coverage (b) all surface binding sites are equal and can be occupied by only one template which occurs if the pre-polymerization complex is good (template-functional monomers) (c) the binding of template is not affected by the presence of template in a neighboring site that occurs if the prepolymerization complex, and subsequently the specific cavities, are distributed homogeneously along the polymeric network. The value of the isotherm constants were calculated by graphing 1/*B* versus 1/*C* where the slope of the intercept/slope corresponds to adsorption constant and 1/intercept to the binding site density. The imprinted polymer shows a higher maximum amount of sorbed species as well as a five-fold increase in the adsorption equilibrium constant. The correlation coefficients (R^2) suggest that the Langmuir model gives a satisfactory fit over the concentration range in the study that suggests that the polymer addresses the premises of the Langmuir model: discrete number of specific

binding sites that are homogenously distributed. The extended version of the Langmuir model was also used to evaluate the adsorption data but fits did not give adequate correlation over the entire range (table 4.2) for both polymer preparations.

Table 4.2 Apparent adsorption constant and binding site density for the adsorption of doxorubicin onto MIP and NIP

	Parameter	R^2	R^2 (extended)
MIP	N = 37.17 k = 0.392	0.993	0.986
NIP	N = 26.38 k = 0.069	0.998	0.859

Final application of the particles as drug delivery system requires a well characterized system, and prediction of the adsoption and release kinetics in a suitable media. The release kinetics of doxorubicin from the imprinted polymer was evaluated. Imprinted polymer particles were loaded with various amounts of doxorubicin (3.75-0.075 µg dox/mg polymer), dried, and placed in dialysis tubing. The extent of release of doxorubicin in water at 37 ºC was measured by taking aliquots at several time points and monitoring the increase in fluorescence at 558 nm. A slow release of doxorubicin was observed over the 26 hour time scale (figure 4.6). The release profile for each concentration is indicative of deviation from Fickian release behavior of particles samples with size distribution when compared to monodispersed samples[269]. Particles below the mean size distribution tend to accelerate the release of drug during the early stages while

particles above the mean suppress the release curve at later time points.[269] This is seen in the rapid release of doxorubicin in the first six hours with a leveling of release in the latter 20 hours.

Characterization of the release characteristics of doxorubicin from the molecularly imprinted polymer was done using the Peppa equation[232, 269] for non-swellable spheres:

$$\frac{B_t}{B_\infty} = kt^n$$

where B_t is the amount of drug released at time t and B_∞ is the amount of drug released at equilibrium. The *k* constant represents the apparent release rate and *n* the diffusion exponent. This model can be applied to describe the kinetics of the adsorption release in order to characterize the MIP as a drug delivery system. A plot of ln(Mt/Mo) vs. ln(t) under the highest loading conditions is shown in figure 4.7. The effect of particle distribution of the samples is seen in the calculated diffusion exponent which is below the theoretical limit for Fickian diffusion (n=0.43) as the value of n is strongly affected by the size and shape of the distribution curve for polydispersed samples.[269] However the drug release profile of drug from the polymer is indicative of controlled release behavior and this confirms the utility of our particles as a drug delivery system.

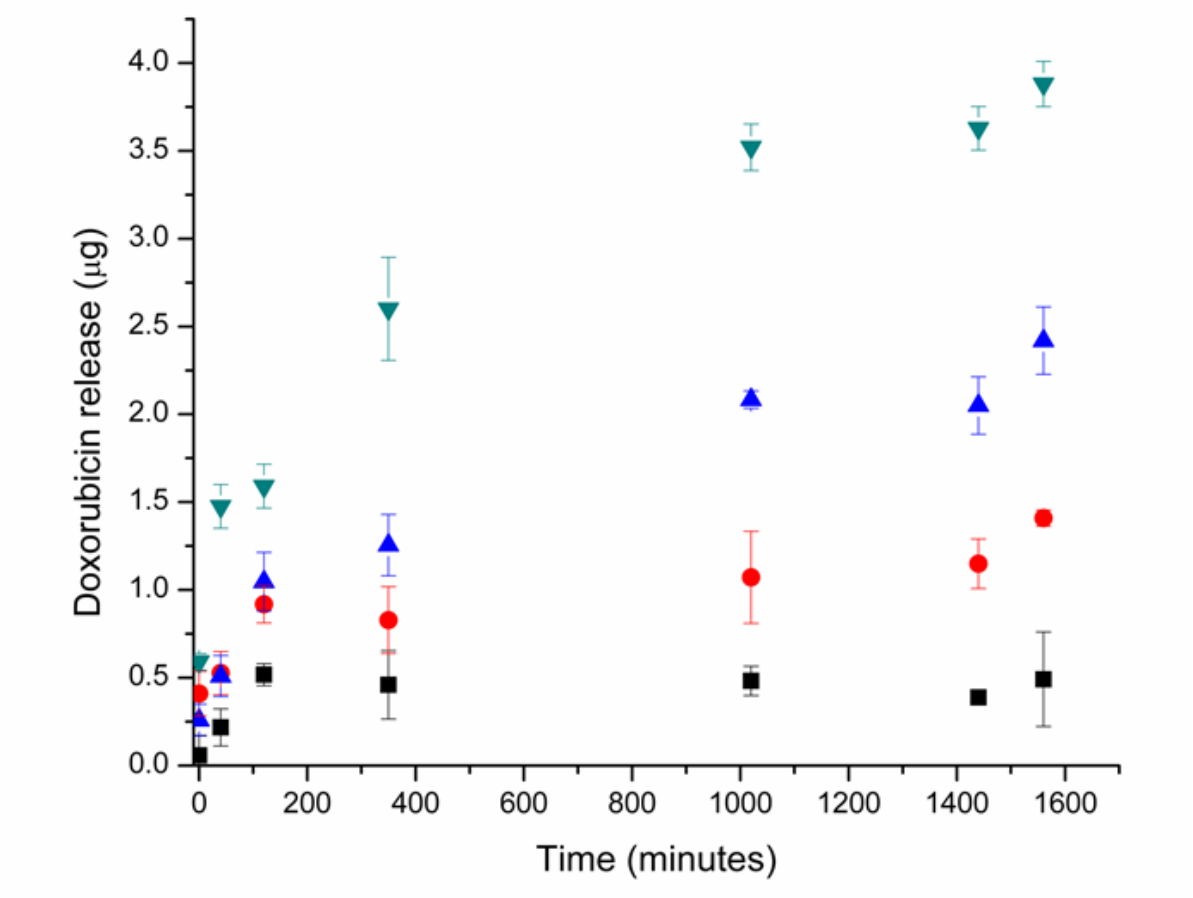

Figure 4.6 Profile of controlled release behavior of molecularly imprinted polymer for loadings of 0.075 µg dox/mg polymer (black), 0.75 µg dox/mg polymer (red), 1.87 µg dox/mg polymer (blue), and 3.75 µg dox/mg polymer (green).

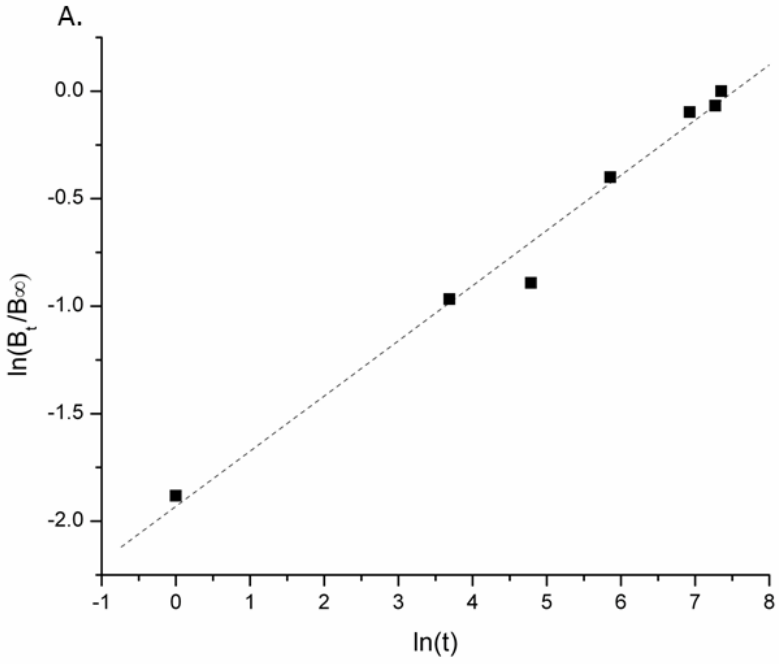

B.

Loading concentration (µg dox/mg polymer)	n	R^2
0.075	0.257	0.984
0.75	0.308	0.962
1.87	0.157	0.886
3.75	0.275	0.833

Figure 4.7 (A) $\ln(M_t/M_\infty)$ versus ln(t) plot for molecularly imprinted polymer loaded with 3.75 µg dox/mg polymer (B) Diffusion exponent calculated from $\ln(M_t/M_\infty)$ versus ln(t) plot of each loading concentration for doxorubicin-loaded polymers in water at 37 ºC

CONCLUSION

In the study we have demonstrated the synthesis and characterization of doxorubicin molecularly imprinted polymers via precipitation polymerization. The MIPs have a higher adsorption capacity than the control polymer which increases with each extraction indicating a high degree of specific binding sites within the polymer. Furthermore the release kinetics of the polymer particles in water are indicative of a diffusion based controlled release mechanism. The dissociation of the doxorubicin from the polymer can be improved by decreasing the concentration of cross linker in the polymerization mixture which produces to more flexible

cavities. The carboxyl groups on the surface of the polymer can be used for further modification for targeting or photo-responsive imprinted polymers.

Chapter 5: Synthesis and Characterization of Silica-Au-Molecularly Imprinted Polymer SERS Substrate for Detection of Thiabendazole

INTRODUCTION

Rapid and accurate monitoring of environmental or biological samples for contaminants for food supply protection to bio-warfare is an important topic in the sensing field[59, 91]. Chemical and biological sensors are gaining increased prominence in the field as of signal transductions become more sophisticated. Chemical and biological sensors typically classified by the method of signal transduction which can be optical, electric, electrochemical, mass sensitive, magnetic, or thermometric[270]. Biological sensors also take advantage of biological macromolecules with specific recognition for ligands to impart a high level of specificity to the system. However, there is a need to develop analytical techniques that are capable of detecting a particular analyte without the aid of a secondary label. In the case of biological sensors, many of the biological macromolecules, such as antibodies or receptors, are particularly sensitive to media composition and storage conditions. This can limited their ability to be integrated into truly field portable devices.

Molecularly imprinted polymers (MIPs), synthetic polymers with specific recognition sites to a target analyte within the material scaffold, have the potential to overcome these challenges. MIPs are normally prepared by copolymerizing a functional monomer(s) with a crosslinker in the presence of a template molecule in solution. After polymerization, the template is removed from the polymeric network revealing cavities with specific molecular recognition properties. The advantages of MIPs, compared to receptors of biological origin, include greater mechanical

and thermal stability, as well as very low cost of preparation [113]. These advantages enable MIPs to function under a wide range of operating conditions, making the technique of molecular imprinting a very useful tool in many analytical fields, such as extraction techniques, chemical separation techniques and chemical sensing. These materials are also simple to prepare, scalable, and can be integrate into a variety of platform like microfluidics. MIPs have been used in a variety of formats and detection applications over the past two decades [271].

Surface Enhanced Raman Spectroscopy (SERS) can be used to tackle the issue of field portability and signal transduction. Surface Enhance Raman is a form of Raman spectroscopy where the transitions between vibrational states are studied when a molecule in-elastically scatters light. The technique is highly sensitive with enhancement factor of at least 10^6 and single molecule detection has been reported[52, 55, 272-276]. The power of this technique lies in the multiplex capability as the Raman spectra has far less spectral overlap compared to fluorescence. SERS substrates have also been used with commercially available hand held devices with *parts per trillion* level detection limits[218]. It is therefore possible to merge the specific capture and retention capability to a MIP with the sensitive analytical capacity of SERS to make a truly field portable, rapid, and specific sensor. For a successful integration of both techniques, the distance between the molecule to be measured and the metal nanoparticles responsible for signal amplification is of great importance. For best signal enhancement, the molecule to be measured needs to be in close vicinity to the metal colloids. There are successful attempts combining both approaches, such as gold nanoparticles embedded in a layer of MIP prepared by emulsion polymerization[210]. However, this approach does not guarantee a precise control of polymer particle size in the nanometer range. Furthermore, since SERS is a phenomenon restricted to the

surface, is convenient to use techniques that allow polymerization on surface controlling the thickness of the MIP layer. Thus, diffusion and access of the target molecule to the polymer matrix is easier and the analyte can be recognized by the MIP in proximity to the metal colloid.

In this regard, polymerization *via-iniferter* (**ini**tiator, trans**fer** agent, **ter**minator) is a suitable approach that permits precise control of the thickness of a layer of polymer prepared from a surface area where the initiator is coupled by varying the UV exposure time [277]. The main advantage of using iniferter-type initiators (eg dithiocarbamates) instead of conventional azo-based initiators, resides in its radical products. Iniferters generate two free radicals, one of which is active and coupled to the surface; another free radical that is inactive and stable in solution but capable of terminating the growing polymer chains by recombination. In this manner, polymerization occurs only via the active radical immobilized onto the support surface, and polymerization in solution is avoided.

In this work we report the development of a prototype SERS-MIP composite microparticles based on the principle of living free radical polymerization of the MIP from the surface of a novel SERS substrate for adsorption and detection of thiabendazole (TBZ), a widely used benzimidazole fungicide.

EXPERIMENTAL

Materials

Phenyltrimethoxysilane (PTMS), methyltrimethoxysilane (MTMS), (3-Aminopropyl) trimethoxysilane (APTMS), (3-Aminopropyl) triethoxysilane (APTES) ethylene glycol dimethacrylate (EGDMA), and methacrylic acid (MAA), thiabendazole (TBZ), tetrachloroauric

(III) acid, sodium citrate, 2-(N-morpholino) ethanesulfonic acid (MES), and sodium diethyldithiocarbamate trihydrate were obtained from Sigma Aldrich. (*p*-Chloromethyl) phenyltrimethoxysilane (CBTMS) was purchased from Gelest. HPLC grade toluene, tetrahydrofuran (THF), and acetonitrile (ACN) were at least HPLC grade from Sigma Aldrich. All other chemicals were used as received.

Methods

Synthesis of gold nanoparticles

Colloidal gold nanoparticles (AuNP) were prepared by reduction of chlorauric acid with sodium citrate, according to a methodology adapted from Frens. [66] In brief, 50 mL of a $HAuCl_4$ (1mM) aqueous solution were heated to boil and a fixed amount of sodium citrate solution (1%) was then added. The reaction mixture was cooled after 20 min of boil. The concentration of AuNPs in the resulting solution was determined by absorbance measurements (λ=520nm) using a Nanodrop ND-1000 spectrophotometer (Thermo Scientific; Rockford, IL) and molar extinction coeffiecients for AuNPs derived from Yguerabide et al. [213]

Synthesis of organically modified core shell silica microspheres

Silica microspheres containing a hydrophobic core with a hydrophilic shell were prepared according to a modification of the procedure described by Koo et al [278]. To form the core, 62 mL of deionized water and 76 µL of HNO_3 was heated to 60 ºC in a 100 mL round bottom flask in a water bath on a hot plate stirrer. Once the temperature of the reaction mixture reached 60 ºC, 707.8 µL (3.72 mmol) of PTMS was added to the flask and the mixture was vigorously stirred for 30 seconds. After which, 15 mL of NH_4OH was added to the flask. The solution was kept

stirring for an additional hour until the solution turned a milky white. The shell was prepared by separately combining 262.7 µL (1.5 mmol), of APTMS, 330 µL (1.5 mmol) of CBTMS, and 641.25 µL (4.5 mmol) of MTMS in a glass vial and adding the mixture to the flask all at once. The suspension was kept stirring for 75 minutes. The resulting particles were vacuum filtered through a 0.45 µm pore size Magna nylon membrane filter (Osmonics, Minnentoka, MN). The microspheres were washed three times with water and then resuspended in 1:2 mixture of water/ethanol and sonicated. The particles were filtered a second time in the same manner and allowed to air dry.

Iniferter Modification of Silica microparticles

250 mg of silica microparticles were resuspended in 2 mL of THF. The suspension was kept stirring while 1 mL of a solution of sodium diethyldithiocarbamate (10 mg/mL) was added dropwise to the suspension. The suspension was stirred for 3 hours and then vacuum filtered through a 0.45 µm pore size Magna nylon membrane filter (Osmonics, Minnentoka, MN) and washed three times with THF. The particles were allowed to air dry overnight.

Preparation of Silica-Gold composite microspheres

200 mg of iniferter modified silica microparticles were suspended in 5 mL of deionized water. 5 mL of Au-NPs were added to the suspension in 1 mL aliquots. The particles were stirred for 1 hour and excess Au-Nps were removed by centrifugation at 1,500 x g in a microcentrifuge. The particles were resuspended in THF centrifuged a second time. The particle pellets were air dried overnight.

Grafting of MIP on Iniferter modified Silica Microparticles

200 mg of iniferter modified silica was suspended in 2 mL of a MIP polymerization mixture containing 11.7 mg of TBZ (1 mmol), 40 mg of MAA (8 mmol) and 460 mg of EGDMA (40 mmol) in 6.25 mL of toluene. The suspension was purged with argon for ten minutes and then the glass vial was tightly sealed. The polymerization was carried out using UV-irradiation at 4 ºC with a Spectroline EB-280C UV lamp (Westbury, NY). The vials were placed on top of an orbital shaker 5 cm from the lamp. After 10 hours of irradiation the Si-MIP particles were centrifuged to remove polymerization mix. The particles were resuspended in toluene and centrifuged to remove the solvent. The template was extracted from the Si-MIP for SERS measurements by four warm sonication baths at 50 ºC using a mixture of acetonitrile/acetic acid (1:1, v/v). The nonimprinted polymer (Si-NIP) was prepared in the same fashion but without the addition of thiabendazole.

Characterization

Dynamic Light Scattering measurements

The size of the microspheres was analyzed through dynamic light scattering (DLS). Dilute suspensions of the different particles were prepared using water as dispersant and transferred to 400 µL disposable sizing cuvettes, measuring the diffusion of the particles moving under Brownian motion using a Zetasizer Nano-ZS (Malvern Instruments Ltd, Worcestershire, UK).

Scanning Electron Microscope Imaging

Scanning Electron Microscope (SEM) was used to characterize the microparticles. The images were obtained using a LEO 1550 FESEM (Keck SEM). The dried particles were first coated with

an electrically conductive gold-palladium coating approximately 10 nm thick and then placed on a silicon wafer for imaging. The resolution at 5 KeV was 2.5nm.

Fourier Transform - Infrared Spectroscopy (FT-IR)

FTIR spectra for the pesticide loaded microparticles were generated using a Bruker Optics - Vertex80v FTIR spectrophotometer equipped with a diamond ATR crystal accessory for analysis of bulk samples. FTIR spectra were acquired between 450-7000cm^{-1}.

SERS Measurements

30 mg of Si-NIP and Si-MIP were incubated overnight in 1.5 mL of TBZ solution in toluene to a final concentration of 100 µM. The particles were centrifuged and resuspended in 300 µL of water. Glass microscope slides were cleaned with nitric acid, thoroughly rinsed with DI water and dried under argon flow. 100 µL of 5 mM APTES solution was deposited on the glass surface for 15 min. The substrates were then rinsed with DI water and dried under argon. A 100 µL aliquot of the Si-NIP and Si-MIP suspension were placed on the APTES modified glass slide and air dried. SERS spectra were obtained using a Renishaw InVia Confocal Microscope system (Renishaw Inc; Hoffman Estates, IL) equipped with a 785 nm edge laser and Renishaw CCD Camera (Renishaw Inc; Hoffman Estates, IL) fitted to a Leica microscope.

RESULTS AND DISCUSSION

Formation of core shell silica nanoparticles

In this work we are presenting the preparation of silica-Au-MIP (Si-Au-MIP) composite SERS substrates for detection of thiabendazole. Figure 5.1A details a schematic of the design process for the composite SERS substrate. The support of the substrate is a silica-based microparticle

decorated with functional amine and phenyl methyl chloride groups. The silica support was designed to have two functionalities. The first function was to serve an initiator surface for polymerization of the MIP layer by grafting from the silica particles [279, 280] taking advantage of this well characterized polymerization chemistry. Its second function is to act as SERS substrate enhancing the Raman signature of the target molecule selectively recognized by the MIP layer. For this purpose, gold nanoparticles are attached to the surface of the silica support, before grafting with the MIP layer.

When designing the Si-Au-MIP composite we must take into account the need for the analyte to be in close proximity to the SERS substrate. While other SERS substrates rely on non-specific binding/interaction of the analyte on the surface, our MIPs can selectively bind and at the same time bring the analyte in close proximity to the surface of the SERS substrate. As only the analyte of interest is trapped close to the SERS substrate, the system proposed here avoids the occurance of background signal of undesired compounds potentially present in the samples, providing added selectivity and sensitivity to the measurements. Thus, this composite material simultaneously acts as both an extracting agent and detection system.

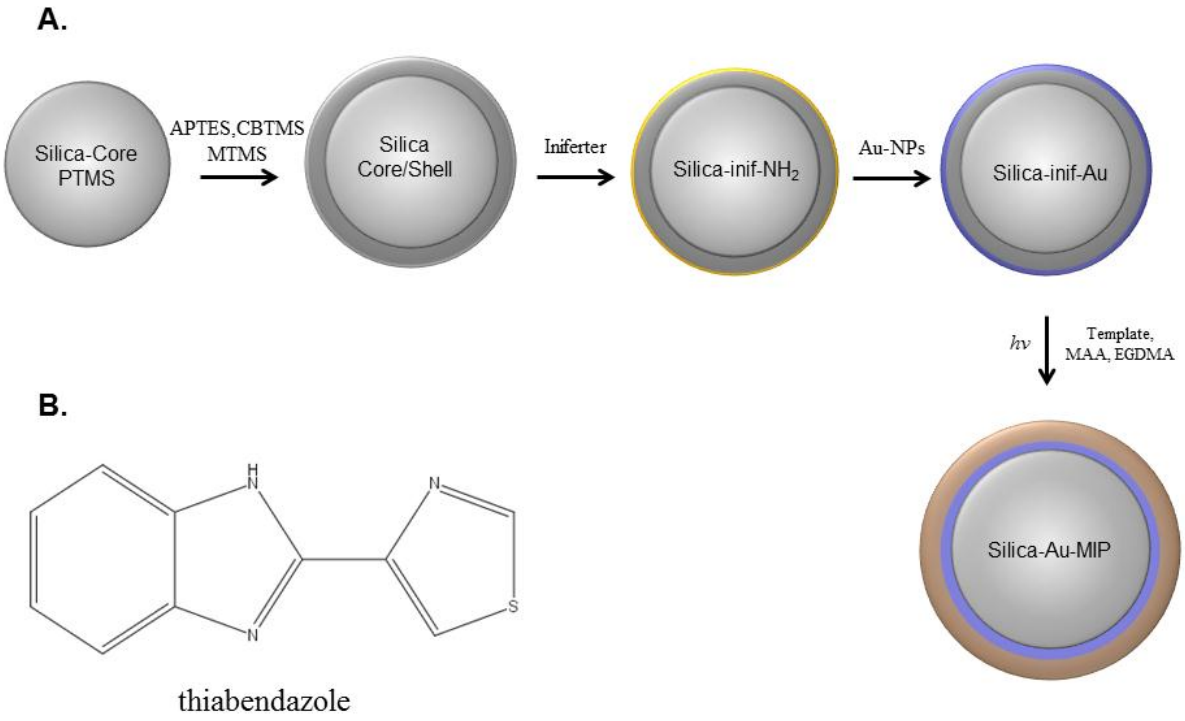

Figure 5.1 (a) Schematic representation of Si-Au-MIP preparation. Process begins with preparation of a hydrophobic phenyltrimethoxysilane (PTMS) core. A hydrophilic shell of methyltrimethoxysilane (MTMS), (3-Aminopropyl) trimethoxysilane (APTMS), and (*p*-Chloromethyl) phenyltrimethoxysilane (CBTMS) was formed around the core. Sodium diethyldithiocarbamate trihydrate reacts with the CBTMES to form the iniferter modified surface. 40 nm Au-NPs attach to the surface via interaction with the amine groups from APTMS. Polymer synthesis is initiated from the surface of the particle through UV formation of iniferter radicals (b) Chemical structure of thiabendazole

Core-shell silica microspheres were synthesized in a two-step synthesis process using the precursors, PTMS, MTMS, APTES, and CBTMS. Initially, 3.72 mmol of PTMS was hydrolyzed in a dilute solution of nitric acid. The silane monomers were then condensed under basic conditions by adding 15 mL of NH_4OH and the solution was stirred for an additional hour to form the hydrophobic core. The size of the particle core can be adjusted by either reducing the concentration of PTMS or increasing the duration of hydrolysis. We designed the synthesis of particle cores that are approximately 1 μm in diameter by using a high concentration of PTMS and a short hydrolysis time. We desired each Raman measurement to be restricted to an individual microsphere surface as studies have shown that variation in signal using microsphere-AuNP composite substrates is independent of the number of microspheres in the sample. [218]

The microspheres cores were capped with a mixture of APTMS, MTMS, and (p-chloromethyl) phenyl –trimethoxysilane (CBTMS). The capping mixture was added to the PTMS core suspension and stirred for 75 minutes. The comparatively more hydrophilic shell of MTMS imparts an increased level of solubility to the microparticles in aqueous solutions. The amine functionality provided by the APTMS is used for formation of microsphere composites with an external layer of gold nanoparticles. The halogenated silane CBTMS, provides functionality for modification of the surface with the dithiocarbamate iniferter molecule for later MIP polymerization. Figure 5.2 shows an SEM image of the unmodified silica microparticles. The core-shell microparticles show no visible signs of aggregation and have a narrow size distribution.

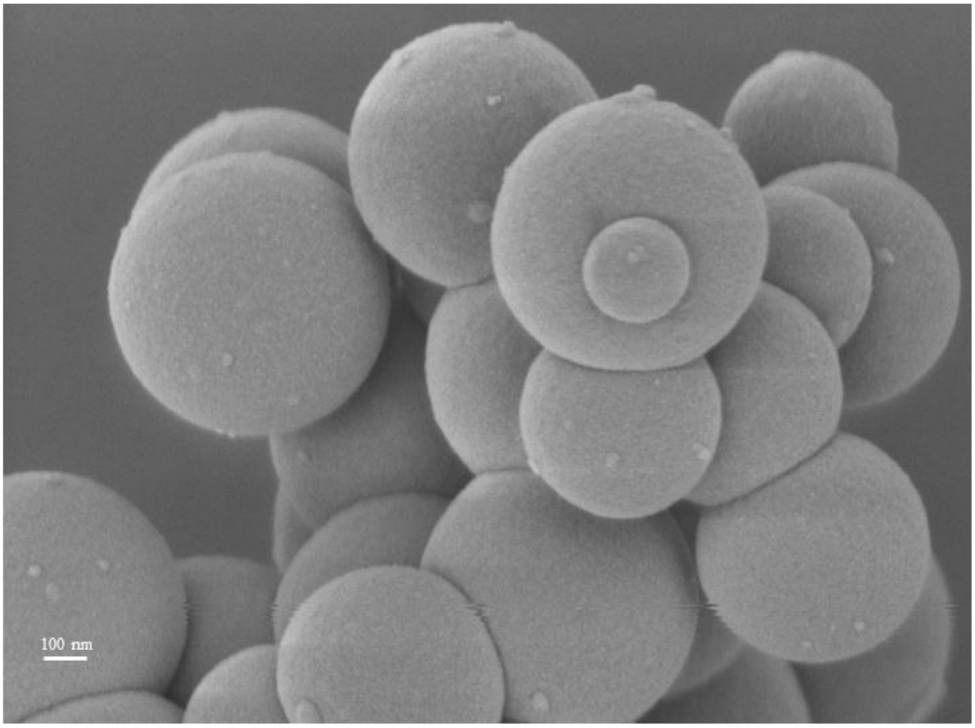

Figure 5.2 Representative SEM image of core-shell silica microparticles prepared with a core layer of trimethoxyphenylsilane (PTMS) and a shell layer consisting of trimethoxymethylsilane (MTMS), (3-aminopropyl)trimethoxysilane (APTES), and (*p*-chloromethyl) phenyl-trimethoxysilane (CBTMS).

After modification of the surface with the dithiocarbamate iniferter, the particles showed no visible differences in morphology (figure 5.3A) The average size of the particles is approximately 1.3 μm which is comparable with the focal volume of the laser (figure 5.3B). The core-shell silica microparticles were then coated with a layer of gold nanoparticles. A SEM image of the composite microparticles is shown in figure 5.3C. The gold attaches to the surface with some clustering. However, the particles are still well distributed across the entire surface forming multiple junctions for potential SERS "hot-spots". The particles also maintained their morphology and did not aggregate in solution. The average size of the particles increased slightly

(figure 5.3D) which was expected after attaching the gold nanoparticles onto the surface via interactions with amine groups.

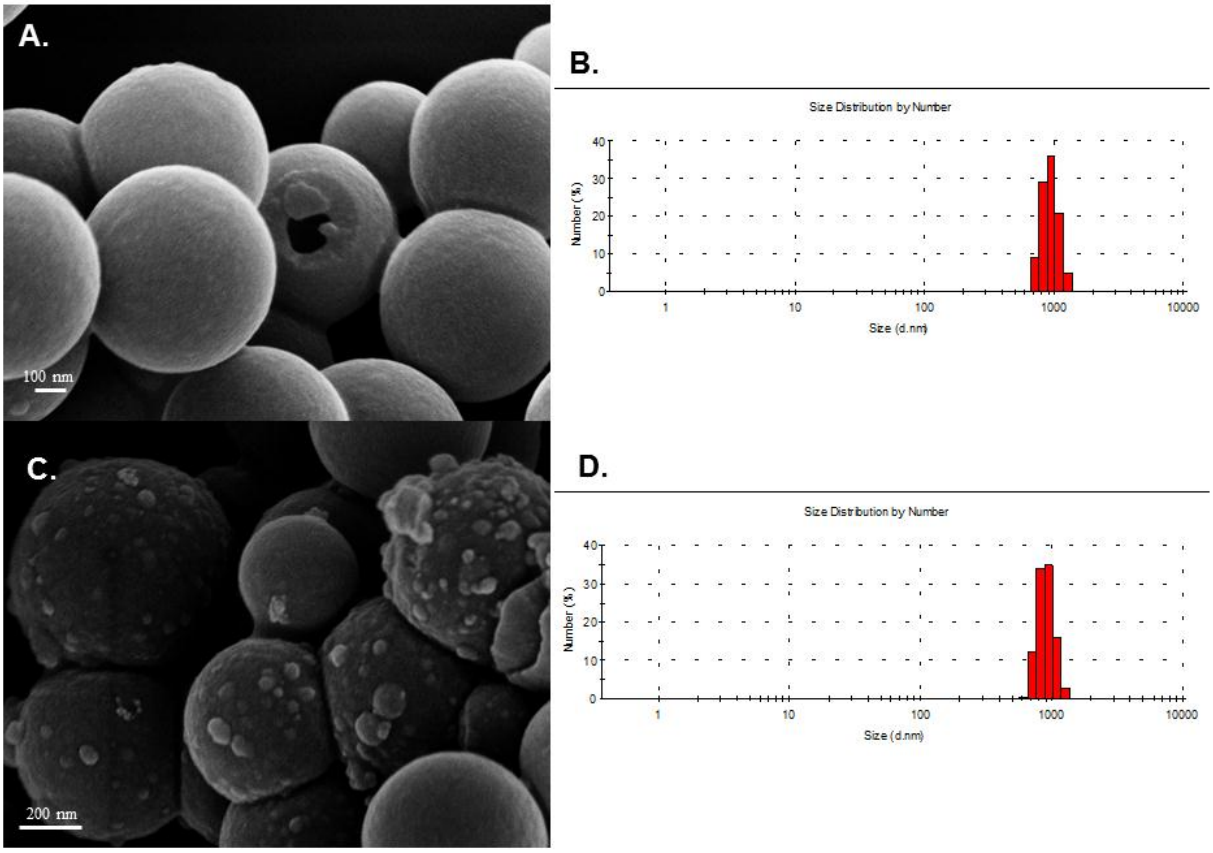

Figure 5.3 (a) Representative SEM image of iniferter modified microspheres. (b) Histogram of number percent size distribution of iniferter modified particles measured using dynamic light scattering. (c) SEM image of Si-Au composite particles after coating with 40 nm gold nanoparticles. (d) Histogram of size distribution of Si-Au composite microparticles.

FTIR characterization of core-shell particle synthesis

An evaluation of the surface modifications during each step of the synthesis of the microsphere composite was carried out using FTIR. The core-shell microparticles showed several characteristic peaks as illustrated in figure 5.4. The peaks between 700-800 cm^{-1} can be assigned to the aliphatic chloro group of CBTMS. The strong band at 1000-1100 cm^{-1} corresponds to the organic siloxane groups contained in all of the monomers. The peak at 1429 cm^{-1} is assigned to the methyl C-H asymmetric/symmetric bend contributed by the CBTMS. The small peak at 1591 cm^{-1} is from the primary amine group on the APTES.

After reaction with the dithiocarbamate group, the FTIR spectra of the iniferter-modified core-shell silica microparticles were compared to the base core-shell particles (figure 5.4). Several distinct peaks were seen in the iniferter-modified particles that did not appear in the unmodified particles. The most obvious distinction is a strong band at 2900-3000 cm^{-1}, assigned to the methyl asymmetric/symmetric stretch from the iniferter terminal methyl groups. Another strong peak appears at 1770-1720 cm^{-1} which can be assigned to the carbamate ester in the iniferter. The iniferter modified core-shell particles still had a strong band for the chlorine of the CBTMS which indicates incomplete reaction of the surface.

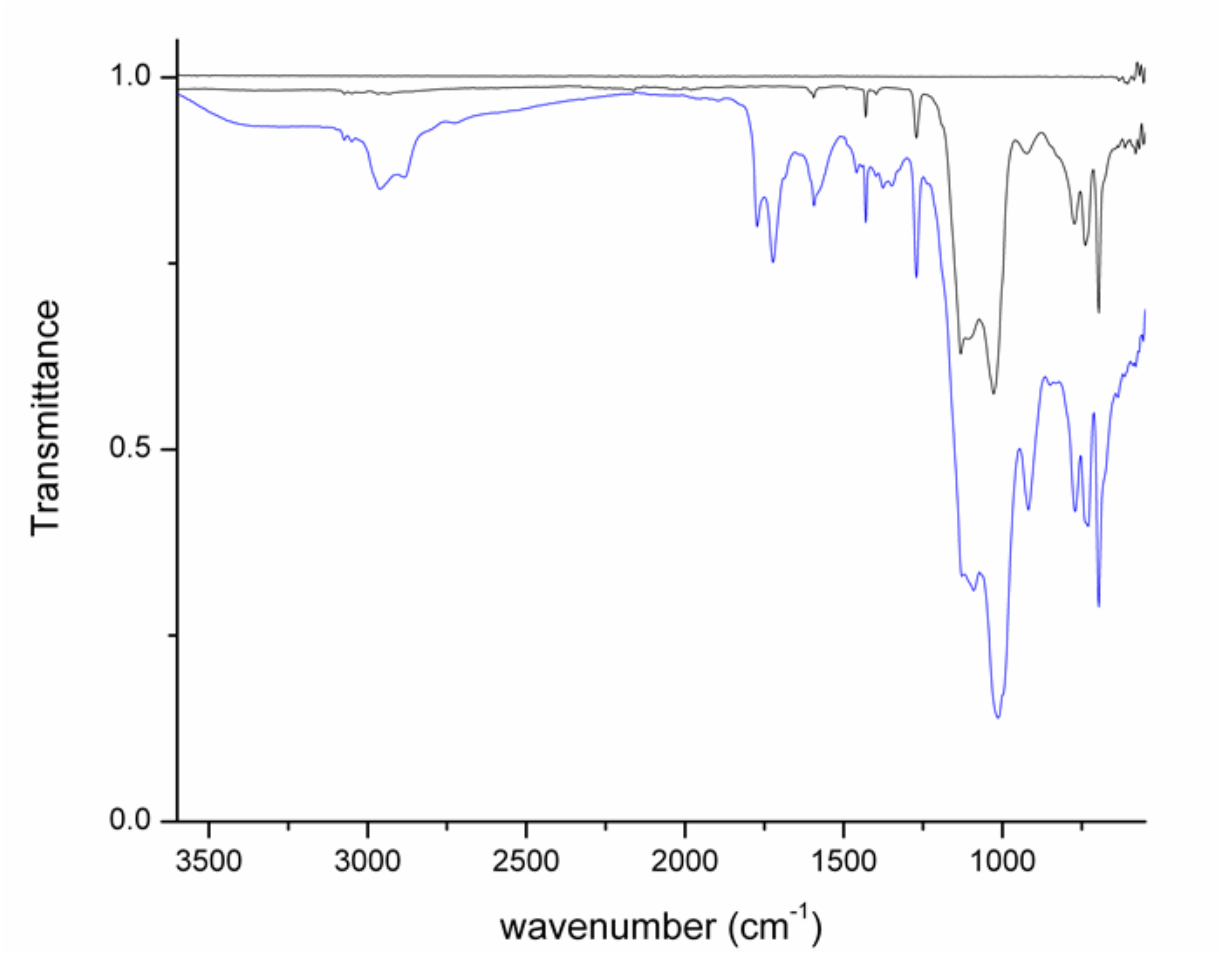

Figure 5.4 FTIR spectra of core-shell particles (black) and iniferter-modified core-shell particles (blue). Characteristic peak of methyl groups contributed by sodium diethyldithiocarbamate trihydrate are seen at 2900 cm^{-1}.

Characterization of Molecularly Imprinted polymers

A MIP for TBZ was polymerized from the surface of the core-shell iniferter modified particles for 12 hours at 4 ºC by UV radiation. This kind of MIPs has been polymerized from the surface of core-shell particles in literature[279, 280]. However, there is a lack of studies reporting this type of polymerization in systems with the presence of gold nanoparticles, which presumably could have an impact in the following MIP grafting. In our work, despite the presence of gold nanoparticles on the surface of the modified silica beads, the polymerization *via-iniferter* was carried out successfully from those regions in the core-particles still exposed to the UV radiation. The particles were subsequently analyzed by SEM to determine if the polymer did form on the surface of the particle. Figure 5.5A shows an SEM image of an extended network of polymer around individual and groups of particles of some thickness for the Si-Au-MIP composites. The relative thickness of the polymer was difficult to analyze as the polymerization resulted in cross reaction of polymer into aggregates. The particles were analyzed by dynamic light scattering (figure 5.5B) which showed an average particle size of approximately 3.5 μm in diameter. However this figure can be attributed to a measure of the aggregate size and not of an individual microparticle thickness.

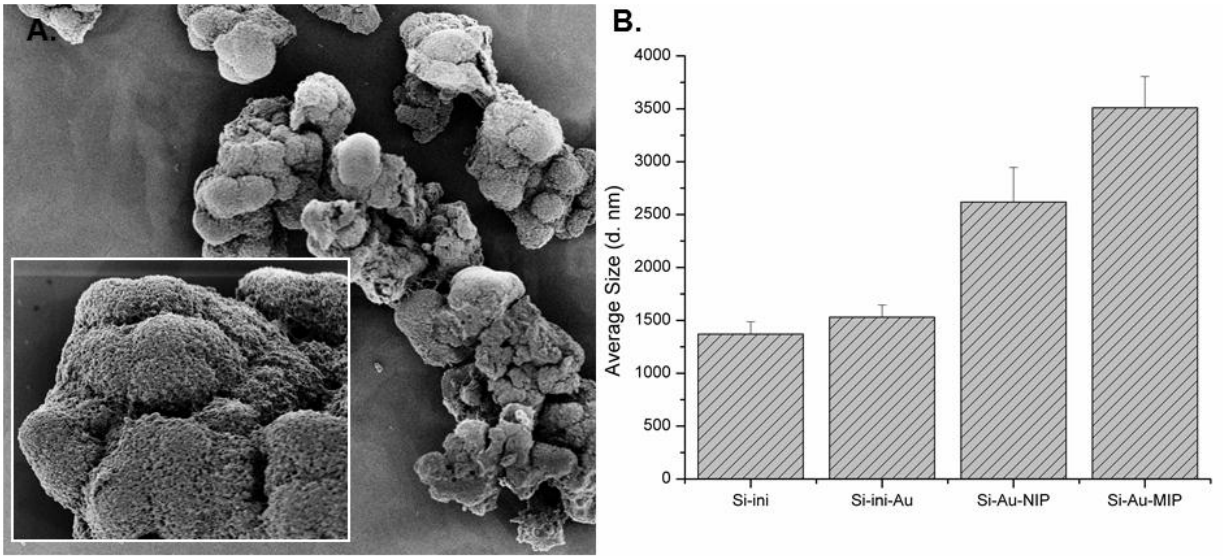

Figure 5.5 (a) SEM image of iniferter modified Si-Au composite microparticles with molecularly imprinted polymer of thiabendazole grown from the surface. Imprinted polymer was made from MAA and EGDMA at a ratio of template to monomers 1:8:40 in toluene. (b) Average diameter of microparticles at different stages in the preparation as analyzed by dynamic light scattering.

The FTIR spectra of the core-shell composites microparticles and the core-shell-MIP microparticles are shown in figure 5.6. There is a marked difference in the spectra which can be attributed to the mechanism of iniferter directed formation of polymer. As the iniferter polymerizes it can also act as a terminator of the polymer chains. Therefore the MIP surface should be decorated with terminating carbamates. Confirmation that this polymer was indeed polymerized from the surface via the iniferter is the strong band at 2900 cm^{-1} that corresponds to the methyl groups of the iniferter. Interestingly this peak does not appear in the Au coated composite particles. Other peaks can be assigned to MAA and EGDMA, in particular the strong peak at 1700 cm-1 is assigned to the carboxyl group of the methacrylic acid. The peak at 1380 cm^{-1} is assigned to the C-CH_3 bending vibrations of the methyl groups of MAA, EGDMA, and dithiocarbamate. The strong peaks between 950 cm^{-1} and 1225 cm^{-1} are contributed by the thiabendazole aromatic C-H in plane bends.

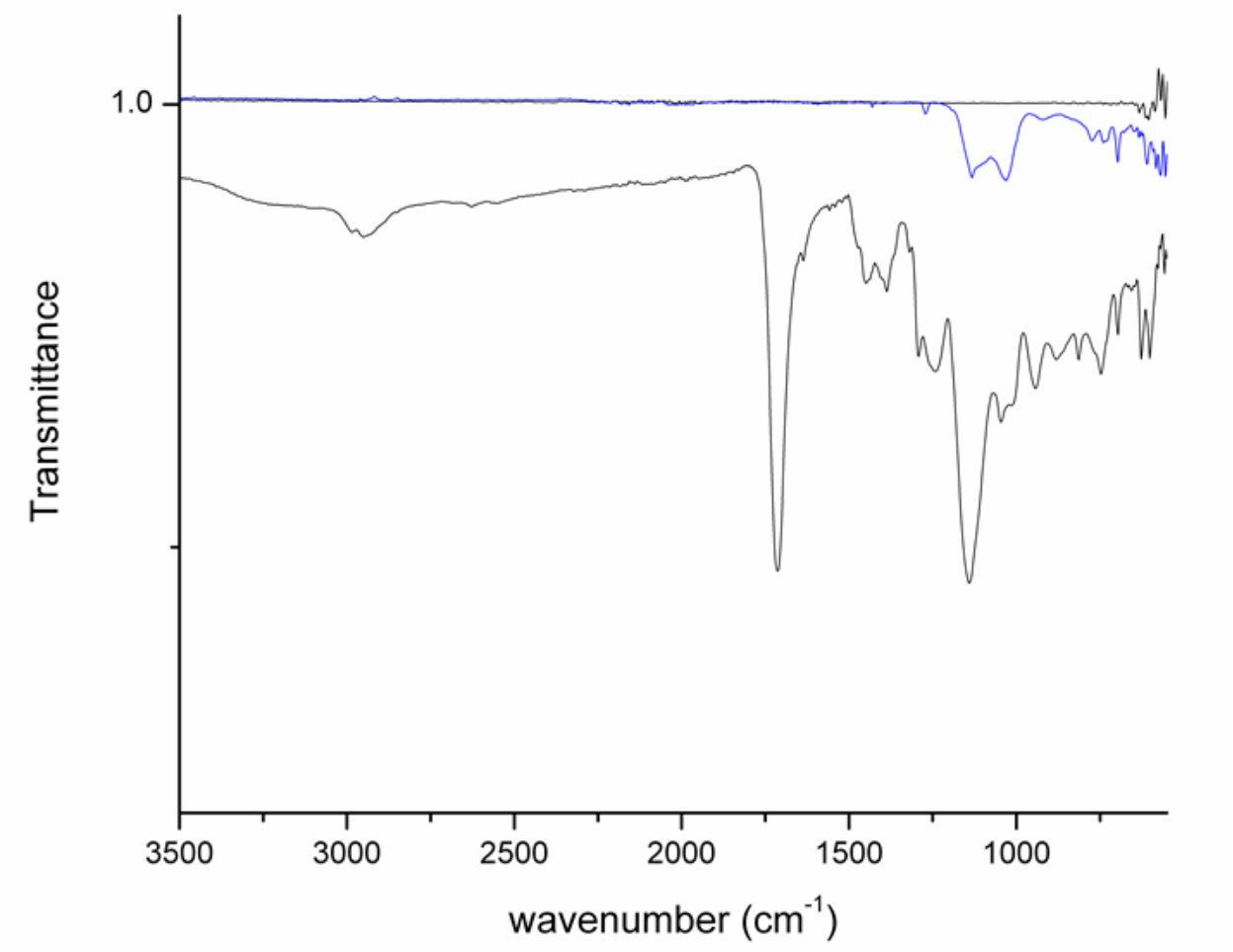

Figure 5.6 FTIR spectra of Si-Au composite particles (blue) and Si-Au-MIP composites (black). The characteristic peak of the iniferter termination is seen at 2900 cm^{-1}. A strong peak for the carboxyl group of MAA is seen at 1700 cm^{-1}.

SERS detection of thiabendazole

To test the Si-MIP composite particles ability to act as a SERS substrate, the template was first extract and then Si-NIP and Si-MIP composite particles were reloaded with 100 μM solution of thiabenzadole in toluene overnight. The particles were washed and analyzed for SERS activity. Reloading of the particles with template in organic media promotes hydrogen bonding interactions in the specific cavities. Depending on the solvent used for reloading we can clarify the origin of the differences in binding specificity between MIP and NIP. Figure 5.7 illustrates the signal generated from the Si-Au-MIP and Si-Au-NIP particles under 10% laser power. Of note is that despite the thick layer, the analyte was capable to access to the specific binding sites in the MIP network, permitting the interaction with the plasmons occurred on the metal colloid surface, allowing thus the desired SERS effect. Our developed Si-Au-MIP particles had a characteristic peak at 1279 cm^{-1} which can be attributed to selective detection of TBZ by our system [281]. The peak at 1279 cm^{-1} as well as the bands at 1580 and 1452 cm^{-1} can be attributed to ring stretching vibrations[281-283]. These peaks are not present in the spectra obtained under the same conditions with the Si-Au-NIP system. Both spectra share a peak at 1000 cm^{-1} that most likely is the dithiocarbamate SERS signal, as the thiol groups can interact with the gold on the surface of the particle. This fact clearly suggests an effective imprinting that permitted to the analyte to access to the proximity of the gold nanoparticles by permeability through the polymer network establishing specific analyte-polymer interactions. However, the formation of aggregates and clusters of the composite material can have the effect of potentially difficult the access of analyte to the surface of the metal. An improved adjustment of the polymerization time can overcome this issue. We successfully demonstrated the possibility of polymerizing via the

iniferter technique from a surface with the presence of AuNP previously attached on it. Moreover, the grafting of a MIP layer showed an effective imprinting, allowing the detection of TBZ in toluene that was not possible with the NIP.

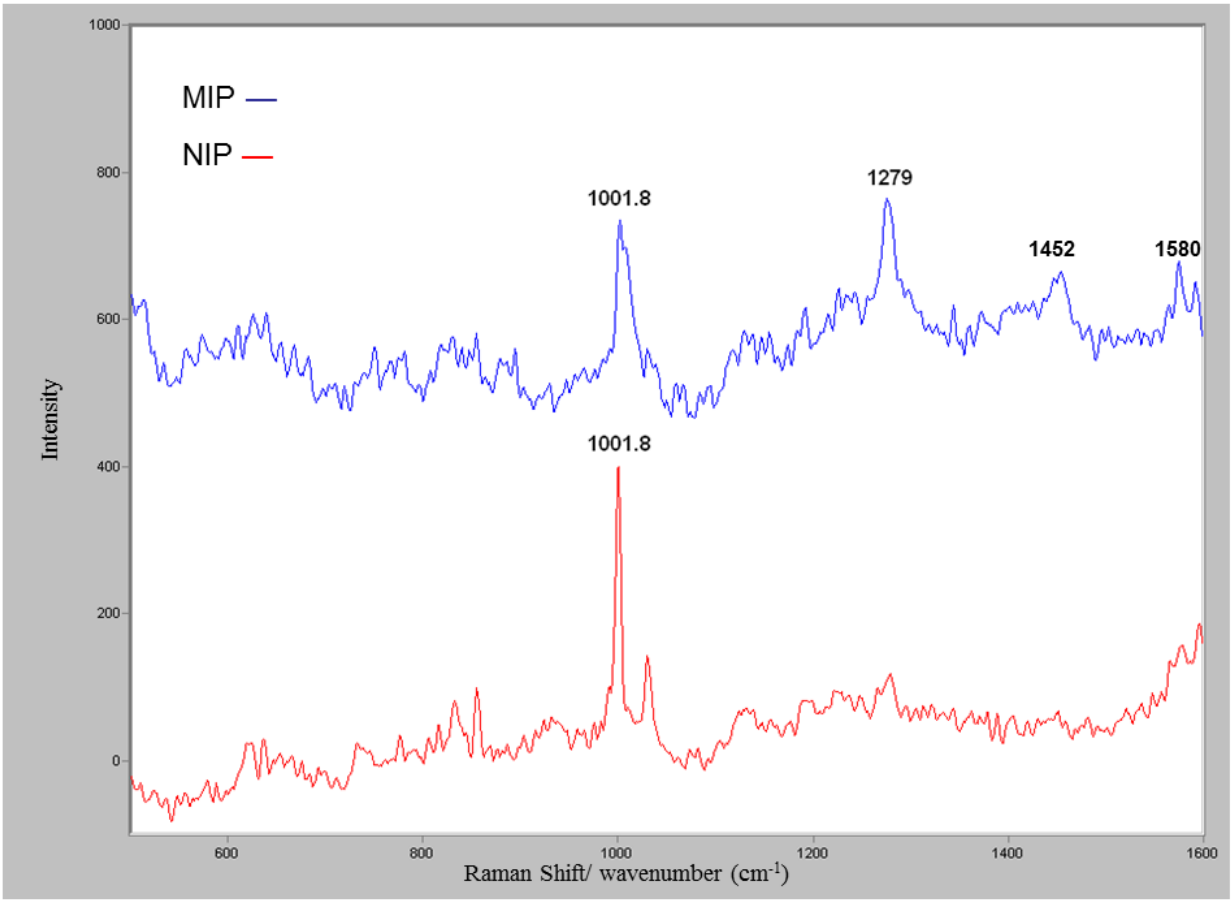

Figure 5.7 Comparison of SERS detection of TBZ using 1279 cm^{-1} peak with Si-Au-MIP and Si-Au-NIP composite substrates: Additional medium intensity bands for TBZ can be found at 1452 cm^{-1} and 1580 cm^{-1}. The substrates were incubated with a 100 µM solution of thiabendazole in water. Spectra are offset for clarity.

CONCLUSION

In summary, this work shows the feasibility of fabrication of a SERS-MIP substrate using iniferter living polymerization from the surface of a gold coated pre-formed particle. Further investigations will address optimal polymer grafting by adjusting the polymerization time. Also the binding capacity of the polymer, and the analytical performance of the SERS substrate will be completed for a more accurate determination of the detection power of the system. Future studies will also test this system in the presence of a mix of related pesticides to clearly demosntrate the specificity provided by this MIP-based sensor for final field applications.

Chapter 6: Teaching bioengineering and nano-technology in the middle school classroom environment.

INTRODUCTION

Use of the scientific method and inquiry based learning in the classroom is not often explored in secondary education. To develop specialized instruction to employ this teaching style, a partnership was developed between a Cornell University graduate student and the 8th grade earth and physical science classes at Boyton Middle located locally in Ithaca, NY and taught by Mrs. Anne Gleed. This collaboration was supported by the National Science Foundation funded GK-12 program, which provides graduate students in the sciences the opportunity to communicate their research to grade school students. Building these collaborative relationships is critical to inquiry based learning; working as a collaboration with the middle school teacher allowed for the teacher to use the resources of an collegiate laboratory [284]. The goal of the curriculum is to increase students' exposure to research as it relates to nanotechnology and bioengineering. For the curriculum guided inquiry based teaching technique was employed and four modules designed for inquiry based learning in a middle school classroom.

The authors of the National Science Education Standards (NSES) define inquiry as a learning process in which the students are engaged in active learning, referring to inquiry as "something the students do, not something that is done to them" [285]. The NSES state that inquiry is central to learning science, allowing students to combine scientific knowledge with reasoning and thinking skills (p.2)[285]. The inquiry teaching method is based on the claim that "knowledge is built primarily from the learner's experiences and interactions with phenomena"[286]. With inquiry

based learning the student is a self-directed learner that processes information, makes observations, forms hypotheses, designs his or her own activities, and shares authority for their conclusions [287, 288]. As opposed to the traditional system where the student is a passive learner recording and memorizing given information, following directions, and deferring to the teacher as the authority [287]. As an active learner the student is able to think scientifically and view the world from a scientific perspective [289].

The facilitator's role is to develop opportunities and the framework in which students are able to generate appropriate conclusions and to guide the students as necessary [286]. The instructor must begin by introducing the students to a concrete concept, followed by encouraging the students to make observation, raise questions, or make generalization from their observations [286].

To accomplish this task, we have developed the module consisted with four components based on the 5-E learning model: Engage, Explore, Explain, Expand, and Evaluate/Assessment [290]. The 5-E model is an instructional model, which allows the learner to build or construct new ideas using previous knowledge. The classroom curriculum included four modules designed with the following learning objectives:

- Learn how researchers use latitude and longitude to track animals in the wild.
- Investigate how a sneeze travels under different conditions.
- Investigate what parts of a marine animal are the most contaminated with foreign microbes and how we use PCR to collect data.
- Determine how to create a surface, which will allow gold nanoparticles to adhere to the surface to form substrates we can use for analytical detection.

The modules are designed to be taught over the course of the school year. Module 1 was conducted after the students studied latitude and longitude. The other modules were interspersed throughout the school year.

MATERIALS

Module 1

Required Supplies:

- Graph paper, Ruler, Pencil

Module 2

Required Supplies:

- 5-6 agar plates (For Each Pair), Over-night culture of B. subtilus in spray bottle , Ruler/meter stick, Masking tape, Marker, Diagram, Cleanser (0.2% bleach solution)

Module 3

Required Supplies:

- Disposable inoculating loop, Swabs, Micropipette, Micropipette tips

Module 4

Required Supplies:

- Microscope slides, Gold nanoparticle solution, (3-aminopropyl) triethoxysilane, Sodium dodecyl sulfate, Water, Micropipette, Micropipette tips

METHODS

Module 1: Sea Turtle

Engage (Time: 5-10min)

Introduce the students to sea turtles and satellite telemetry. Explain how humans use tracking to map sea turtle movements to study the behavior of the animal. In an earth science class this lesson works well after students have completed the section on mapping. Have the students review latitude and longitude as a class and how to use tracking data to create a map.

Explore (Time: 20-30min)

Students pick a set of data they would like to map (Casey Key Loggerhead, Gulf of Mexico, winter) and choose the appropriate map. The students summarize the tracking data by choosing 15 points from the data set. The summarized data set should be recorded on their worksheet in the following manner.

Date	Longitude	Latitude
7/9/2007	82.5 W	27.0 N
7/10/2007	83.0 W	27.0 N

The students can begin plotting their data on the map. They should begin to see a pattern develop. After the class has finished drawing their maps, collectively discuss the data. Have the groups come to the front of the class and describe how their animal was migrating during that time of year.

Explain (Time: 10 min)

The goal of this exercise is to show students that sea turtles, in particular females, have different migratory behavioral patterns depending on the time of year. The student should attempt to figure out whether the animal was nesting, resting, foraging, or migrating in their data set.

Expand (Time: Homework)

The students can create more detailed maps using the seaturtle.org *Maptool*. This tool allows students to add data such as sea currents, coastlines, country names, and sea surface temperatures. They can also notice if there were any weather patterns that could have affects the migration pattern of the animal (i.e. Hurricane). Students can also adopt a sea turtle and track its movements online.

Module 2: Sneeze Lab

Engage (Time: 5-10min)

This module is designed for students to determine how far a sneeze travels and if covering ones nose/mouth while sneezing has an effect on transmission. In addition they will learn how to identify and count bacterial colonies on an agar plate. The students will review basic concepts on microbes and scientific method terminology. Before the student design their experiment the teacher must discuss positive and negative controls. Let the class figure out how to make a positive control plate and a negative control plate. By the end of the lesson, students should have learned how to use the scientific method to test a hypothesis and how to work in groups to run an experiment.

Explore (Time: 20-30min)

1) The students (4-5) should set up their experiment by mapping out the locations of the agar plates with a measuring stick and marking the location with masking tape. The agar plates should be placed at specified locations on the work bench.

2) Students should each record the experimental set up on the worksheet. They should label each

agar plates with the group name, date, and the position. If they are a group that is testing covering the nose, they should label the agar plates with the appropriate information.

3) The students should remove each of the lids and place them next to the plates. I came to each group and sprayed the bottle allowing the mist to settle for a few seconds. The group can then replace the lids. If the group had a positive control I made the control by spraying the culture mist directly onto an empty plate.

4) Use the bleach solution to clean the work area after spraying the bacteria.

5) Let the plates incubate overnight and store at 4 ºC until next class period.

6) During the next class period, students will count colonies on their plates. They should record the number of colonies on their worksheet and compare the results with the rest of the class. If their plate became a lawn of bacteria, I explained the difference between a lawn and single colonies.

Explain (Time: 10 min)

The students should learn how to make controls and run a simple experiment. They should understand how to make and test a hypothesis, making sure the different sets of data are comparable. Students should also learn how bacteria spread and grow. Students should be able to describe the scientific method by the end of the lesson.

Module 3: Marine Wildlife CSI

Engage (Time: 10min)

This module is designed to connect basic laboratory research with the activity of tracking sea turtles. In this activity student are tasked to be forensic pathologists and help animal doctors discover if bacterial pathogens are the cause of the animals in their hospital becoming ill. In the process of the discovery of microbiome of the diseased animals, student will learn the basics of polymerase chain reaction (PCR) and techniques for analyzing PCR products. Students will need to keep a detailed record of samples. Students will also learn how to use a micropipette and how to properly take a sample from a contaminated culture swab or specimen. At the conclusion of the lesson the student should demonstrate proficiency with several basic laboratory skills. In the process, students will discover the impact of human activity on the waters in the Gulf of Mexico as it relates to introduction of foreign pathogens into the Gulf ecosystem.

Explore (Time: 20-30min)

1. Sample preparation
    a. Students begin activity by putting a 20 µl aliquot of water into a PCR tube. The students should familiarize themselves with a micropipette and how to adjust the settings to the proper volume. Every student should get an opportunity to use the pipette so I had each student prepare at least one sample.
2. Collection
    a. Once all tubes have been filled with the proper amount of liquid, the students can begin to sample. One student should be tasked with collecting a control from the room. The student should use the cleanroom swab to collect the sample

b. Another student can be charged with collecting biofilm from the specimen. Use the disposable inoculating loops to perform this task. I monitored this step so that students would be careful with the specimen.

c. The inoculation loop should be dipped into the PCR tube. Close the microcentrifuge tube.

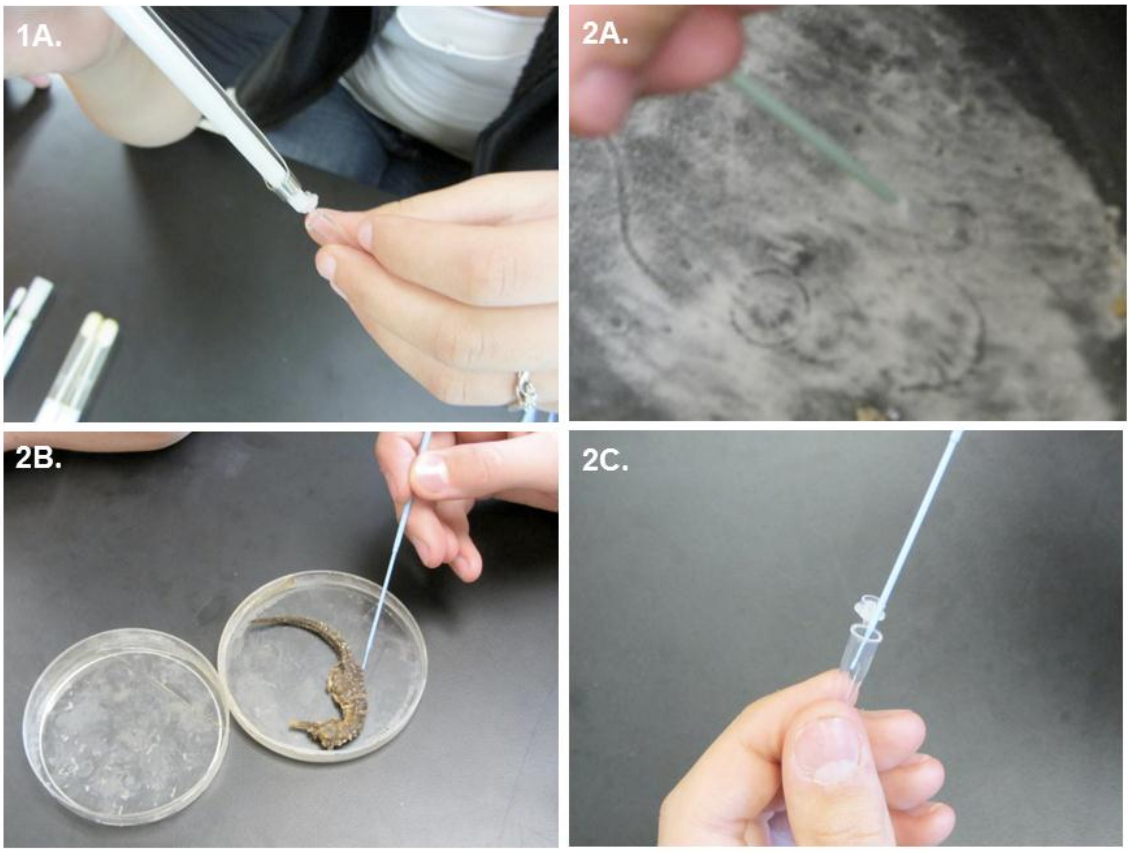

Figure 6.1 Snapshots of student preparing reactions and taking specimen samples for PCR. 1A. Students begin by aliquoting 20 µL of sterile deionized water into a microcentrifuge tube. 2A. Using a sterile culture swab or inoculating loop, students collect a sample from a surface in the classroom or specimen (2B). 2C. Students inoculate microcentrifuge tube with sample.

d. Student will then move to collecting samples from the swabs. Each group will be

given 4-5 swabs taken from various body parts (foot, armpit, urogenital) of a marine animal (manatee, dolphin, penguin, etc.). An extension of the exercise would be to give each student an anatomical diagram of the animal and have them label the location they are sampling.

Figure 6.2 Snapshot of student taking samples from marine animal swabs for PCR identification of bacteria.

3. Data Analysis (Day 1)
    a. In an effort to maximize class time I prepared a DNA agarose gel before class and ran samples I had previous collected. I explained how DNA travels through the gel and how we can visualize the DNA in the gel. Students took turns lighting up the gel under the dark reader.
4. Data Analysis (Day 2)
    a. After the first class period, I added a ready-to-use PCR reaction mixture containing Taq polymerase to all of the samples and recorded the sample information. The PCR reactions were completed in the laboratory and I analyzed the samples by gel electrophoresis. The next class period we used for data analysis. The students were

shown which samples they collected were positive for bacteria.

Explain (Time: 10 min)

During the explanation student should understand how PCR can amplify DNA. I quizzed students on how many cycles it would take to produce billions of pieces of DNA. Students had to make connections to how some bacteria found in humans can infect an animal in the Gulf of Mexico.

Expand (Time: Homework)

Highly motivated students can learn more about 16S rDNA sequencing as a method of bacterial identification.

Module 4: Nano-Engineers

Engage (Time: 5-10min)

This module is designed as an activity to show how we can use nanotechnology to create devices we can use for research. The goal is to teach students what nano-scale means and how we can manipulate objects on the nano-scale. Students are first introduced to an EM image of the growth of silicon nanowires from a gold surface that looked like a forest under false color. The student can make inferences on how small the objects were in the image. The activity also includes a short introduction to chemistry. The students need to understand that only certain molecules on the surface of their substrate can react with the chemical that will allow the gold to attach to the surface.

Explore (Time: 45min)

The goal of this activity is to allow the student as much freedom as possible to create the device.

The experiment can be conducted in one of two ways. The first way would be to use one chemical (APTES) and have the student vary the surface they use. In practice, a typical polystyrene surface does not react well with the APTES. This surface should not have as much gold attached as the glass surface treated with the APTES. The students can record the differences in the gold coating on the glass between the surfaces.

Another possible lesson would be to introduce more variables into the system. For a more advanced class, I explained the surface chemistry principle and it was their responsibility to find the right chemical and surface that would give the most gold on the surface. They then had to identify the chemical and show why one would work over another. They also identified the control in the experiment.

a) After picking a surface, students take a 50-100 μL aliquot of chemical solution and place it on the surface. Draw a circle around the drop with a marker. Allow the reaction to take place for at least 15 minutes.
b) Thoroughly rinse off the surface with water. Dry the surface, careful not to touch the area inside the circle.
c) Place a drop of gold inside the circle on the surface. Depending on the type of surface, the drop may spread outside of the circle. If this happens, reduce the volume of the gold solution added to the surface. Let the gold incubate on the surface for another 15 minutes. If time is limited the gold can incubate on the surface overnight. Keep the surface covered to limit evaporation.
d) Rinse the gold from the surface and allow the plate to dry. The plates can be left to dry overnight and analyzed during the following class period.

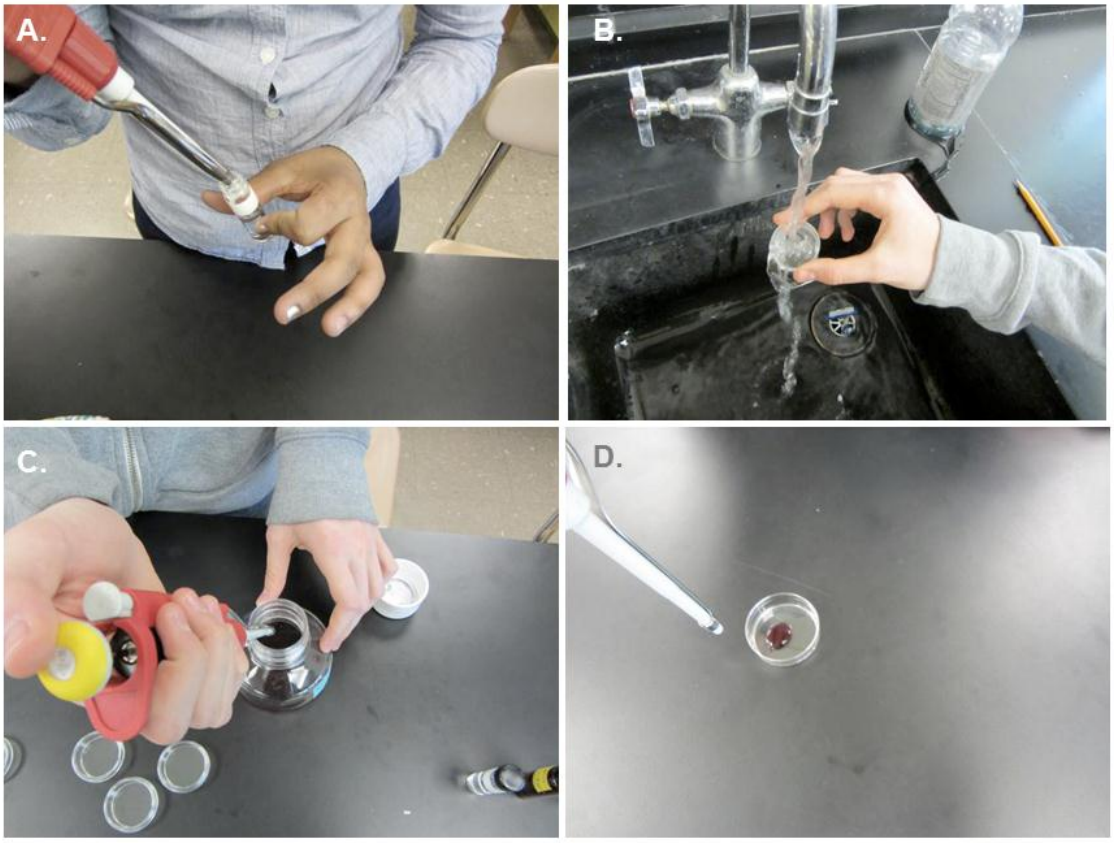

Figure 6.3 Snapshot of students preparing Surface Enhanced Raman substrates using gold nanoparticles chemically modified petri dishes. A. Students dispense 50-100 µL of APTES solution onto a glass microscope slide fitted into a small petri dish. B. The slide is rinsed after 10 minutes of incubation. C. 50 µL of gold nanoparticle solution is placed on the rinsed microscope slide. D. The particles incubate on the surface for 15 minutes and excess particle solution is rinsed off.

Explain (Time: 10 min)

By the end of the lesson students should see the differences between the various substrates used in the experiment and if the chemical used reacted with the surface to allow the gold to bind. At the end of the experiment, students should be able to describe in general terms why some surfaces bind gold as others do not. They should also familiarize themselves with some basic chemistry principles.

Expand (Time: Homework)

Highly motivated students can have their surface characterized using Scanning Electron Microscopy (SEM). An example of a gold coated glass surface created using the APTES reaction can be found in the appendix.

RESULTS AND DISCUSSION

Module 1: This module consists of student picking an animal to track, marking the animal's location of a map, and connecting the mark to visualize the animal's path. This activity requires some preparation by the teacher before the lesson. First the teacher must visit www.seaturtle.org and sign up for free access to tracking data for the classroom. Once access to the data has been granted, the teacher can choose data from several different species of sea turtle. The teacher must then identify what ocean the sea turtles are located in so they can download/print the appropriate tracking map also located on the website.

Next, the teacher must divide the tracking data up by season (Spring-Winter). Some animals have more tracking data than others, so for this exercise it is important to choose several animals with large sets of data. Preparation time is approximately 3 hours.

Module 2: This module will require the teacher to prepare or purchase as many as 30 LB agar plates. The number of agar plates can be decreased by altering the size of the work groups. The teacher will also need to prepare a spray bottle of nonpathogenic bacteria. The recommended cell

line for this experiment would be *Bacillus subtilus*. The teacher will also need to prepare a diagram showing to possible plate locations for the students to test.

Module 3: This module requires preparation by the teacher to maximize the lesson time. The teacher will need to distribute and label all materials before the beginning of the lesson. The figure below shows an example of how to lay out the materials before the lesson. If the teacher is using specimens, it is recommended that the teacher distribute when the group is ready. If the teacher is going to show an agarose gel during the class, the gel must prepared and run before the class period. To prepare the gel dissolve 0.4 g of agarose into 50 ml of TAE buffer (Tris, acetate, EDTA) and add 0.5 µl of gel green dye of DNA visualization. Allow the gel to cool in a mold with comb. Run the gel at 100 V for 1 hour with pre-prepared samples. Store the gel in a sealed container until students are ready to see the gel. Due to the limited time, the PCR cannot be completed in one class period. The teacher should collect the samples and add the remaining 25 µl of pre-mixed PCR reaction mixture to complete the PCR reaction. The teacher can then place the samples in a thermocycler to run overnight and analyze in the next class period. Lesson will take approximately 2 ½ class periods to complete.

Module 4: This module requires some preparation by the teacher. The teacher must prepare all of the materials and reagents before the beginning of the activity. It is helpful to organize the materials similar to the layout below. The gold nanoparticles should be aliquoted into microcentrifuge tubes for each group. Also give each group an aliquot of each chemical. Be sure the students circle the drop they make on the surface so they can place the gold in the correct spot later on.

Assessment

The following rubric can be used to assess students during each part of the activity. The term "expectations" here refers to the content, process and attitudinal goals for this activity. Evidence for understanding may be in the form of oral as well as written communication, both with the teacher as well as observed communication with other students. Specifics are listed in the table below.

1= exceeds expectations
2= meets expectations consistently
3= meets expectations occasionally
4= not meeting expectations

Module	Engage	Explore	Explain	Expand/Synthesis
1	Student is eager to participate in group discussion. Offers help to his or her class mates during the discussion and uses prior knowledge develop a hypothesis for the lesson	Student is highly engaged in the experiment and allowed others to participate in the lesson. They record their data correctly and required little assistance setting up experiment	Student offers an insightful description the phenomena of the modules and develops a well thought out hypothesis.	Student is an active participant in developing a conclusion to the lesson. They help their class mates understand the concepts discussed and ask for further examples.
2	Student participated in discussion	Student was engaged in activity; they recorded their data, and completed the lab assignment.	Student was an active participant in the class discussion	Student developed proper conclusion to the lesson
3	Student only participated in discussion if asked	Student was not highly engaged in the activity or did not allow others to participate. Assignments were incomplete.	Student was a modest participant in discussion	Student developed conclusion but not correct based on the results.
4	Student does not participate in the discussion and/or is a distraction to the rest of the group	Student does not complete laboratory assignment and shows little interest in the activity	Student does not participate or is a distraction during the discussion	Student does not participate and did not reach a conclusion from the lesson

CHAPTER 7: CONCLUSIONS & FUTURE DIRECTIONS

The work presented in this dissertation demonstrates the utility to molecularly imprinted polymers and aptamers use with surface enhanced Raman spectroscopy. The aptamer system provides a level of specificity to a SERS substrate that is not seen in most SERS based platforms. Furthermore there exists an extensive library of aptamer that bind small molecules and proteins which makes this system transferable to many fields. Molecularly imprinted polymers are potentially more attractive in that they are much more stable across a spectrum of conditions and the synthesis costs are a fraction of the cost of oligonucleotide synthesis.

A potentially powerful drug delivery system was generated with molecular imprinting of doxorubicin. The common chemotherapy has a short serum half-life and is highly toxic. This molecularly imprinted polymer addresses these two factors in its specific trapping of the molecule within the polymer network which is resistance to enzymatic degradation. Future work will involve modifying the surface of the particles with a laser adsorption layer. The photo initiated heating of the polymer would cause a swelling of the matrix and result in burst release. The particles could then be conjugated with a targeting antibody and only a substantial release drug would occur when irradiated by a plasmon matching laser.

Future work with CT antigens will involve development of Virus-Like Particles (VLP) decorated with the CT antigen NY-ESO-1 enhanced immunogenicity. Currently work is being conducted to modify norovirus P particle surface loops with either the MHC epitope of NY-ESO-1 or the full antigen and express the protein at the large scale in *Pichia pastoris*.

REFERENCES

1. Dougan, M.; Dranoff, G., Immune Therapy for Cancer. In *Annual Review of Immunology*, Annual Reviews: Palo Alto, 2009; Vol. 27, pp 83-117.
2. Lesterhuis, W. J.; Haanen, J.; Punt, C. J. A., Cancer immunotherapy - revisited. *Nature Reviews Drug Discovery* **2011,** 10, (8), 591-600.
3. Waldmann, T. A., Immunotherapy: past, present and future. *Nature Medicine* **2003,** 9, (3), 269-277.
4. Miller, R. A.; Maloney, D. G.; Warnke, R.; Levy, R., Treatment of B-Cell Lymphoma with Monoclonal Anti-Idiotype Antibody. *New England Journal of Medicine* **1982,** 306, (9), 517-522.
5. Gajewski, T. F., Cancer immunotherapy. *Molecular Oncology* **2012,** 6, (2), 242-250.
6. Pijpers, F.; Faint, R.; Saini, N., Therapeutic cancer vaccines. *Nature Reviews Drug Discovery* **2005,** 4, (8), 623-624.
7. Huang, C. J.; Lowe, A. J.; Batt, C. A., Recombinant immunotherapeutics: current state and perspectives regarding the feasibility and market. *Applied Microbiology and Biotechnology* **2010,** 87, (2), 401-410.
8. Adams, G. P.; Weiner, L. M., Monoclonal antibody therapy of cancer. *Nature Biotechnology* **2005,** 23, (9), 1147-1157.
9. Kohler, G.; Milstein, C., Continuous Cultures of Fused Cells Secreting Antibody of Predefined Specificity *Nature* **1975,** 256, (5517), 495-497.
10. Norman, D. J., An Overview of the Use of the Monoclonal-Antibody OKT3 in Renal-Transplantation. *Transplantation Proceedings* **1988,** 20, (6), 1248-1252.
11. Queen, C.; Schneider, W. P.; Selick, H. E.; Payne, P. W.; Landolfi, N. F.; Duncan, J. F.; Avdalovic, N. M.; Levitt, M.; Junghans, R. P.; Waldmann, T. A., A humanized antibody that binds to the Interleukin-2 receptor. *Proceedings of the National Academy of Sciences of the United States of America* **1989,** 86, (24), 10029-10033.
12. Riechmann, L.; Clark, M.; Waldmann, H.; Winter, G., Reshaping human antibodies for therapy. *Nature* **1988,** 332, (6162), 323-327.
13. Witzig, T. E.; Gordon, L. I.; Cabanillas, F.; Czuczman, M. S.; Emmanouilides, C.; Joyce, R.; Pohlman, B. L.; Bartlett, N. L.; Wiseman, G. A.; Padre, N.; Grillo-Lopez, A. J.; Multani, P.; White, C. A., Randomized controlled trial of yttrium-90-labeled ibritumomab tiuxetan radioimmunotherapy versus rituximab immunotherapy for patients with relapsed or refractory low-grade, follicular, or transformed B-cell non-Hodgkin's lymphoma. *Journal of Clinical Oncology* **2002,** 20, (10), 2453-2463.
14. Baselga, J.; Norton, L.; Albanell, J.; Kim, Y. M.; Mendelsohn, J., Recombinant humanized anti-HER2 antibody (Herceptin (TM)) enhances the antitumor activity of paclitaxel and doxorubicin against HER2/neu overexpressing human breast cancer xenografts. *Cancer Research* **1998,** 58, (13), 2825-2831.
15. Hudis, C. A., Drug therapy: Trastuzumab - Mechanism of action and use in clinical practice. *New England Journal of Medicine* **2007,** 357, (1), 39-51.
16. Slamon, D. J.; Leyland-Jones, B.; Shak, S.; Fuchs, H.; Paton, V.; Bajamonde, A.; Fleming, T.; Eiermann, W.; Wolter, J.; Pegram, M.; Baselga, J.; Norton, L., Use of

chemotherapy plus a monoclonal antibody against HER2 for metastatic breast cancer that overexpresses HER2. *New England Journal of Medicine* **2001,** 344, (11), 783-792.
17. Chames, P.; Van Regenmortel, M.; Weiss, E.; Baty, D., Therapeutic antibodies: successes, limitations and hopes for the future. *British Journal of Pharmacology* **2009,** 157, (2), 220-233.
18. Kelley, B., Industrialization of mAb production technology: The bioprocessing industry at a crossroads. *mAbs* **2009,** 1, (5), 443-452.
19. Nelson, A. L.; Reichert, J. M., Development trends for therapeutic antibody fragments. *Nature Biotechnology* **2009,** 27, (4), 331-337.
20. Davis, J. P., Experience with hepatitis A and B vaccines. *American Journal of Medicine* **2005,** 118, 7-15.
21. Lin, W. W.; Karin, M., A cytokine-mediated link between innate immunity, inflammation, and cancer. *Journal of Clinical Investigation* **2007,** 117, (5), 1175-1183.
22. Quadrivalent Vaccine against Human Papillomavirus to Prevent High-Grade Cervical Lesions. *New England Journal of Medicine* **2007,** 356, (19), 1915-1927.
23. Garland, S. M.; Hernandez-Avila, M.; Wheeler, C. M.; Perez, G.; Harper, D. M.; Leodolter, S.; Tang, G. W. K.; Ferris, D. G.; Steben, M.; Bryan, J.; Taddeo, F. J.; Railkar, R.; Esser, M. T.; Sings, H. L.; Nelson, M.; Boslego, J.; Sattler, C.; Barr, E.; Koutsky, L. A., Quadrivalent vaccine against human papillomavirus to prevent anogenital diseases. *New England Journal of Medicine* **2007,** 356, (19), 1928-1943.
24. Bryan, J. T., Developing an HPV vaccine to prevent cervical cancer and genital warts. *Vaccine* **2007,** 25, (16), 3001-3006.
25. Novellino, L.; Castelli, C.; Parmiani, G., A listing of human tumor antigens recognized by T cells: March 2004 update. *Cancer Immunology, Immunotherapy* **2005,** 54, (3), 187-207.
26. Simpson, A. J. G.; Caballero, O. L.; Jungbluth, A.; Chen, Y. T.; Old, L. J., Cancer/testis antigens, gametogenesis and cancer. *Nature Reviews Cancer* **2005,** 5, (8), 615-625.
27. Knuth, A.; Danowski, B.; Oettgen, H. F.; Old, L. J., T-cell-mediated cyto-toxicity against autologous malignant-melanoma - analysis with Interleukin 2-dependent T-cell cultues. *Proceedings of the National Academy of Sciences of the United States of America-Biological Sciences* **1984,** 81, (11), 3511-3515.
28. Knuth, A.; Wolfel, T.; Klehmann, E.; Boon, T.; Zumbuschenfelde, K. H. M., Cytolytic T-cell clones against an autologous human-melanoma - specificity study and definition of 3 antigens by immunoselection. *Proceedings of the National Academy of Sciences of the United States of America* **1989,** 86, (8), 2804-2808.
29. Sahin, U.; Tureci, O.; Schmitt, H.; Cochlovius, B.; Johannes, T.; Schmits, R.; Stenner, F.; Luo, G. R.; Schobert, I.; Pfreundschuh, M., Human Neoplasms Elicit Multiple Specific Immune-Responses in the Autologous Host. *Proceedings of the National Academy of Sciences of the United States of America* **1995,** 92, (25), 11810-11813.
30. Chen, Y., Identification of human tumor antigens by serological expression cloning: an online review on SEREX. *Cancer Immunity* **2004,** [updated 2004 Mar 10; cited 2004 Apr 1], URL: http://www.cancerimmunity.org/serex.
31. Tureci, O.; Sahin, U.; Schobert, I.; Koslowski, M.; Schmitt, H.; Schild, H. J.; Stenner, F.; Seitz, G.; Rammensee, H. G.; Pfreundschuh, M., The SSX-2 gene, which is involved in the

t(X;18) translocation of synovial sarcomas, codes for the human tumor antigen HOM-MEL-40. *Cancer Research* **1996,** 56, (20), 4766-4772.
32. Chen, Y. T.; Scanlan, M. J.; Sahin, U.; Tureci, O.; Gure, A. O.; Tsang, S. L.; Williamson, B.; Stockert, E.; Pfreundschuh, M.; Old, L. J., A testicular antigen aberrantly expressed in human cancers detected by autologous antibody screening. *Proceedings of the National Academy of Sciences of the United States of America* **1997,** 94, (5), 1914-1918.
33. Kirkin, A. F.; Dzhandzhugazyan, K. N.; Zeuthen, J., Cancer/Testis Antigens: Structural and Immunobiological Properties. *Cancer Investigation* **2002,** 20, (2), 222.
34. Suri, A., Cancer testis antigens - their importance in immunotherapy and in the early detection of cancer. *Expert Opinion on Biological Therapy* **2006,** 6, (4), 379-389.
35. Atanackovic, D.; Altorki, N. K.; Cao, Y.; Ritter, E.; Ferrara, C. A.; Ritter, G.; Hoffman, E. W.; Bokemeyer, C.; Old, L. J.; Gnjatic, S., Booster vaccination of cancer patients with MAGE-A3 protein reveals long-term immunological memory or tolerance depending on priming. *Proceedings of the National Academy of Sciences of the United States of America* **2008,** 105, (5), 1650-1655.
36. Brichard, V. G.; Lejeune, D., GSK's antigen-specific cancer immunotherapy programme: Pilot results leading to Phase III clinical development. *Vaccine* **2007,** 25, B61-B71.
37. Fujita, S.; Wada, H.; Jungbluth, A. A.; Sato, S.; Nakata, T.; Noguchi, Y.; Doki, Y.; Yasui, M.; Sugita, Y.; Yasuda, T.; Yano, M.; Ono, T.; Chen, Y. T.; Higashiyama, M.; Gnjatic, S.; Old, L. J.; Nakayama, E.; Monden, M., NY-ESO-1 expression and immunogenicity in esophageal cancer. *Clinical Cancer Research* **2004,** 10, (19), 6551-6558.
38. Sato, S.; Noguchi, Y.; Wada, H.; Fujita, S.; Nakamura, S.; Tanaka, R.; Nakada, T.; Hasegawa, K.; Nakagawa, K.; Koizumi, F.; Ono, T.; Nouso, K.; Jungbluth, A.; Chen, Y. T.; Old, L. J.; Shiratori, Y.; Nakayama, E., Quantitative real-time RT-PCR analysis of NY-ESO-1 and LAGE-1a mRNA expression in normal tissues and tumors, and correlation of the protein expression with the mRNA copy number. *International Journal of Oncology* **2005,** 26, (1), 57-63.
39. Sugita, Y.; Wada, H.; Fujita, S.; Nakata, T.; Sato, S.; Noguchi, Y.; Jungbluth, A. A.; Yamaguchi, M.; Chen, Y. T.; Stockert, E.; Gnjatic, S.; Williamson, B.; Scanlan, M. J.; Ono, T.; Sakita, I.; Yasui, M.; Miyoshi, Y.; Tamaki, Y.; Matsuura, N.; Noguchi, S.; Old, L. J.; Nakayama, E.; Monden, M., NY-ESO-1 expression and immunogenicity in malignant and benign breast tumors. *Cancer Research* **2004,** 64, (6), 2199-2204.
40. Gnjatic, S.; Nishikawa, H.; Jungbluth, A. A.; Gure, A. O.; Ritter, G.; Jager, E.; Chen, Y. T.; Old, L. J., NY-ESO-1: Review of an immunogenic tumor antigen. In *Advances in Cancer Research, Vol 95*, VandeWoude, G. F.; Klein, G., Eds. Elsevier Academic Press Inc: San Diego, 2006; Vol. 95, pp 1-30.
41. Davis, I. D.; Chen, W. S.; Jackson, H.; Parente, P.; Shackleton, M.; Hopkins, W.; Chen, Q. Y.; Dimopoulos, N.; Luke, T.; Murphy, R.; Scott, A. M.; Maraskovsky, E.; McArthur, G.; MacGregor, D.; Sturrock, S.; Tai, T. Y.; Green, S.; Cuthbertson, A.; Maher, D.; Miloradovic, L.; Mitchell, S. V.; Ritter, G.; Jungbluth, A. A.; Chen, Y. T.; Gnjatic, S.; Hoffman, E. W.; Old, L. J.; Cebon, J. S., Recombinant NY-ESO-1 protein with ISCOMATRIX adjuvant induces broad integrated antibody and CD4+ and CD8+ T cell responses in humans. *Proceedings of the National Academy of Sciences of the United States of America* **2004,** 101, (29), 10697-10702.

42. Chomez, P.; De Backer, O.; Bertrand, M.; De Plaen, E.; Boon, T.; Lucas, S., An Overview of the MAGE Gene Family with the Identification of All Human Members of the Family. *Cancer Research* **2001,** 61, (14), 5544-5551.
43. Balasse, E.; Gatouillat, G.; Patigny, D.; Andry, M. C.; Madoulet, C., In vivo anti-melanoma activities of the Melan-A/MART-1(101-115) T CD4+cell peptide. *Vaccine* **2009,** 27, (44), 6107-6109.
44. Gardiner, D. J.; Graves, P. R.; Bowley, H. J., *Practical Raman spectroscopy*. Springer-Verlag: Berlin; New York, 1989.
45. Raman, C. V.; Krishnan, K. S., A new type of secondary radiation. *Nature* **1928,** 121, 501-502.
46. Albrecht, M. G.; Creighton, J. A., Anomalously intense Raman spectra of pyridine at a silver electrode. *J Am Chem Soc* **1977,** 99, (15), 5215-5217.
47. Fleischmann, M.; Hendra, P. J.; McQuilla, A., Raman-spectra of pyridine adsorbed at a silver electrode. *Chemical Physics Letters* **1974,** 26, (2), 163-166.
48. Jeanmaire, D., Surface Raman spectroelectrochemistry Part I. Heterocyclic, aromatic, and aliphatic amines adsorbed on the anodized silver electrode. *J Electroanal Chem* **1977,** 84, (1), 1-20.
49. Howard, R. E.; Liao, P. F.; Skocpol, W. J.; Jackel, L. D.; Craighead, H. G., Microfabrication as a scientific tool. *Science* **1983,** 221, (4606), 117-121.
50. Liao, P. F.; Bergman, J. G.; Chemla, D. S.; Wokaun, A.; Melngailis, J.; Hawryluk, A. M.; Economou, N. P., Surface-enhanced Raman-scattering from microlithographic silver particle surfaces. *Chemical Physics Letters* **1981,** 82, (2), 355-359.
51. Campion, A.; Kambhampati, P., Surface-enhanced Raman scattering. *Chemical Society Reviews* **1998,** 27, (4), 241-250.
52. Stiles, P. L.; Dieringer, J. A.; Shah, N. C.; Van Duyne, R. P., Surface-Enhanced Raman Spectroscopy. *Annu Rev Anal Chem* **2008,** 1, (1), 601-626.
53. Schatz, G. C.; Young, M. A.; Van Duyne, R. P., Electromagnetic mechanism of SERS. *Surface-Enhanced Raman Scattering: Physics and Applications* **2006,** 103, 19-45.
54. Willets, K. A.; Van Duyne, R. P., Localized surface plasmon resonance spectroscopy and sensing. In *Annual Review of Physical Chemistry*, 2007; Vol. 58, pp 267-297.
55. Sharma, B.; Frontiera, R. R.; Henry, A. I.; Ringe, E.; Van Duyne, R. P., SERS: Materials, applications, and the future. *Materials Today* **2012,** 15, (1-2), 16-25.
56. Lombardi, J. R.; Birke, R. L.; Lu, T. H.; Xu, J., Charge-transfer theory of surface enhanced Raman-spectroscopy - Herzberg-Teller contributions. *Journal of Chemical Physics* **1986,** 84, (8), 4174-4180.
57. Jensen, L.; Aikens, C. M.; Schatz, G. C., Electronic structure methods for studying surface-enhanced Raman scattering. *Chemical Society Reviews* **2008,** 37, (5), 1061-1073.
58. Morton, S. M.; Jensen, L., Understanding the Molecule-Surface Chemical Coupling in SERS. *Journal of the American Chemical Society* **2009,** 131, (11), 4090-4098.
59. Bantz, K. C.; Meyer, A. F.; Wittenberg, N. J.; Im, H.; Kurtulus, è.; Lee, S. H.; Lindquist, N. C.; Oh, S.-H.; Haynes, C. L., Recent progress in SERS biosensing. *Phys Chem Chem Phys* **2011,** 13, (24), 11551-11567.

60. Lee, K.; Irudayaraj, J., Periodic and Dynamic 3-D Gold Nanoparticle-DNA Network Structures for Surface-Enhanced Raman Spectroscopy-Based Quantification. *Journal of Physical Chemistry C* **2009,** 113, (15), 5980-5983.
61. Fan, M.; Andrade, G. F. S.; Brolo, A. G., A review on the fabrication of substrates for surface enhanced Raman spectroscopy and their applications in analytical chemistry. *Analytica Chimica Acta* **2011,** 693, (1-2), 7-25.
62. Brown, R. J. C.; Milton, M. J. T., Nanostructures and nanostructured substrates for surface-enhanced Raman scattering (SERS). *Journal of Raman Spectroscopy* **2008,** 39, (10), 1313-1326.
63. Lin, X.-M.; Cui, Y.; Xu, Y.-H.; Ren, B.; Tian, Z.-Q., Surface-enhanced Raman spectroscopy: substrate-related issues. *Analytical and Bioanalytical Chemistry* **2009,** 394, (7), 1729-1745.
64. Aroca, R. F.; Alvarez-Puebla, R. A.; Pieczonka, N.; Sanchez-Cortez, S.; Garcia-Ramos, J. V., Surface-enhanced Raman scattering on colloidal nanostructures. *Advances in Colloid and Interface Science* **2005,** 116, (1â€“3), 45-61.
65. Pieczonka, N. P. W.; Aroca, R. F., Inherent Complexities of Trace Detection by Surface-Enhanced Raman Scattering. *Chemphyschem* **2005,** 6, (12), 2473-2484.
66. Frens, G., Controlled Nucleation for Regulation of Particle-Size in Monodisperse Gold Suspensions. *Nature* **1973,** 241, (105), 20-22.
67. Leopold, N.; Lendl, B., A new method for fast preparation of highly surface-enhanced Raman scattering (SERS) active silver colloids at room temperature by reduction of silver nitrate with hydroxylamine hydrochloride. *Journal of Physical Chemistry B* **2003,** 107, (24), 5723-5727.
68. Zhou, J.; An, J.; Tang, B.; Xu, S.; Cao, Y.; Zhao, B.; Xu, W.; Chang, J.; Lombardi, J. R., Growth of tetrahedral silver nanocrystals in aqueous solution and their SERS enhancement. *Langmuir* **2008,** 24, (18), 10407-10413.
69. Esenturk, E. N.; Walker, A. R. H., Surface-enhanced Raman scattering spectroscopy via gold nanostars. *Journal of Raman Spectroscopy* **2009,** 40, (1), 86-91.
70. Jana, S.; Pande, S.; Sinha, A. K.; Sarkar, S.; Pradhan, M.; Basu, M.; Saha, S.; Pal, T., A Green Chemistry Approach for the Synthesis of Flower-like Ag-Doped MnO2 Nanostructures Probed by Surface-Enhanced Raman Spectroscopy. *Journal of Physical Chemistry C* **2009,** 113, (4), 1386-1392.
71. Guo, H. Y.; Ruan, F. X.; Lu, L. H.; Hu, J. W.; Pan, J. A.; Yang, Z. L.; Ren, B., Correlating the Shape, Surface Plasmon Resonance, and Surface-Enhanced Raman Scattering of Gold Nanorods. *Journal of Physical Chemistry C* **2009,** 113, (24), 10459-10464.
72. Orendorff, C. J.; Gearheart, L.; Jana, N. R.; Murphy, C. J., Aspect ratio dependence on surface enhanced Raman scattering using silver and gold nanorod substrates. *Physical Chemistry Chemical Physics* **2006,** 8, (1), 165-170.
73. Liao, Q.; Mu, C.; Xu, D. S.; Ai, X. C.; Yao, J. N.; Zhang, J. P., Gold Nanorod Arrays with Good Reproducibility for High-Performance Surface-Enhanced Raman Scattering. *Langmuir* **2009,** 25, (8), 4708-4714.
74. Cialla, D.; Marz, A.; Bohme, R.; Theil, F.; Weber, K.; Schmitt, M.; Popp, J., Surface-enhanced Raman spectroscopy (SERS): progress and trends. *Analytical and Bioanalytical Chemistry* **2012,** 403, (1), 27-54.

75. Fan, M.; Brolo, A. G., Silver nanoparticles self assembly as SERS substrates with near single molecule detection limit. *Physical Chemistry Chemical Physics* **2009,** 11, (34), 7381-7389.
76. Kinnan, M. K.; Chumanov, G., Surface enhanced Raman scattering from silver nanoparticle arrays on silver mirror films: Plasmon-induced electronic coupling as the enhancement mechanism. *Journal of Physical Chemistry C* **2007,** 111, (49), 18010-18017.
77. Sisco, P. N.; Murphy, C. J., Surface-Coverage Dependence of Surface-Enhanced Raman Scattering from Gold Nanocubes on Self-Assembled Monolayers of Analyte. *Journal of Physical Chemistry A* **2009,** 113, (16), 3973-3978.
78. Li, J. F.; Huang, Y. F.; Ding, Y.; Yang, Z. L.; Li, S. B.; Zhou, X. S.; Fan, F. R.; Zhang, W.; Zhou, Z. Y.; Wu, D. Y.; Ren, B.; Wang, Z. L.; Tian, Z. Q., Shell-isolated nanoparticle-enhanced Raman spectroscopy. *Nature* **2010,** 464, (7287), 392-395.
79. Dieringer, J. A.; McFarland, A. D.; Shah, N. C.; Stuart, D. A.; Whitney, A. V.; Yonzon, C. R.; Young, M. A.; Zhang, X. Y.; Van Duyne, R. P., Surface enhanced Raman spectroscopy: new materials, concepts, characterization tools, and applications. *Faraday Discussions* **2006,** 132, 9-26.
80. Biggs, K. B.; Camden, J. P.; Anker, J. N.; Van Duyne, R. P., Surface-Enhanced Raman Spectroscopy of Benzenethiol Adsorbed from the Gas Phase onto Silver Film over Nanosphere Surfaces: Determination of the Sticking Probability and Detection Limit Time. *Journal of Physical Chemistry A* **2009,** 113, (16), 4581-4586.
81. Baia, L.; Baia, M.; Popp, J.; Astilean, S., Gold films deposited over regular arrays of polystyrene nanospheres as highly effective SERS substrates from visible to NIR. *Journal of Physical Chemistry B* **2006,** 110, (47), 23982-23986.
82. Quagliano, L. G., Observation of molecules adsorbed on III-V semiconductor quantum dots by surface-enhanced Raman scattering. *Journal of the American Chemical Society* **2004,** 126, (23), 7393-7398.
83. Qiu, C.; Zhou, H.; Yang, H.; Chen, M.; Guo, Y.; Sun, L., Investigation of n-Layer Graphenes as Substrates for Raman Enhancement of Crystal Violet. *Journal of Physical Chemistry C* **2012,** 115, (20), 10019-10025.
84. Musumeci, A.; Gosztola, D.; Schiller, T.; Dimitrijevic, N. M.; Mujica, V.; Martin, D.; Rajh, T., SERS of Semiconducting Nanoparticles (TiO2 Hybrid Composites). *Journal of the American Chemical Society* **2009,** 131, (17), 6040-+.
85. Strickland, A. D.; Batt, C. A., Detection of Carbendazim by Surface-Enhanced Raman Scattering Using Cyclodextrin Inclusion Complexes on Gold Nanorods. *Analytical Chemistry* **2009,** 81, (8), 2895-2903.
86. Jia, J. L.; Xu, H. H.; Zhang, G. R.; Hu, Z.; Xu, B. Q., High quality gold nanorods and nanospheres for surface-enhanced Raman scattering detection of 2,4-dichlorophenoxyacetic acid. *Nanotechnology* **2012,** 23, (49), 8.
87. Lyandres, O.; Shah, N. C.; Yonzon, C. R.; Walsh, J. T.; Glucksberg, M. R.; Van Duyne, R. P., Real-time glucose sensing by surface-enhanced Raman spectroscopy in bovine plasma facilitated by a mixed decanethiol/mercaptohexanol partition layer. *Analytical Chemistry* **2005,** 77, (19), 6134-6139.

88. Sha, M. Y.; Xu, H.; Natan, M. J.; Cromer, R., Surface-Enhanced Raman Scattering Tags for Rapid and Homogeneous Detection of Circulating Tumor Cells in the Presence of Human Whole Blood. *Journal of the American Chemical Society* **2008,** 130, (51), 17214-+.
89. Stuart, D. A.; Yonzon, C. R.; Zhang, X. Y.; Lyandres, O.; Shah, N. C.; Glucksberg, M. R.; Walsh, J. T.; Van Duyne, R. P., Glucose sensing using near-infrared surface-enhanced Raman spectroscopy: Gold surfaces, 10-day stability, and improved accuracy. *Analytical Chemistry* **2005,** 77, (13), 4013-4019.
90. Stuart, D. A.; Yuen, J. M.; Lyandres, N. S. O.; Yonzon, C. R.; Glucksberg, M. R.; Walsh, J. T.; Van Duyne, R. P., In vivo glucose measurement by surface-enhanced Raman spectroscopy. *Analytical Chemistry* **2006,** 78, (20), 7211-7215.
91. Golightly, R. S.; Doering, W. E.; Natan, M. J., Surface-enhanced Raman spectroscopy and homeland security: A perfect match? *ACS Nano ACS Nano* **2009,** 3, (10), 2859-2869.
92. Zhang, X.; Shah, N. C.; Van Duyne, R. P., Sensitive and selective chem/biosensing based on surface-enhanced Raman spectroscopy (SERS). *Vibrational Spectroscopy* **2006,** 42, (1), 2-8.
93. Zhang, X. Y.; Young, M. A.; Lyandres, O.; Van Duyne, R. P., Rapid detection of an anthrax biomarker by surface-enhanced Raman spectroscopy. *Journal of the American Chemical Society* **2005,** 127, (12), 4484-4489.
94. Barhoumi, A.; Zhang, D.; Tam, F.; Halas, N. J., Surface-enhanced Raman spectroscopy of DNA. *Journal of the American Chemical Society* **2008,** 130, (16), 5523-5529.
95. Neumann, O.; Zhang, D.; Tam, F.; Lal, S.; Wittung-Stafshede, P.; Halas, N. J., Direct Optical Detection of Aptamer Conformational Changes Induced by Target Molecules. *Anal Chem* **2009,** 81, (24), 10002-10006.
96. Jarvis, R. M.; Brooker, A.; Goodacre, R., Surface-enhanced Raman spectroscopy for bacterial discrimination utilizing a scanning electron microscope with a Raman spectroscopy interface. *Analytical Chemistry* **2004,** 76, (17), 5198-5202.
97. Jarvis, R. M.; Brooker, A.; Goodacre, R., Surface-enhanced Raman scattering for the rapid discrimination of bacteria. *Faraday Discussions* **2006,** 132, 281-292.
98. Premasiri, W. R.; Moir, D. T.; Klempner, M. S.; Krieger, N.; Jones, G.; Ziegler, L. D., Characterization of the Surface Enhanced Raman Scattering (SERS) of bacteria. *Journal of Physical Chemistry B* **2005,** 109, (1), 312-320.
99. Grubisha, D. S.; Lipert, R. J.; Park, H. Y.; Driskell, J.; Porter, M. D., Femtomolar detection of prostate-specific antigen: An immunoassay based on surface-enhanced Raman scattering and immunogold labels. *Analytical Chemistry* **2003,** 75, (21), 5936-5943.
100. Lowe, A. J.; Huh, Y. S.; Strickland, A. D.; Erickson, D.; Batt, C. A., Multiplex Single Nucleotide Polymorphism Genotyping Utilizing Ligase Detection Reaction Coupled Surface Enhanced Raman Spectroscopy. *Analytical Chemistry* **2010,** 82, (13), 5810-5814.
101. Mohs, A. M.; Mancini, M. C.; Singhal, S.; Provenzale, J. M.; Leyland-Jones, B.; Wang, M. D.; Nie, S., Hand-held Spectroscopic Device for In Vivo and Intraoperative Tumor Detection: Contrast Enhancement, Detection Sensitivity, and Tissue Penetration. *Analytical Chemistry* **2010,** 82, (21), 9058-9065.
102. Stevenson, R.; Ingram, A.; Leung, H.; McMillan, D. C.; Graham, D., Quantitative SERRS immunoassay for the detection of human PSA. *Analyst* **2009,** 134, (5), 842-844.

103. An, J.-H.; El-Said, W. A.; Yea, C.-H.; Kim, T.-H.; Choi, J.-W., Surface-Enhanced Raman Scattering of Dopamine on Self-Assembled Gold Nanoparticles. *Journal of Nanoscience and Nanotechnology* **2011,** 11, (5), 4424-4429.
104. Beier, H. T.; Cowan, C. B.; Chou, I. H.; Pallikal, J.; Henry, J. E.; Benford, M. E.; Jackson, J. B.; Good, T. A.; Cote, G. L., Application of surface-enhanced Raman spectroscopy for detection of beta amyloid using nanoshells. *Plasmonics* **2007,** 2, (2), 55-64.
105. Puoci, F.; Cirillo, G.; Curcio, M.; Parisi, O. I.; Iemma, F.; Picci, N., Molecularly imprinted polymers in drug delivery: state of art and future perspectives. *Expert Opinion on Drug Delivery* **2011,** 8, (10), 1379-1393.
106. Andersson, L. I.; Muller, R.; Vlatakis, G.; Mosbach, K., Mimics of the Binding-Sites of Opiod Receptors Obtained by Molecular Imprinting of Enkephalin and Morphine. *Proceedings of the National Academy of Sciences of the United States of America* **1995,** 92, (11), 4788-4792.
107. Ramstrom, O.; Ye, L.; Mosbach, K., Artificial antibodies to corticosteroids prepared by molecular imprinting. *Chemistry & Biology* **1996,** 3, (6), 471-477.
108. Vlatakis, G.; Andersson, L. I.; Muller, R.; Mosbach, K., Drug assay using antibody mimics made by molecular imprinting. *Nature* **1993,** 361, (6413), 645-647.
109. Wulff, G., Enzyme-like catalysis by molecularly imprinted polymers. *Chemical Reviews* **2002,** 102, (1), 1-27.
110. Cormack, P. A. G.; Elorza, A. Z., Molecularly imprinted polymers: synthesis and characterisation. *Journal of Chromatography B* **2004,** 804, (1), 173-182.
111. Cunliffe, D.; Kirby, A.; Alexander, C., Molecularly imprinted drug delivery systems. *Advanced Drug Delivery Reviews* **2005,** 57, (12), 1836-1853.
112. Sellergren, B., *Molecularly imprinted polymers : man-made mimics of antibodies and their applications in analytical chemistry*. Elsevier: Amsterdam; New York, 2001.
113. Alexander, C.; Andersson, H. S.; Andersson, L. I.; Ansell, R. J.; Kirsch, N.; Nicholls, I. A.; O'Mahony, J.; Whitcombe, M. J., Molecular imprinting science and technology: a survey of the literature for the years up to and including 2003. *Journal of Molecular Recognition* **2006,** 19, (2), 106-180.
114. Sarhan, A.; Wulff, G., Enzyme-analog built polymers .13. on the introduction of amino and boronic acid groups into chiral polymer cavities *Makromolekulare Chemie-Macromolecular Chemistry and Physics* **1982,** 183, (1), 85-92.
115. Wulff, G.; Stellbrink, H., On the chemistry of binding-sites .7. enantioselective binding using chiral boronic acids. *Recueil Des Travaux Chimiques Des Pays-Bas-Journal of the Royal Netherlands Chemical Society* **1990,** 109, (3), 216-221.
116. Wulff, G.; Haarer, J., Enzyme-Analog Built Polymers - 29: The Preparation of Defined Chiral Cavities for the Racemic-Resolution of Free Sugars. *Makromolekulare Chemie-Macromolecular Chemistry and Physics* **1991,** 192, (6), 1329-1338.
117. Wulff, G.; Schauhoff, S., Enzyme-Analog-Built Polymers -27: Racemic-Resolution of Free Sugars with Macroporous Polymers Prepared by Molecular Imprinting - Selectivity Dependence on the Arrangement of Functional-Groups Versus Spatial Requirements. *Journal of Organic Chemistry* **1991,** 56, (1), 395-400.
118. Sarhan, A., Racemic Separation of Amygdalinic Acid on Polymers with Chiral Spaces -1: The Synthesis of Suitable Polymers with Phenylboronic Acid as a Bound Group. *Makromolekulare Chemie-Rapid Communications* **1982,** 3, (7), 489-493.

119. Shea, K. J.; Thompson, E. A., Template Synthesis of Macromolecules - Selective Functionalization of an Organic Polymer. *Journal of Organic Chemistry* **1978,** 43, (21), 4253-4255.
120. Shea, K. J.; Thompson, E. A.; Pandey, S. D.; Beauchamp, P. S., Template synthesis of macromolecules. Synthesis and chemistry of functionalized macroporous poly(divinylbenzene). *Journal of the American Chemical Society* **1980,** 102, (9), 3149-3155.
121. Arshady, R.; Mosbach, K., Synthesis of substrate-selective polymers by host-guest polymerization. *Die Makromolekulare Chemie* **1981,** 182, (2), 687-692.
122. Garcia-Calzon, J. A.; Diaz-Garcia, M. E., Characterization of binding sites in molecularly imprinted polymers. *Sensors and Actuators B-Chemical* **2007,** 123, (2), 1180-1194.
123. Cormack, P. A. G.; Elorza, A. Z., Molecularly imprinted polymers: synthesis and characterisation. *Journal of Chromatography B-Analytical Technologies in the Biomedical and Life Sciences* **2004,** 804, (1), 173-182.
124. Dong, H.; Tong, A. J.; Li, L. D., Syntheses of steroid-based molecularly imprinted polymers and their molecular recognition study with spectrometric detection. *Spectrochimica Acta Part a-Molecular and Biomolecular Spectroscopy* **2003,** 59, (2), 279-284.
125. Nomura, Y.; Muguruma, H.; Yano, K.; Kugimiya, A.; McNiven, S.; Ikebukuro, K.; Karube, I., Selective recognition of 2,4-dichlorophenoxyacetic acid using a molecularly imprinted polymer. *Analytical Letters* **1998,** 31, (6), 973-980.
126. Spivak, D. A.; Shea, K. J., Binding of nucleotide bases by imprinted polymers. *Macromolecules* **1998,** 31, (7), 2160-2165.
127. Liu, X. Y.; Guan, Y.; Ding, X. B.; Peng, Y. X.; Long, X. P.; Wang, X. C.; Chang, K., Design of temperature sensitive imprinted polymer hydrogels based on multiple-point hydrogen bonding. *Macromolecular Bioscience* **2004,** 4, (7), 680-684.
128. Puoci, F.; Cirillo, G.; Curcio, M.; Iemma, F.; Parisi, O. I.; Castiglione, M.; Picci, N., Molecularly imprinted polymers for alpha-tocopherol delivery. *Drug Delivery* **2008,** 15, (4), 253-258.
129. Puoci, F.; Iemma, F.; Cirillo, G.; Picci, N.; Matricardi, P.; Alhaique, F., Molecularly imprinted polymers for 5-fluorouracil release in biological fluids. *Molecules* **2007,** 12, (4), 805-814.
130. Kriz, D.; Mosbach, K., Competitive amperometric morphine sensor-based on an agarose immobilized molecularly imprinted polymer. *Analytica Chimica Acta* **1995,** 300, (1-3), 71-75.
131. Nam, G. H.; Kim, D., Separation characteristics of molecular imprinted poly(methacrylic acid) for retinoid derivatives. *Journal of Applied Polymer Science* **2003,** 90, (4), 1081-1087.
132. Svenson, J.; Nicholls, I. A., On the thermal and chemical stability of molecularly imprinted polymers. *Analytica Chimica Acta* **2001,** 435, (1), 19-24.
133. Yoshizako, K.; Hosoya, K.; Iwakoshi, Y.; Kimata, K.; Tanaka, N., Porogen imprinting effects. *Analytical Chemistry* **1998,** 70, (2), 386-389.
134. Wulff, G.; Kemmerer, R.; Vietmeier, J.; Poll, H. G., Chirality of Vinyl-Polymers - The Preparation of Chiral Cavities in Synthetic-Polymers. *Nouveau Journal De Chimie-New Journal of Chemistry* **1982,** 6, (12), 681-687.
135. Wulff, G.; Poll, H. G., Enzyme-Analog Built Polymers 23: Influence of the Structure of the Binding-Sites on the Selectivity for Racemic-Resolution. *Makromolekulare Chemie-Macromolecular Chemistry and Physics* **1987,** 188, (4), 741-748.

136. Wulff, G.; Vietmeier, J.; Poll, H. G., Enzyme-Analog Built Polymers 22: Influence of the Nature of the Cross-Linking Agent on the Performance of Imprinted Polymers in Racemic-Resolution. *Makromolekulare Chemie-Macromolecular Chemistry and Physics* **1987,** 188, (4), 731-740.
137. Oshannessy, D. J.; Ekberg, B.; Mosbach, K., Molecular Imprinting of Amino-Acid Derivatives at Low-Temperature (0-Degrees-C) Using Photolytic Homolysis of Azobisnitriles. *Analytical Biochemistry* **1989,** 177, (1), 144-149.
138. Otsu, T.; Yoshida, M., Role of initiator-transfer agent-terminator (iniferter) in radical polymerizations - polymer design by organic disulfides as iniferters. *Makromolekulare Chemie-Rapid Communications* **1982,** 3, (2), 127-132.
139. Sellergren, B.; Shea, K. J., Influence of Polymer Morphology on the Ability of Imprinted Network Polymers to Resolve Enantiomers. *Journal of Chromatography* **1993,** 635, (1), 31-49.
140. Haupt, K.; Dzgoev, A.; Mosbach, K., Assay system for the herbicide 2,4-dichlorophenoxyacetic acid using a molecularly imprinted polymer as an artificial recognition element. *Analytical Chemistry* **1998,** 70, (3), 628-631.
141. Karlsson, J. G.; Andersson, L. I.; Nicholls, I. A., Probing the molecular basis for ligand-selective recognition in molecularly imprinted polymers selective for the local anaesthetic bupivacaine. *Analytica Chimica Acta* **2001,** 435, (1), 57-64.
142. Pap, T.; Horvath, V.; Tolokan, A.; Horvai, G.; Sellergren, B., Effect of solvents on the selectivity of terbutylazine imprinted polymer sorbents used in solid-phase extraction. *Journal of Chromatography A* **2002,** 973, (1-2), 1-12.
143. Kempe, M., Antibody-Mimicking polymers as chiral stationary phases in HPLC. *Analytical Chemistry* **1996,** 68, (11), 1948-1953.
144. Levi, R.; McNiven, S.; Piletsky, S. A.; Cheong, S. H.; Yano, K.; Karube, I., Optical detection of chloramphenicol using molecularly imprinted polymers. *Analytical Chemistry* **1997,** 69, (11), 2017-2021.
145. Takeuchi, T.; Haginaka, J., Separation and sensing based on molecular recognition using molecularly imprinted polymers. *Journal of Chromatography B* **1999,** 728, (1), 1-20.
146. Yu, C.; Mosbach, K., Influence of mobile phase composition and cross-linking density on the enantiomeric recognition properties of molecularly imprinted polymers. *Journal of Chromatography A* **2000,** 888, (1-2), 63-72.
147. Andersson, L. I., Efficient sample pre-concentration of bupivacaine from human plasma by solid-phase extraction on molecularly imprinted polymers. *Analyst* **2000,** 125, (9), 1515-1517.
148. Arthur, C. L.; Pawliszyn, J., Solid-phase microextraction with thermal-desorption using fused-silica optical fibers. *Analytical Chemistry* **1990,** 62, (19), 2145-2148.
149. Kawaguchi, M.; Hayatsu, Y.; Nakata, H.; Ishii, Y.; Ito, R.; Saito, K.; Nakazawa, H., Molecularly imprinted solid phase extraction using stable isotope labeled compounds as template and liquid chromatography-mass spectrometry for trace analysis of bisphenol A in water sample. *Analytica Chimica Acta* **2005,** 539, (1-2), 83-89.
150. Masque, N.; Marce, R. M.; Borrull, F.; Cormack, P. A. G.; Sherrington, D. C., Synthesis and evaluation of a molecularly imprinted polymer for selective on-line solid-phase extraction of 4-nitrophenol from environmental water. *Analytical Chemistry* **2000,** 72, (17), 4122-4126.
151. Muldoon, M. T.; Stanker, L. H., Molecularly imprinted solid phase extraction of atrazine from beef liver extracts. *Analytical Chemistry* **1997,** 69, (5), 803-808.

152. Perez-Moral, N.; Mayes, A. G., Direct rapid synthesis of MIP beads in SPE cartridges. *Biosensors & Bioelectronics* **2006,** 21, (9), 1798-1803.
153. Silva, R. G. D.; Augusto, F., Sol-gel molecular imprinted ormosil for solid-phase extraction of methylxanthines. *Journal of Chromatography A* **2006,** 1114, (2), 216-223.
154. Zhou, S. N.; Lai, E. P. C.; Miller, J. D., Analysis of wheat extracts for ochratoxin A by molecularly imprinted solid-phase extraction and pulsed elution. *Analytical and Bioanalytical Chemistry* **2004,** 378, (8), 1903-1906.
155. Bossi, A.; Bonini, F.; Turner, A. P. F.; Piletsky, S. A., Molecularly imprinted polymers for the recognition of proteins: The state of the art. *Biosensors & Bioelectronics* **2007,** 22, (6), 1131-1137.
156. Busam, K. J.; Jungbluth, A. A., Melan-A, a new melanocytic differentiation marker. *Advances in Anatomic Pathology* **1999,** 6, (1), 12-18.
157. Berman, H. M.; Battistuz, T.; Bhat, T. N.; Bluhm, W. F.; Bourne, P. E.; Burkhardt, K.; Iype, L.; Jain, S.; Fagan, P.; Marvin, J.; Padilla, D.; Ravichandran, V.; Schneider, B.; Thanki, N.; Weissig, H.; Westbrook, J. D.; Zardecki, C., The Protein Data Bank. *Acta Crystallographica Section D-Biological Crystallography* **2002,** 58, 899-907.
158. Coulie, P. G.; Brichard, V.; Vanpel, A.; Wolfel, T.; Schneider, J.; Traversari, C.; Mattei, S.; Deplaen, E.; Lurquin, C.; Szikora, J. P.; Renauld, J. C.; Boon, T., A NEW GENE CODING FOR A DIFFERENTIATION ANTIGEN RECOGNIZED BY AUTOLOGOUS CYTOLYTIC T-LYMPHOCYTES ON HLA-A2 MELANOMAS. *Journal of Experimental Medicine* **1994,** 180, (1), 35-42.
159. Kawakami, Y.; Eliyahu, S.; Jennings, C.; Sakaguchi, K.; Kang, X. Q.; Southwood, S.; Robbins, P. F.; Sette, A.; Appella, E.; Rosenberg, S. A., RECOGNITION OF MULTIPLE EPITOPES IN THE HUMAN-MELANOMA ANTIGEN GP100 BY TUMOR-INFILTRATING T-LYMPHOCYTES ASSOCIATED WITH IN-VIVO TUMOR-REGRESSION. *Journal of Immunology* **1995,** 154, (8), 3961-3968.
160. Busam, K. J.; Chen, Y.-T.; Old, L. J.; Stockert, E.; Iversen, K.; Coplan, K. A.; Rosai, J.; Barnhill, R. L.; Jungbluth, A. A., Expression of Melan-A (MART1) in Benign Melanocytic Nevi and Primary Cutaneous Malignant Melanoma. *The American Journal of Surgical Pathology* **1998,** 22, (8), 976-982.
161. Vanderbruggen, P.; Traversari, C.; Chomez, P.; Lurquin, C.; Deplaen, E.; Vandeneynde, B.; Knuth, A.; Boon, T., A GENE ENCODING AN ANTIGEN RECOGNIZED BY CYTOLYTIC LYMPHOCYTES-T ON A HUMAN-MELANOMA. *Science* **1991,** 254, (5038), 1643-1647.
162. Lowe, A. J.; Anderson, K. A.; Bardliving, C. L.; Huang, C., Jr.; Teixeira, L. M.; Damasceno, L. M.; Ritter, G.; Old, L. J.; Batt, C. A., Expression and purification of cGMP grade NY-ESO-1 for clinical trials. *Biotechnology Progress* **2011,** 27, (2), 435-441.
163. Huang, C., Jr.; Anderson, K.; Damasceno, L.; Ritter, G.; Old, L.; Batt, C., Improved secretion of the cancer-testis antigen SSX2 in <i>Pichia pastoris</i> by deletion of its nuclear localization signal. *Applied Microbiology and Biotechnology* 86, (1), 243-253.
164. Ayyoub, M.; Hesdorffer, C. S.; Montes, M.; Merlo, A.; Speiser, D.; Rimoldi, D.; Cerottini, J. C.; Ritter, G.; Scanlan, M.; Old, L. J.; Valmori, D., An immunodominant SSX-2-derived epitope recognized by CD4(+) T cells in association with HLA-DR. *Journal of Clinical Investigation* **2004,** 113, (8), 1225-1233.

165. Jαger, E.; Gnjatic, S.; Nagata, Y.; Stockert, E.; JÃ¤ger, D.; Karbach, J.; Neumann, A.; Rieckenberg, J.; Chen, Y.-T.; Ritter, G.; Hoffman, E.; Arand, M.; Old, L. J.; Knuth, A., Induction of primary NY-ESO-1 immunity: CD8+ T lymphocyte and antibody responses in peptide-vaccinated patients with NY-ESO-1+ cancers. *Proceedings of the National Academy of Sciences* **2000,** 97, (22), 12198-12203.
166. Bettinotti, M. P.; Kim, C. J.; Lee, K. H.; Roden, M.; Cormier, J. N.; Panelli, M.; Parker, K. K.; Marincola, F. M., Stringent allele/epitope requirements for MART-1/Melan A immunodominance: Implications for peptide-based immunotherapy. *Journal of Immunology* **1998,** 161, (2), 877-889.
167. Kang, X. Q.; Kawakami, Y.; Elgamil, M.; Wang, R. F.; Sakaguchi, K.; Yannelli, J. R.; Appella, E.; Rosenberg, S. A.; Robbins, P. F., Identification of a Tyrosinase Epitope Recognized by HLA-A24-Restricted, Tumor-Infiltrating Lyphocytes. *Journal of Immunology* **1995,** 155, (3), 1343-1348.
168. Lopes, L.; Fletcher, K.; Ikeda, Y.; Collins, M., Lentiviral vector expression of tumour antigens in dendritic cells as an immunotherapeutic strategy. *Cancer Immunology Immunotherapy* **2006,** 55, (8), 1011-1016.
169. Plog, M. S.; Guyre, C. A.; Roberts, B. L.; Goldberg, M.; George, J. A. S.; Perricone, M. A., Preclinical safety and biodistribution of adenovirus-based cancer vaccines after intradermal delivery. *Human Gene Therapy* **2006,** 17, (7), 705-716.
170. Schutz, A.; Oertli, D.; Marti, W. R.; Noppen, C.; Padovan, E.; Spagnoli, G. C.; Heberer, M.; Zajac, P., Immunogenicity of nonreplicating recombinant vaccinia expressing HLA-A201 targeted or complete MART-1/Melan-A antigen. *Cancer Gene Therapy* **2001,** 8, (9), 655-661.
171. Zajac, P.; Oertli, D.; Marti, W.; Adamina, M.; Bolli, M.; Guller, U.; Noppen, C.; Padovan, E.; Schultz-Thater, E.; Heberer, M.; Spagnoli, G., Phase I/II clinical trial of a nonreplicative vaccinia virus expressing multiple HLA-A0201-restricted tumor-associated epitopes and costimulatory molecules in metastatic melanoma patients. *Human Gene Therapy* **2003,** 14, (16), 1497-1510.
172. Lienard, D.; Avril, M. F.; Le Gal, F. A.; Baumgaertner, P.; Vermeulen, W.; Blom, A.; Geldhof, C.; Rimoldi, D.; Pagliusi, S.; Romero, P.; Dietrich, P. Y.; Corvaia, N.; Speiser, D. E., Vaccination of Melanoma Patients With Melan-A/Mart-1 Peptide and Klebsiella Outer Membrane Protein P40 as an Adjuvant. *Journal of Immunotherapy* **2009,** 32, (8), 875-883.
173. Eggermont, A. M. M.; Testori, A.; Maio, M.; Robert, C., Anti-CTLA-4 Antibody Adjuvant Therapy in Melanoma. *Seminars in Oncology* **2010,** 37, (5), 455-459.
174. Leach, D. R.; Krummel, M. F.; Allison, J. P., Enhancement of antitumor immunity by CTLA-4 blockade. *Science* **1996,** 271, (5256), 1734-1736.
175. Shrikant, P.; Khoruts, A.; Mescher, M. F., CTLA-4 blockade reverses CD8(+) T cell tolerance to tumor by a CD4(+) T cell-and IL-2-dependent mechanism. *Immunity* **1999,** 11, (4), 483-493.
176. Jazirehi, A. R.; Baritaki, S.; Koya, R. C.; Bonavida, B.; Economou, J. S., Molecular Mechanism of MART-1+/A*0201+ Human Melanoma Resistance to Specific CTL-Killing Despite Functional Tumor-CTL Interaction. *Cancer Res*.
177. Dangoor, A.; Lorigan, P.; Keilholz, U.; Schadendorf, D.; Harris, A.; Ottensmeier, C.; Smyth, J.; Hoffmann, K.; Anderson, R.; Cripps, M.; Schneider, J.; Hawkins, R., Clinical and

immunological responses in metastatic melanoma patients vaccinated with a high-dose poly-epitope vaccine. *Cancer Immunology Immunotherapy* 59, (6), 863-873.
178. Guillaume, P.; Baumgaertner, P.; Neff, L.; Rufer, N.; Wettstein, P.; Speiser, D. E.; Luescher, I. F., Novel soluble HLA-A2/MELAN-A complexes selectively stain a differentiation defective subpopulation of CD8+ T cells in patients with melanoma. *International Journal of Cancer* 127, (4), 910-923.
179. Ayyoub, M.; Zippelius, A.; Pittet, M. l. J.; Rimoldi, D.; Valmori, D.; Cerottini, J.-C.; Romero, P.; Lejeune, F.; LiÃ©nard, D.; Speiser, D. E., Activation of Human Melanoma Reactive CD8+ T Cells by Vaccination with an Immunogenic Peptide Analog Derived from Melan-A/Melanoma Antigen Recognized by T Cells-1. *Clinical Cancer Research* **2003,** 9, (2), 669-677.
180. Speiser, D. E.; LiÃ©nard, D.; Rufer, N.; Rubio-Godoy, V.; Rimoldi, D.; Lejeune, F.; Krieg, A. M.; Cerottini, J.-C.; Romero, P., Rapid and strong human CD8+ T cell responses to vaccination with peptide, IFA, and CpG oligodeoxynucleotide 7909. *The Journal of Clinical Investigation* **2005,** 115, (3), 739-746.
181. Good Manufacturing Practice Guide for Active Pharmaceutical Ingredients Q7. In *ICH Harmonised Tripartite Guideline*, Silver Spring, MD, 2000; Vol. 4.
182. Huang, C. J.; Chen, R. H.; Vannelli, T.; Lee, F.; Ritter, E.; Ritter, G.; Old, L. J.; Batt, C. A., Expression and purification of the cancer antigen SSX2: a potential cancer vaccine. *Protein Expr Purif* **2007,** 56, (2), 212-9.
183. Ishihama, Y.; Oda, Y.; Tabata, T.; Sato, T.; Nagasu, T.; Rappsilber, J.; Mann, M., Exponentially modified protein abundance index (emPAI) for estimation of absolute protein amount in proteomics by the number of sequenced peptides per protein. *Molecular & cellular proteomics : MCP* **2005,** 4, (9), 1265-72.
184. Kane, J. F., EFFECTS OF RARE CODON CLUSTERS ON HIGH-LEVEL EXPRESSION OF HETEROLOGOUS PROTEINS IN ESCHERICHIA-COLI. *Current Opinion in Biotechnology* **1995,** 6, (5), 494-500.
185. Miroux, B.; Walker, J. E., Over-production of Proteins inEscherichia coli: Mutant Hosts that Allow Synthesis of some Membrane Proteins and Globular Proteins at High Levels. *Journal of Molecular Biology* **1996,** 260, (3), 289-298.
186. Martínez-Murcia A.J.; Antón A.I.; Rodríguez-Valera F., Patterns of sequence variation in two regions of the 16S rRNA multigene family of Escherichia coli. *International Journal of Systematic and Evolutionary Microbiology* **1999,** 49, 601-610.
187. Kim, B.; Lee, S.; Lee, S.; Chang, Y.; Chang, H., High cell density fed-batch cultivation of <i>Escherichia coli</i> using exponential feeding combined with pH-stat. *Bioprocess and Biosystems Engineering* **2004,** 26, (3), 147-150.
188. Suzuki, T.; Yamane, T.; Shimizu, S., Phenomenological Background and Some Preliminary Trials of Automated Substrate Supply in pH-Stat Modal Fed-Batch Culture Using a Setpoint of High Limit. *Journal of Fermentation and Bioengineering* **1990,** 69, (5), 292-297.
189. Chen, R. H.; Huang, C., Jr.; Newton, B. S.; Ritter, G.; Old, L. J.; Batt, C. A., Factors affecting endotoxin removal from recombinant therapeutic proteins by anion exchange chromatography. *Protein Expression and Purification* **2009,** 64, (1), 76-81.

190. Specifications: Test Procedures and Acceptance Criteria for Biotechnological/Biological Products Q6B. In *ICH Harmonised Tripartite Guideline*, US Food and Drug Administration: Silver Spring, MD, 1999; Vol. 4.
191. Carrio, M. M.; Villaverde, A., Localization of Chaperones DnaK and GroEL in Bacterial Inclusion Bodies. *Journal of Bacteriology* **2005,** 187, (10), 3599-3601.
192. Carrió, M. M.; Villaverde, A., Role of molecular chaperones in inclusion body formation. *FEBS Letters* **2003,** 537, (1-3), 215-221.
193. González-Montalbán, N.; Carrió, M. M.; Cuatrecasas, S.; Arís, A.; Villaverde, A., Bacterial inclusion bodies are cytotoxic in vivo in absence of functional chaperones DnaK or GroEL. *Journal of Biotechnology* **2005,** 118, (4), 406-412.
194. Tripp, R. A.; Dluhy, R. A.; Zhao, Y., Novel nanostructures for SERS biosensing. *Nano Today* **2008,** 3, (3-4), 31-37.
195. Bonner, M. R.; Coble, J.; Blair, A.; Beane Freeman, L. E.; Hoppin, J. A.; Sandler, D. P.; Alavanja, M. C. R., Malathion Exposure and the Incidence of Cancer in the Agricultural Health Study. *Am J Epidemiol* **2007,** 166, (9), 1023-1034.
196. Edwards, D., Reregistration Eligibility Decision for Malathion. In EPA, Ed. US Environmental Protection Agency - Prevention, Pesticides and Toxic Substances: 2006; Vol. 9.
197. Borras, E.; Sanchez, P.; Munoz, A.; Tortajada-Genaro, L. A., Development of a gas chromatography-mass spectrometry method for the determination of pesticides in gaseous and particulate phases in the atmosphere. *Analytica Chimica Acta* **2012,** 699, (1), 57-65.
198. Saito, T.; Miura, N.; Namera, A.; Oikawa, H.; Miyazaki, S.; Nakamoto, A.; Inokuchi, S., Mixed-mode TiO-C18 monolithic spin-column extraction and GC-MS for simultaneous assay of organophosphorus compounds, glyphosate, and glufosinate in human serum and urine. *Forensic Toxicology* **2011,** 30, (1), 1-10.
199. Samadi, S.; Sereshti, H.; Assadi, Y., Ultra-preconcentration and determination of thirteen organophosphorus pesticides in water samples using solid-phase extraction followed by dispersive liquid-liquid microextraction and gas chromatography with flame photometric detection. *J Chromatogr A* **2011,** 1219, 61-65.
200. González-Curbelo, M.; Hernández-Borges, J.; Borges-Miquel, T. M.; Rodríguez-Delgado, M., Determination of pesticides and their metabolites in processed cereal samples. *Food Addit Contam Part A Chem Anal Control Expo Risk Assess* **2012,** 29, (1), 104-16.
201. Gonzalez-Curbelo, M. A.; Asensio-Ramos, M.; Hernandez-Borges, J.; Dionis-Delgado, S., Pesticide analysis in toasted barley and chickpea flours. *J Sep Sci* **2012,** 35, (2), 299-307.
202. González-Curbelo, M. A.; Asensio-Ramos, M.; Herrera-Herrera, A. V.; Hernández-Borges, J., Pesticide residue analysis in cereal-based baby foods using multi-walled carbon nanotubes dispersive solid-phase extraction. *Anal Bioanal Chem* **2012,** 404, (1), 183-96.
203. Ebrahimi, M.; Es'haghi, Z.; Samadi, F.; Bamoharram, F. F.; Hosseini, M. S., Rational design of heteropolyacid-based nanosorbent for hollow fiber solid phase microextraction of organophosphorus residues in hair samples. *J Chromatogr A* **2012,** 1225, 37-44.
204. Ebrahimi, M.; Es'haghi, Z.; Samadi, F.; Hosseini, M. S., Ionic liquid mediated sol-gel sorbents for hollow fiber solid-phase microextraction of pesticide residues in water and hair samples. *J Chromatogr A* **2012,** 1218, (46), 8313-8321.
205. Pareja, L.; Fernandez-Alba, A. R.; Cesio, V.; Heinzen, H.; BioCop, I. I. M. c. c. i. f., Analytical methods for pesticide residues in rice. *Trends Analyt Chem* **2011,** 30, (2), 270-291.

206. Chen, Y.; Guo, Z.; Wang, X.; Qiu, C., Sample preparation. *J. Chromatogr. A Journal of Chromatography A* **2008,** 1184, (1-2), 191-219.
207. Fan, M. K.; Wang, P. H.; Escobedo, C.; Sinton, D.; Brolo, A. G., Surface-enhanced Raman scattering (SERS) optrodes for multiplexed on-chip sensing of nile blue A and oxazine 720. *Lab Chip* **2012,** 12, (8), 1554-1560.
208. Ryu, K.; Haes, A. J.; Park, H.-Y.; Nah, S.; Kim, J.; Chung, H.; Yoon, M.-Y.; Han, S.-H., Use of peptide for selective and sensitive detection of an Anthrax biomarker via peptide recognition and surface-enhanced Raman scattering. *J Raman Spectrosc* **2011,** 41, (2), 121-124.
209. Huang, G. G.; Hossain, M. K.; Han, X. X.; Ozaki, Y., A novel reversed reporting agent method for surface-enhanced Raman scattering; highly sensitive detection of glutathione in aqueous solutions. *Analyst* **2009,** 134, (12), 2468-2474.
210. Bompart, M.; De Wilde, Y.; Haupt, K., Chemical Nanosensors Based on Composite Molecularly Imprinted Polymer Particles and Surface-Enhanced Raman Scattering. *Advanced Materials* **2010,** 22, (21), 2343-2348.
211. Strickland, A. D.; Batt, C. A., Detection of Carbendazim by Surface-Enhanced Raman Scattering Using Cyclodextrin Inclusion Complexes on Gold Nanorods. *Anal Chem* **2009,** 81, (8), 2895-2903.
212. Chen, J. W.; Jiang, J. H.; Gao, X.; Liu, G. K.; Shen, G. L.; Yu, R. Q., A New Aptameric Biosensor for Cocaine Based on Surface-Enhanced Raman Scattering Spectroscopy. *Chemistry-a European Journal* **2008,** 14, (27), 8374-8382.
213. Yguerabide, J.; Yguerabide, E. E., Light-scattering submicroscopic particles as highly fluorescent analogs and their use as tracer labels in clinical and biological applications - II. Experimental characterization. *Analytical Biochemistry* **1998,** 262, (2), 157-176.
214. Bruno, J.; Carrillo, M.; Phillips, T.; King, B., Development of DNA aptamers for cytochemical detection of acetylcholine. *In Vitro Cell Dev Biol* **2008,** 44, (3-4), 63-72.
215. Bruno, J. G., Chanpong, Joseph. Methods of Producing Competitive Aptamer FRET Reagents and Assays. 2009, 2009.
216. Taton, T. A., Preparation of Gold Nanoparticle–DNA Conjugates. In *Current Protocols in Nucleic Acid Chemistry*, John Wiley & Sons, Inc.: 2001.
217. Yong, K. T.; Sahoo, Y.; Swihart, M. T.; Prasad, P. N., Synthesis and plasmonic properties of silver and gold nanoshells on polystyrene cores of different size and of gold-silver core-shell nanostructures. *Colloids Surf A Physicochem Eng Asp* **2006,** 290, (1-3), 89-105.
218. Schmit, V. L.; Martoglio, R.; Scott, B.; Strickland, A. D.; Carron, K. T., Lab-on-a-Bubble: Synthesis, Characterization, and Evaluation of Buoyant Gold Nanoparticle-Coated Silica Spheres. *J Am Chem Soc* **2011,** 134, (1), 59-62.
219. Pierre, M. C. S.; Mackie, P. M.; Roca, M.; Haes, A. J., Correlating Molecular Surface Coverage and Solution-Phase Nanoparticle Concentration to Surface-Enhanced Raman Scattering Intensities. *J Phys Chem C* **2011,** 115, (38), 18511-18517.
220. Demers, L. M.; Mirkin, C. A.; Mucic, R. C.; Reynolds, R. A.; Letsinger, R. L.; Elghanian, R.; Viswanadham, G., A fluorescence-based method for determining the surface coverage and hybridization efficiency of thiol-capped oligonucleotides bound to gold thin films and nanoparticles. *Analytical Chemistry* **2000,** 72, (22), 5535-5541.
221. Rouhana, L. L.; Jaber, J. A.; Schlenoff, J. B., Aggregation-Resistant Water-Soluble Gold Nanoparticles. *Langmuir* **2007,** 23, (26), 12799-12801.

222. Barhoumi, A.; Zhang, D.; Tam, F.; Halas, N. J., Surface-Enhanced Raman Spectroscopy of DNA. *J Am Chem Soc* **2008,** 130, (16), 5523-5529.
223. Chen, J.; Jiang, J.; Gao, X.; Liu, G.; Shen, G.; Yu, R., A New Aptameric Biosensor for Cocaine Based on Surface-Enhanced Raman Scattering Spectroscopy. *Chemistry – A European Journal* **2008,** 14, (27), 8374-8382.
224. Pagba, C. V.; Lane, S. M.; Wachsmann-Hogiu, S., Raman and surface-enhanced Raman spectroscopic studies of the 15-mer DNA thrombin-binding aptamer. *J Raman Spectrosc* **2010,** 41, (3), 241-247.
225. Tanner, P. A.; Leung, K.-H., Spectral Interpretation and Qualitative Analysis of Organophosphorus Pesticides Using FT-Raman and FT-Infrared Spectroscopy. *Appl. Spectrosc.* **1996,** 50, (5), 565-571.
226. Thompson, M.; Ellison, S. L. R.; Wood, R., Harmonized guidelines for single-laboratory validation of methods of analysis - (IUPAC technical report). *Pure Appl Chem* **2002,** 74, (5), 835-855.
227. Yu, W. W.; White, I. M., A simple filter-based approach to surface enhanced Raman spectroscopy for trace chemical detection. *Analyst* **2012,** 137, (5), 1168-1173.
228. Gervais, J. A., Luukinen, B., Buhl, K., Stone, D. *Malathion Technical Fact Sheet*; Oregon State University Extension Services: 2009.
229. Rowe, R. C.; Sheskey, P. J.; Owen, S. C.; American Pharmacists, A., *Handbook of pharmaceutical excipients*. Pharmaceutical Press ; American Pharmacists Association: London; Greyslake, IL; Washington, DC, 2006.
230. Duncan, R., The dawning era of polymer therapeutics. *Nature Reviews Drug Discovery* **2003,** 2, (5), 347-360.
231. Duncan, R., Polymer conjugates as anticancer nanomedicines. *Nature Reviews Cancer* **2006,** 6, (9), 688-701.
232. Liechty, W. B.; Kryscio, D. R.; Slaughter, B. V.; Peppas, N. A., Polymers for Drug Delivery Systems. In *Annual Review of Chemical and Biomolecular Engineering, Vol 1*, Prausnitz, J. M.; Doherty, M. F.; Segalman, M. A., Eds. Annual Reviews: Palo Alto, 2010; Vol. 1, pp 149-173.
233. Greco, F.; Vicent, M. J.; Gee, S.; Jones, A. T.; Gee, J.; Nicholson, R. I.; Duncan, R., Investigating the mechanism of enhanced cytotoxicity of HPMA copolymer-Dox-AGM in breast cancer cells. *Journal of Controlled Release* **2007,** 117, (1), 28-39.
234. Greco, F.; Vicent, M. J.; Penning, N. A.; Nicholson, R. I.; Duncan, R., HPMA copolymer-aminoglutethimide conjugates inhibit aromatase in MCF-7 cell lines. *Journal of Drug Targeting* **2005,** 13, (8-9), 459-470.
235. Krakovicova, H.; Etrych, T.; Ulbrich, K., HPMA-based polymer conjugates with drug combination. *European Journal of Pharmaceutical Sciences* **2009,** 37, (3-4), 405-412.
236. Vicent, M. J.; Greco, F.; Nicholson, R. I.; Paul, A.; Griffiths, P. C.; Duncan, R., Polymer therapeutics designed for a combination therapy of hormone-dependent cancer. *Angewandte Chemie-International Edition* **2005,** 44, (26), 4061-4066.
237. Lammers, T.; Subr, V.; Ulbrich, K.; Peschke, P.; Huber, P. E.; Hennink, W. E.; Storm, G., Simultaneous delivery of doxorubicin and gemcitabine to tumors in vivo using prototypic polymeric drug carriers. *Biomaterials* **2009,** 30, (20), 3466-3475.

238. Byrne, M. E.; Salian, V., Molecular imprinting within hydrogels II: Progress and analysis of the field. *International Journal of Pharmaceutics* **2008,** 364, (2), 188-212.
239. Mullett, W. M., Determination of drugs in biological fluids by direct injection of samples for liquid-chromatographic analysis. *Journal of Biochemical and Biophysical Methods* **2007,** 70, (2), 263-273.
240. Sambe, H.; Hoshina, K.; Hosoya, K.; Haginaka, J., Simultaneous determination of bisphenol A and its halogenated derivatives in river water by combination of isotope imprinting and liquid chromatographyâ€“mass spectrometry. *Journal of Chromatography A* **2006,** 1134, (1-2), 16-23.
241. Haginaka, J.; Sakai, Y.; Narimatsu, S., Uniform-Sized Molecularly Imprinted Polymer Material for Propranolol. Recognition of Propranolol and Its Metabolites. *Analytical Sciences* **1998,** 14, (4), 823-826.
242. Haginaka, J.; Takehira, H.; Hosoya, K.; Tanaka, N., Molecularly Imprinted Uniform-Sized Polymer-Based Stationary Phase for Naproxen. *Chemistry Letters* **1997,** 26, (6), 555-556.
243. Azodi-Deilami, S.; Abdouss, M.; Hasani, S., Preparation and utilization of a molecularly imprinted polymer for solid phase extraction of tramadol. *Central European Journal of Chemistry* **2010,** 8, (4), 861-869.
244. Caro, E.; MarcÃ©, R. M.; Borrull, F.; Cormack, P. A. G.; Sherrington, D. C., Application of molecularly imprinted polymers to solid-phase extraction of compounds from environmental and biological samples. *TrAC Trends in Analytical Chemistry* **2006,** 25, (2), 143-154.
245. Moller, K.; Nilsson, U.; Crescenzi, C., Investigation of matrix effects of urine on a molecularly imprinted solid-phase extraction. *Journal of Chromatography B* **2004,** 811, (2), 171-176.
246. Theodoridis, G.; Zacharis, C. K.; Tzanavaras, P. D.; Themelis, D. G.; Economou, A., Automated sample preparation based on the sequential injection principle: Solid-phase extraction on a molecularly imprinted polymer coupled on-line to high-performance liquid chromatography. *Journal of Chromatography A* **2004,** 1030, (1â€“2), 69-76.
247. Chen, G.; Guan, Z.; Chen, C.-T.; Fu, L.; Sundaresan, V.; Arnold, F. H., A glucose-sensing polymer. *Nat Biotech* **1997,** 15, (4), 354-357.
248. Kriz, D.; Mosbach, K., Competitive amperometric morphine sensor based on an agarose immobilised molecularly imprinted polymer. *Analytica Chimica Acta* **1995,** 300, (1-3), 71-75.
249. Turkewitsch, P.; Wandelt, B.; Darling, G. D.; Powell, W. S., Fluorescent Functional Recognition Sites through Molecular Imprinting. A Polymer-Based Fluorescent Chemosensor for Aqueous cAMP. *Analytical Chemistry* **1998,** 70, (10), 2025-2030.
250. Anderson, C. D.; Shea, K. J.; Rychnovsky, S. D., Strategies for the generation of molecularly imprinted polymeric nitroxide catalysts. *Organic Letters* **2005,** 7, (22), 4879-4882.
251. Fischer, L.; Mueller, R.; Ekberg, B.; Mosbach, K., Direct enantioseparation of .beta.-adrenergic blockers using a chiral stationary phase prepared by molecular imprinting. *Journal of the American Chemical Society* **1991,** 113, (24), 9358-9360.
252. Lin, J. M.; Nakagama, T.; Uchiyama, K.; Hobo, T., Molecularly imprinted polymer as chiral selector for enantioseparation of amino acids by capillary gel electrophoresis. *Chromatographia* **1996,** 43, (11-12), 585-591.

253. Lin, J. M.; Nakagama, T.; Uchiyama, K.; Hobo, T., Enantioseparation of D,L-phenylalanine by molecularly imprinted polymer particles filled capillary electrochromatography. *Journal of Liquid Chromatography & Related Technologies* **1997,** 20, (10), 1489-1506.
254. Suedee, R.; Songkram, C.; Petmoreekul, A.; Sangkunakup, S.; Sankasa, S.; Kongyarit, N., Direct enantioseparation of adrenergic drugs via thin-layer chromatography using molecularly imprinted polymers. *Journal of Pharmaceutical and Biomedical Analysis* **1999,** 19, (3-4), 519-527.
255. Yin, J. F.; Yang, G. L.; Chen, Y., Rapid and efficient chiral separation of nateglinide and its L-enantiomer on monolithic molecularly imprinted polymers. *Journal of Chromatography A* **2005,** 1090, (1-2), 68-75.
256. Greco, F.; Vicent, M. J., Combination therapy: Opportunities and challenges for polymer-drug conjugates as anticancer nanomedicines. *Advanced Drug Delivery Reviews* **2009,** 61, (13), 1203-1213.
257. Puoci, F.; Iemma, F.; Muzzalupo, R.; Spizzirri, U. G.; Trombino, S.; Cassano, R.; Picci, N., Spherical Molecularly Imprinted Polymers (SMIPs) via a Novel Precipitation Polymerization in the Controlled Delivery of Sulfasalazine. *Macromolecular Bioscience* **2004,** 4, (1), 22-26.
258. Alvarez-Lorenzo, C.; Concheiro, A., Molecularly imprinted polymers for drug delivery. *Journal of Chromatography B-Analytical Technologies in the Biomedical and Life Sciences* **2004,** 804, (1), 231-245.
259. Karukstis, K. K.; Thompson, E. H. Z.; Whiles, J. A.; Rosenfeld, R. J., Deciphering the fluorescence signature of daunomycin and doxorubicin. *Biophysical Chemistry* **1998,** 73, (3), 249-263.
260. Xu, Z. F.; Kuang, D. Z.; Feng, Y. L.; Zhang, F. X., Combination of hydrophobic effect and electrostatic interaction in imprinting for achieving efficient recognition in aqueous media. *Carbohydrate Polymers* **2010,** 79, (3), 642-647.
261. Piletsky, S. A.; Piletska, E. V.; Karim, K.; Freebairn, K. W.; Legge, C. H.; Turner, A. P. F., Polymer Cookery:â€‰ Influence of Polymerization Conditions on the Performance of Molecularly Imprinted Polymers. *Macromolecules* **2002,** 35, (19), 7499-7504.
262. Turner, N. W.; Piletska, E. V.; Karim, K.; Whitcombe, M.; Malecha, M.; Magan, N.; Baggiani, C.; Piletsky, S. A., Effect of the solvent on recognition properties of molecularly imprinted polymer specific for ochratoxin A. *Biosensors and Bioelectronics* **2004,** 20, (6), 1060-1067.
263. Mosbach, K.; Yu, Y. H.; Andersch, J.; Ye, L., Generation of new enzyme inhibitors using imprinted binding sites: The anti-idiotypic approach, a step toward the next generation of molecular imprinting. *Journal of the American Chemical Society* **2001,** 123, (49), 12420-12421.
264. Yu, Y. H.; Ye, L.; Haupt, K.; Mosbach, K., Formation of a class of enzyme inhibitors (drugs), including a chiral compound, by using imprinted polymers or biomolecules as molecular-scale reaction vessels. *Angewandte Chemie-International Edition* **2002,** 41, (23), 4459-+.
265. Norell, M. C.; Andersson, H. S.; Nicholls, I. A., Theophylline molecularly imprinted polymer dissociation kinetics: a novel sustained release drug dosage mechanism. *Journal of Molecular Recognition* **1998,** 11, (1-6), 98-102.

266. Suedee; Srichana; Rattananont, Enantioselective Release of Controlled Delivery Granules Based on Molecularly Imprinted Polymers. *Drug Delivery* **2002,** 9, (1), 19-30.
267. Janssen, M.; Crommelin, D.; Storm, G.; Hulshoff, A., Doxorubicin decomposition on storage. Effect of pH, type of buffer and liposome encapsulation. *International Journal of Pharmaceutics International Journal of Pharmaceutics* **1985,** 23, (1), 1-11.
268. Coates, J., Interpretation of Infrared Spectra, A Practical Approach. In *Encyclopedia of Analytical Chemistry*, John Wiley & Sons, Ltd: 2006.
269. Ritger, P. L.; Peppas, N. A., A simple equation for description of solute release I. Fickian and non-fickian release from non-swellable devices in the form of slabs, spheres, cylinders or discs. *Journal of Controlled Release* **1987,** 5, (1), 23-36.
270. Taylor, R. F.; Schultz, J. S., *Handbook of chemical and biological sensors*. Institute of Physics Pub.: Bristol; Philadelphia, 1996.
271. Turiel, E.; Martin-Esteban, A., Molecularly imprinted polymers for sample preparation: A review. *Analytica Chimica Acta* **2010,** 668, (2), 87-99.
272. Kneipp, K.; Wang, Y.; Kneipp, H.; Perelman, L. T.; Itzkan, I.; Dasari, R.; Feld, M. S., Single molecule detection using surface-enhanced Raman scattering (SERS). *Physical Review Letters* **1997,** 78, (9), 1667-1670.
273. Doering, W. E.; Nie, S. M., Single-molecule and single-nanoparticle SERS: Examining the roles of surface active sites and chemical enhancement. *Journal of Physical Chemistry B* **2002,** 106, (2), 311-317.
274. Pettinger, B., Single-molecule surface- and tip-enhanced raman spectroscopy. *Molecular Physics* **2010,** 108, (16), 2039-2059.
275. Bjerneld, E. J.; Foldes-Papp, Z.; Kall, M.; Rigler, R., Single-molecule surface-enhanced Raman and fluorescence correlation spectroscopy of horseradish peroxidase. *Journal of Physical Chemistry B* **2002,** 106, (6), 1213-1218.
276. Kleinman, S. L.; Ringe, E.; Valley, N.; Wustholz, K. L.; Phillips, E.; Scheidt, K. A.; Schatz, G. C.; Van Duyne, R. P., Single-Molecule Surface-Enhanced Raman Spectroscopy of Crystal Violet Isotopologues: Theory and Experiment. *Journal of the American Chemical Society* **2011,** 133, (11), 4115-4122.
277. Ruckert, B.; Hall, A. J.; Sellergren, B., Molecularly imprinted composite materials via iniferter-modified supports. *Journal of Materials Chemistry* **2002,** 12, (8), 2275-2280.
278. Koo, Y. E. L.; Cao, Y. F.; Kopelman, R.; Koo, S. M.; Brasuel, M.; Philbert, M. A., Real-time measurements of dissolved oxygen inside live cells by organically modified silicate fluorescent nanosensors. *Analytical Chemistry* **2004,** 76, (9), 2498-2505.
279. Barahona, F.; Turiel, E.; Cormack, P. A. G.; Martin-Esteban, A., Chromatographic Performance of Molecularly Imprinted Polymers: Core-Shell Microspheres by Precipitation Polymerization and Grafted MIP Films via Iniferter-Modified Silica Beads. *Journal of Polymer Science Part a-Polymer Chemistry* **2010,** 48, (5), 1058-1066.
280. Sellergren, B.; Ruckert, B.; Hall, A. J., Layer-by-layer grafting of molecularly imprinted polymers via iniferter modified supports. *Advanced Materials* **2002,** 14, (17), 1204-+.
281. Kim, M. S.; Kim, M. K.; Lee, C. J.; Jung, Y. M.; Lee, M. S., Surface-enhanced Raman Spectroscopy of Benzimidazolic Fungicides: Benzimidazole and Thiabendazole. *Bulletin of the Korean Chemical Society* **2009,** 30, (12), 2930-2934.

282. Forster, M.; Girling, R. B.; Hester, R. E., Infared, Raman and Resonance Raman Investigations of Methylviologen and its Radical Cation. *Journal of Raman Spectroscopy* **1982,** 12, (1), 36-48.
283. Sundaraganesan, N.; Ilakiamani, S.; Subramani, P.; Joshua, B. D., Comparison of experimental and ab initio HF and DFT vibrational spectra of benzimidazole. *Spectrochimica Acta Part a-Molecular and Biomolecular Spectroscopy* **2007,** 67, (3-4), 628-635.
284. Powell, K.; Stiller, J., What's living in your world? Building research partnerships for inquiry-based learning. *The Science Teacher* **2005,** 72, 20+.
285. National Committee on Science Education, S.; Assessment; National Research, C., *National Science Education Standards*. The National Academies Press: 1996.
286. Grumbine, R. A.; Hecker, L.; Littlefield, A. P.; Abedon, B.; Coleman, K. D.; Hinckley, T. R.; Rubin, J.; Tolman, C.; Whittemore, S.; Landmark College . National, I., *Biology success! : teaching diverse learners, a resource manual for biology educators*. National Institute at Landmark College: Putney, Vt., 2005.
287. Anderson, R. A., Reforming Science Teaching: What Research says about Inquiry. *Journal of Science Teacher Education* **2002,** 13, (1), 1-12.
288. Bell, R. L., L. Smetana, and I. Binns., Simplifying inquiry instruction: Assessing the inquiry level of classroom activities. *The Science Teacher* **2005,** 72, (7), 30-33.
289. Bogiages, C. A.; Lotter, C., Modeling natural selection: using model-based inquiry and wikis to learn about evolution. *The Science Teacher* 78, 34.
290. Trowbridge, L. W.; Bybee, R. W.; Carlson-Powell, J., *Teaching secondary school science : strategies for developing scientific literacy*. Merrill: Upper Saddle River, N.J., 2000.